Ultra-Sensitive Absorption Measurements Through Cavity-Enhanced Spectroscopy

Thesis by

Timothy McGarvey

In Partial Fulfillment of the Requirements

for the Degree of

Doctor of Philosophy

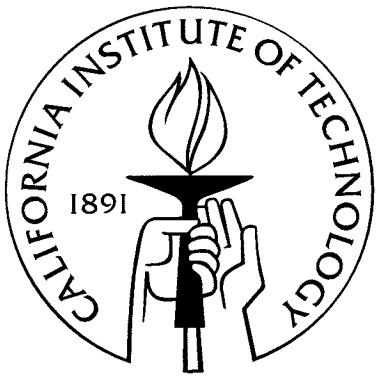

California Institute of Technology

Pasadena, California

2006

(Defended May 12, 2006)

Acknowledgements

First and foremost, I would like to thank my advisor, Hideo Mabuchi, for his guidance and patience in my learning process. I came into the group not even knowing what 'Quantum Optics' meant and not understanding much of what was discussed during group meetings. Having been trained in Molecular Biology and Organic Chemistry, the world of (Quantum) Optical Physics was quite foreign indeed. I wanted to be involved in an interdisciplinary project, however. I was interested in developing a new technique for observing protein dynamics. After speaking with Hideo and doing some initial investigation, I became convinced that cavity-enhanced spectroscopy was a promising technique with which to probe and observe such dynamics. Five years later, we completed the proof-of-principle experiments and cavity-enhanced spectroscopy is ready for its next phase of development and eventual implementation for characterizing the protein dynamics of a photosynthetic reaction center or some other system. This project was a phenomenal learning and growing experience for me and I would not trade it for anything in the world. I learned more in my years at Caltech than in any period of my life and, for that, I am grateful to Hideo and all of the other members (past and present) of the Mabuchi Group: Mike Armen, André Conjusteau, Andy Berglund, Kevin McHale, John Stockton, Benjamin Lev, Andrew Doherty, John Au, J. M. Geremia, Jen Sokol, and many others. In particular, I would like to thank André Conjusteau for patiently introducing me to and helping me with nearly all aspects of this project. I would also like to give a special thanks to special Mikey Armen. Mike was instrumental in helping me to diagnose some difficult problems with my servo and some of the electro-optic components in my experiment. Next I would like to thank Andrew Berglund for patiently (or mostly patiently) answering my endless

questions about mathematics, MATLAB, and control theory. Last but not least, a special thank you to Kevin McHale for his general willingness to help and for his guidance in MATLAB and LATEX.

Abstract

The desire to increase the sensitivity of solution-based optical absorption spectroscopy is motivated by the need for label-free biosensing (which provides a more authentic indication of the state of a biological system) and by the usefulness of characterizing the kinetics of biologically relevant reactions (which may not be accurately characterizable at reagent concentrations required by standard methods). Our current device has a demonstrated detection threshold of $1.7 \times 10^{-7}/\sqrt{Hz}$ ($4.36 \times 10^{-6} cm^{-1}$), which could with further technical work be improved to a shot-noise limited sensitivity of $1.93 \times 10^{-10}/\sqrt{Hz}$ ($1.06 \times 10^{-8} cm^{-1}$). The latter would correspond to an average of 700 strong absorbers ($\epsilon = 10^5 M^{-1} cm^{-1}$) in the optical beam volume. The shot-noise limited detection threshold of our measurement method could potentially be improved by up to two orders of magnitude by incorporating state-of-the-art optical mirrors. With such mirrors, cavity-enhanced absorption experiments performed with gas-phase samples have previously demonstrated single molecule sensitivity. We have established that solution-based cavity-enhanced absorption measurements are more sensitive than standard single-pass measurements by the predicted enhancement factor for our present device ($\sim 20,000$). These measurements provide the proof-of-principle for solution-based, cavity-enhanced spectroscopy and serve as the intermediate step towards the attainment of the theoretical sensitivity of this technique. We believe that this device will be of broad interest to the scientific because it is presently the most sensitive solution-based spectroscopic device, it can make real-time absorption measurements which would allow monitoring of the kinetics of chemical reactions in which the spectral properties of reactants change by even a small amount, and, near its theoretical limit of sensitivity (given currently available mirrors), such a device could

potentially resolve single-molecule absorption events on the sub-millisecond timescale and below.

Contents

List of Figures

Chapter 1

Introduction

In this experiment, we have performed absorption measurements that provide the proof-of-principle for solution-based, cavity-enhanced spectroscopy and serve as the intermediate step towards the attainment of our larger goal of observing structural dynamics on a small population of protein complexes. We have established that solution-based cavity-enhanced absorption measurements are more sensitive than standard single-pass measurements by the predicted enhancement factor for our present device ($\sim 20,000$) and we have demonstrated a detection threshold of of $1.7 \times 10^{-7}/\sqrt{Hz}$ ($4.36 \times 10^{-6} cm^{-1}$), which could with further technical work be improved to a shot-noise limited sensitivity of $1.93 \times 10^{-10}/\sqrt{Hz}$ ($1.06 \times 10^{-8} cm^{-1}$). The latter would correspond to an average of 700 strong absorbers ($\epsilon = 10^5 M^{-1} cm^{-1}$) in the optical beam volume.

1.1 Experimental Motivation

Our initial motivation in developing a solution-based cavity-enhanced spectroscopic device was to examine a light-sensitive biological system at a level of sensitivity that pre-existing devices could not attain. We needed to choose a system that had a light-induced spectral shift on a slow enough time scale as to be measurable, given what we understood to be our bandwidth limitations. After some research, we chose the bacterial photosynthetic reaction center of *R. sphaeroides*, largely because its x-ray crystal structure had been solved at high resolution [1] [2] [3] [4] [5] and the kinetics of electron transfer had been well-characterized [6] [7] [8] [9][10].

In order to discuss the particular event we were interested in characterizing, it will first be necessary to discuss photosynthesis and the structure of the reaction center. Photosynthesis is the mechanism by which certain biological organisms convert light energy into biological energy in the form of adenosine triphosphate (ATP). The photosynthetic reaction center is the protein in which this process takes place in certain types of purple bacteria, such as *R. sphaeroides*. Most of what is known about the specific steps in electron transfer has been determined using bulk absorption difference measurements (using optical pulses) and the x-ray structures of the reaction center. The absorption difference measurements identify changes in absorption in each chromaphore due to the presence of a local electric field (the Stark Effect) caused by charge separation caused by a mobile electron or due to the fact that one of the chromaphores is in an excited electronic state. The x-ray structures identify the exact position and structure of each chromaphore and the local protein environment around and between each. The structure of each chromaphore and its local environment provide important information concerning the nature of the ionization of bacteriochlorophyll and the subsequent path of the electron in its journey to the final electron-accepting molecule in the reaction center, ubiquinone. Based upon these, the reaction center is known to contain six chlorophyll-like chromaphores and two ubiquinone electron acceptors. A structure of this *R. sphaeroides* reaction center is presented in Figure 1.1 ([1]. Two of the chromaphores are at the top of the reaction center in the form of a bacteriochlorophyll dimer (D). Additionally, there are two individual bacteriochlorophyll molecules (BA and BB) about 7 Å on either side of the dimer. The last two chromaphores are individual bacteriopheophytin (HA and HB) (very similar in structure to bacteriochlorophyll) molecules and are located 13 Å down from the individual bacteriochlorophyll molecules. The ubiquinone molecules (QA and QB) are located 10 Å down from the bacteriopheophytin molecules and are themselves 15 Å apart. The electron is initially liberated from the bacteriochlorophyll dimer upon absorption of excitation energy either directly from a photon or from other nearby chromaphores. It is then known to travel to BA and then to QA and finally on to QB. There is no solid

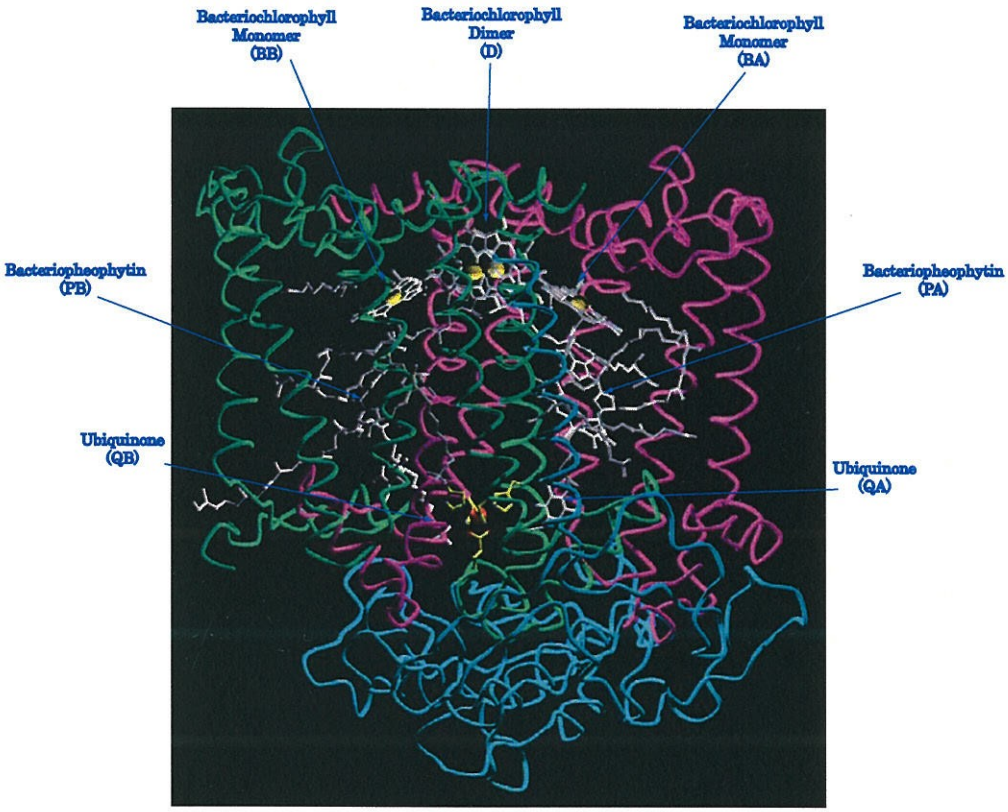

Figure 1.1: Chromaphores in a Bacterial Reaction Center (*R. sphaeroides*)

evidence that it ever directly travels to HA or that it ever travels along the 'B' pathway (BB and HB). In fact, the 'purpose' of the 'B' pathway is unknown. The kinetics of electron transfer between the dimer and the bacteriochlorophyll and bacteriopheophytin are too fast (psec and faster) to monitor with cavity-enhanced spectroscopy. The transfer of an electron from QA to QB is accompanied by a spectral shift in the near infrared that is on the order of hundreds of microseconds to a millisecond [8] [7]. This transfer event is thought to be accompanied by a conformational change in the reaction center protein and to involve a 180 degree flip in the position of QB in its binding pocket within the reaction center [11]. This change in the position of QB was demonstrated to be a necessary condition for electron transfer between QA and QB at low temperatures ($\sim$ 90 K) [12]. This suggests that the QB flip is thermal-mediated, which is consistent with the observed differences in the positions of certain amino acid side chains in the reaction center in the presence versus the absence of light [11]. What particularly caught our attention was that, in the 'dark structure' (i.e. the reaction center structure in the absence of light), although most of the quinone electron density suggested a QB in the 'pre-flip' state (which seems to inhibit the ability of QA to transfer its electron to QB), some residual electron density suggested some relatively small population of reaction centers contained the QB in the 'post-flip' state, in which QA can readily transfer its electron to QB. This was clear evidence that the picture provided by bulk measurements was likely averaging out improbable events, events which, if characterized could enhance our knowledge of this particular step in electron transfer. Our hope, therefore, was that we might be able to use cavity-enhanced spectroscopy to observe this relatively slow and seemingly thermal-mediated transfer of electrons between the two quinones in a much smaller population of reaction centers, small enough to observe that were imperceptible in bulk.

1.2 Improving the Sensitivity of Solution-Based Absorption Measurements

Absorption measurements traditionally have been done in bulk because of the need to be able to discriminate between a change in light intensity due to absorption or scattering (this difference represents the signal we are trying to measure) and a variation in the signal due to amplitude or frequency noise on the light source or to electronic noise associated with photo detection and laser frequency control, for example. In the characterization of reaction center kinetics, these bulk measurements consisted largely in pulse propagation of light in a single pass through a medium that contained the reaction centers. One way in which the absorption of a smaller population of molecules can be measured is by causing light to make multiple passes through the molecules of interest. There are a number of techniques by which such increasingly sensitive measurements have been made, including incoherent cavity-enhanced spectroscopy, cavity ringdown spectroscopy, microsphere-based whispering-gallery mode sensing, and our cavity-enhanced measurements. A brief review of each technique and its sensitivity will be presented. The focus of this discussion is on the sensitivity of each technique and its potential applications. Discussions of the details of each technique are presented in a number of recent papers [13] [14] [15]. One of the challenges in reviewing these different techniques is that each one has its own unique vocabulary and conventions of measuring loss/absorption. In the realm of traditional biochemistry and biophysics, the conventional units of absorption are those of absorbance or optical density. It is rare that these units are used in physics, largely because they represent the base 10 log of the incident power over the transmitted power. Standard units in Physics are either roundtrip loss factors, which are in units of cm^{-1}, to show the natural log of the incident over the transmitted or reflected power for some path length. The path length factor is particularly important in techniques in which the effective path length over which the measurement is made is on the order of tens of meters and longer. These units can be converted to units of absorbance by dividing by ln(10). Another complicating factor is that sensitivity can be reported in terms of the effective

detection bandwidth (i.e. $losses/\sqrt{BW}$), since the ultimate sensitivity one reports is a function of the amount of time over which the detected signal is averaged (i.e. the effective bandwidth).

1.2.1 Cavity Ringdown Spectroscopy

Cavity Ringdown Spectroscopy (CRDS) is a technique in which a coherent optical beam pulse (or continuous wave laser shuttered with an acousto-optic modulator) is sent into a cavity. The beam makes many round trips within the cavity before being transmitted out. A simple description of this type of system is:

$$P = P_i e^{-t/\tau} \tag{1.1}$$

where τ is the exponential decay constant, which is a function of the round trip distance within the cavity, the reflectivity of the cavity mirrors, and intra-cavity losses due to absorption and scattering. The intra-cavity losses due to absorption can be determined by comparing the decay constant in the presence and absence of the absorber. Zare et al. uses CRDS to make solution-based absorption measurements of copper (II) acetate, LD700 laser dye, and Indigo Carmine[16] and methylene blue [17] [18]. They report that their method has a sensitivity of $1.0 \times 10^{-6}\ cm^{-1}$ and their actual measurements have a sensitivity of $\sim 1 \times 10^{-4} cm^{-1}$. In [17], they made kinetic measurements of the reduction of methylene blue by ascorbic acid in nanomolar to hundreds of picomolar concentrations. Pippino et al. uses evanescent wave (EW) CRDS to make very sensitive absorption measurements on solid films (2.2×10^{-6}) [19] [20]. This technique may have the potential to measure absorption of absorber-containing phospholipid bilayers.

1.2.2 Microsphere-Based Whispering Gallery Mode Sensing

Microspheres have been used to make solution-based absorption measurements. Light propagates around the microspheres through total internal reflection within the sphere in what are called whispering gallery modes (WGMs). The evanescent field of the

WGM (which is the surface mode) extends hundreds of nanometers from the surface of the sphere into the surrounding medium, whether it be air, liquid, or a thin film. Microspheres are characterized by a quality (Q) factor which is analogous to cavity finesse. These microsphere resonators have the general advantage of having very high Q factors (on the order of 10^9) and very long effective pathlengths (on the order of hundreds of meters). The Q factors are affected by certain physical features of the microsphere (e.g. radius of curvature, surface anomalies, etc.) and by absorption and scattering in the medium on the exterior of the microsphere. Thus, absorptive losses can be determined by measuring the change in the Q factor in the presence and absence of the absorber. Nadeau *et al.* measured the absorption of a fluorescent stain (T-3605) in methanol (at 670 nm) and reported a microcavity Q^{-1} consistent with a detection threshold of $1 \times 10^{-2} cm^{-1}$ for the measurements they actually performed and with the potential to reduce that by at least one order of magnitude with that particular experimental setup [21]. They were also able to coat microspheres with biotin and streptavidin with cavity Q factors around 1.0×10^{-6} and greater. Based on its sensitivity and the ability to coat the microspheres with protein, this technique would seem to show promise for measuring absorption in biological systems.

1.2.3 Incoherent Cavity-Enhanced Spectroscopy

In this somewhat rogue technique, incoherent light from a commercially-available spectrophotometer is sent through a cavity in order to increase the interaction distance and the sensitivity of the measurement over a standard, single-pass spectrophotometer. In this particular experiment, the fifth C-H stretch of benzene was measured with a detection threshold of approximately $1 \times 10^{-6} cm^{-1}$ [22].

Chapter 2

Modeling the Optical Beam for Cavity-Enhanced Spectroscopy

2.1 The Scalar Wave Equation

One way in which the interaction distance can be increased is by sending the light through a Fabry-Perot resonator. How we choose to model optical beams turns out to be an important feature in describing the principles by which cavity-enhanced spectroscopy amplifies the optical signal; therefore, we will spend some time carefully specifying our model. Since optical beams are electro-magnetic waves, Maxwell's Equations provides the necessary guidelines for determining some fundamental characteristics of optical beam propagation. The fundamental property with which we are concerned is the Scalar Wave Equation, in which it is assumed that the wave is traveling in a neutral, homogeneous, isotropic medium such as air or glass or an uncharged liquid A derivation of the scalar wave equation is presented in the first appendix. The scalar wave equation is:

$$[\Delta^2 + k^2](\mathbf{e}\tilde{E}(q)) = 0 \tag{2.1}$$

2.2 Plane Wave Approximation

A simple solution to the wave equation would be a spherical wave propagating from the origin. The amplitude of the beam is assumed to be constant (which would not be

helpful in the physical case):

$$\tilde{E} = \frac{1}{r} E_0 e^{i(\mathbf{k}\cdot\mathbf{r})} \tag{2.2}$$

A solution to (8.12) in the first appendix would be the time-dependent version of our general solution:

$$\tilde{E} = \frac{1}{r} E_0 e^{-i(\omega t + \mathbf{k}\cdot\mathbf{r})} \tag{2.3}$$

If we want to work in rectangular coordinates, we can assume the field is propagating only in the z direction, with the x and y components of k assumed to be zero. We call this the plane wave approximation and it is directly analogous to our spherical wave solution.

$$\tilde{E} = E_0 e^{-i(\omega t + kz)} \tag{2.4}$$

For the first part of our description of the cavity, we will use a plane wave approximation. This model will adequately represent the z propagation of the optical beam for our present purposes. In a later section, we will consider the variation in the phase and scalar amplitude as a function of z propagation and some initial conditions.

2.2.1 Initial Cavity Description

Our cavity contains two highly reflective mirrors separated by a distance, L, as shown in Figure 2.1 . We will assume that the only surfaces on which the beam is reflected or through which it is transmitted are the highly reflective dielectric coatings on the inside surface of the mirrors. The electric field circulating within the cavity, $\tilde{E}_{circ}$, is given by:

$$\tilde{E}_{circ} = it_1 \tilde{E}_{inc} + \tilde{g}_{rt} \tilde{E}_{circ} \tag{2.5}$$

A small fraction of the incident field is transmitted through the first mirror with amplitude transmittivity, t_1. This contributes $it_1\tilde{E}_{inc}$. In order to distinguish between reflectivity and transmittivity, amplitude transmittivity is expressed as 'it' and reflectivity as 'r.' Within the cavity, the circulating field is affected by the round-trip gain factor, $\tilde{g}_{rt}$ and contributes $\tilde{g}_{rt}\tilde{E}_{circ}$. In one round trip within the cavity, the electric field

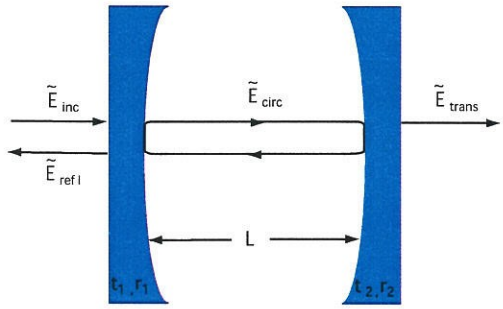

Figure 2.1: Fabry-Perot cavity

will propagate a distance, p, equal to twice the length of the cavity, in what we will arbitrarily call the z direction with propagation constant, k ($k = \frac{2\pi}{\lambda}$). The round-trip gain factor, therefore, will include a phase term that takes into consideration the distance the light propagates within each round-trip, the amplitude reflectivities of each mirror, r_1 and r_2, and an amplitude loss factor, α_0, which will account for intracavity losses due to imperfections in the mirrors, scattering, or absorption. Our expression for the round trip gain factor, therefore, is:

$$\tilde{g}_{rt} = r_1 r_2 e^{-ikp-\alpha_0 p} \tag{2.6}$$

For the purposes of this particular discussion, we will limit our representation of the spatial propagation of the optical beam to the area between the cavity mirrors. Our expression for the round trip gain factor handles this sufficiently; therefore, we will represent the incident field merely as:

$$\tilde{E}_{inc} = E_{inc} e^{-i\omega t} \tag{2.7}$$

The ratio of the circulating field to the incident field provides us with an indication of the buildup that occurs within the cavity under certain conditions:

$$\frac{\tilde{E}_{circ}}{\tilde{E}_{inc}} = \frac{it_1}{1 - \tilde{g}_{rt}} = \frac{it_1}{1 - r_1 r_2 e^{-(ik+\alpha_0)p}} \tag{2.8}$$

Assuming a homogeneous medium (such as air) with dielectric constant (ϵ) and magnetic permeability(μ) of one, we have:

$$\frac{\tilde{E}_{circ}}{\tilde{E}_{inc}} = \frac{it_1}{1 - r_1 r_2 e^{-(i\omega/c+\alpha_0)p}} \tag{2.9}$$

We can see that whenever $\frac{\omega p}{c}$ is a multiple of 2π, $e^{-i\omega p/c}$ becomes one and the circulating intensity reaches a maximum value. This condition is satisfied when the round trip distance within the cavity, p, is a whole-number multiple of the wavelength of light:

$$\frac{\omega p}{c} = \frac{2\pi f p}{c} = \frac{2\pi p}{\lambda} = 2\pi q \Rightarrow p = q\lambda \tag{2.10}$$

When this condition is met, assuming identical mirrors and no internal losses, we have:

$$\frac{\tilde{E}_{circ}}{\tilde{E}_{inc}} = \frac{it_1}{1 - r_1^2} = \frac{i}{t_1} \tag{2.11}$$

Since we can only detect intensity or power with a photodiode, we need an expression for circulating intensity:

$$\frac{I_{circ}}{I_{inc}} = |(\frac{\tilde{E}_{circ}}{\tilde{E}_{inc}})(\frac{\tilde{E}_{circ}}{\tilde{E}_{inc}})^*| = \frac{t_1^2}{r_1^2 r_2^2 e^{-2\alpha_0 p} - 2r_1 r_2 cos(\omega p/c) e^{-\alpha_0 p} + 1} \tag{2.12}$$

As before, when the resonance condition is met, $\omega p/c = q2\pi$. Under these conditions, the cosine term is one and we have:

$$\frac{I_{circ}}{I_{inc}} = \frac{t_1^2}{(1 - e^{(-\alpha_0 p)} r_1 r_2)^2} \tag{2.13}$$

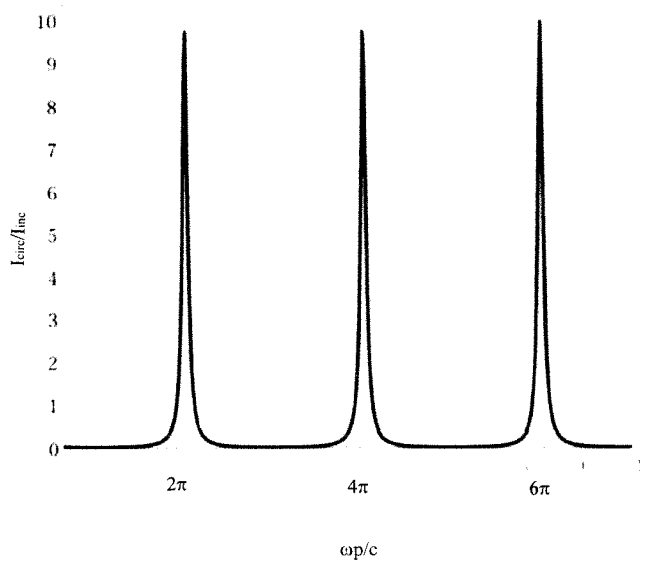

Figure 2.2: Circulating Intensity

Assuming identical mirrors and no internal losses, we have:

$$\frac{I_{circ}}{I_{inc}} = \frac{1}{t_1^2} = \frac{1}{T_1} \tag{2.14}$$

With mirrors that have a power reflectivity of 0.9 (and a corresponding transmittivity of 0.1)$(R_1 + T_1 = 1)$(given the sign conventions we're using), the intra-cavity intensity would be 10 times higher than the incident intensity:

$$\frac{I_{circ}}{I_{inc}} = \frac{1}{0.1} = 10 \tag{2.15}$$

One can also view the resonance condition in terms of frequency, as can be inferred from (2.10):

$$\frac{2\pi f p}{c} = 2\pi q \Rightarrow f = q\frac{c}{2L} \tag{2.16}$$

We can understand this equation as stating that the resonance condition is satisfied

every $c/2L$ in frequency space. (This frequency should not be confused with the frequency of the optical signal, which is often many orders of magnitude higher, since the cavity perimeter is often much larger than the optical wavelength.) The frequency spacing between resonances is commonly referred to as axial spacing, (Δf_{ax}) or free spectral range (Δf_{FSR}). Our discussion of the circulating field and intensity was convenient to illustrate the conditions under which cavity-enhanced light buildup occurs; however, the intensity of the circulating light cannot be directly measured. Only the intensity of the light that is transmitted through (I_{trans}) or reflected from the cavity (I_{refl}) can be detected. The light that is reflected has two components: one that is directly reflected by the first mirror and one that is transmitted through the first mirror from the circulating field. Thus, the total reflected field can be described as:

$$\tilde{E}_{refl} = r_1 \tilde{E}_{inc} + it_1 \tilde{E}_{circ} \frac{\tilde{g}_{rt}(\omega)}{r_1} \tag{2.17}$$

The first component is merely the incident field ($\tilde{E}_{inc}$) times the amplitude reflectivity of the first mirror (r_1). The second component is the circulating field ($\tilde{E}_{circ}$) multiplied by the amplitude transmittivity of the first mirror (it_1) and the round trip gain factor ($\tilde{g}_{rt}(\omega)$). This term must be divided by r_1 since the circulating field is transmitted, not reflected, through the first mirror on the last round trip (the round trip gain factor assumes reflection on both mirrors). After a bit of algebra, we have:

$$\frac{\tilde{E}_{refl}}{\tilde{E}_{inc}} = \frac{r_1 - r_2 e^{-\alpha_0 p - i\omega p/c}}{1 - r_1 r_2 e^{-\alpha_0 p - i\omega p/c}} \tag{2.18}$$

This ratio is also often referred to as the reflection coefficient ($F(\omega)$). On resonance, we have:

$$\frac{\tilde{E}_{refl}}{\tilde{E}_{inc}} = \frac{r_1 - r_2 e^{-\alpha_0 p}}{1 - r_1 r_2 e^{-\alpha_0 p}} \tag{2.19}$$

We can see that, on resonance, the reflected field is at a minimum. If $r_1 = r_2 e^{-\alpha_0 p}$, the reflected field would be zero. When this condition is met, we say that the cavity is impedance-matched. Since we can detect only intensity or power, we need an

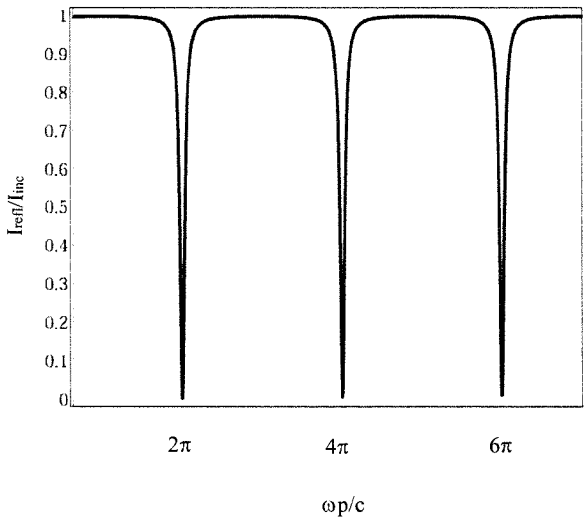

Figure 2.3: Reflected Intensity

expression for the reflected intensity:

$$\frac{I_{refl}}{I_{inc}} = \left(\frac{\tilde{E}_{refl}}{\tilde{E}_{inc}}\right)\left(\frac{\tilde{E}_{refl}}{\tilde{E}_{inc}}\right)^{*} = \left(\frac{r_1 - r_2 e^{-\alpha_0 p - i\omega p/c}}{1 - r_1 r_2 e^{-\alpha_0 p - i\omega p/c}}\right)\left(\frac{r_1 - r_2 e^{-\alpha_0 p + i\omega p/c}}{1 - r_1 r_2 e^{-\alpha_0 p + i\omega p/c}}\right)$$
$$= \frac{r_2^2 e^{-2\alpha_0 p} - 2r_1 r_2 cos(\omega p/c) e^{-\alpha_0 p} + r_1^2}{r_1^2 r_2^2 e^{-2\alpha_0 p} - 2r_1 r_2 cos(\omega p/c) e^{-\alpha_0 p} + 1} \tag{2.20}$$

This denominator is identical to the denominator in our expression for the circulating intensity; however, the numerator is notably different.

As before, on resonance, the cosine term becomes one and we have:

$$\frac{I_{refl}}{I_{inc}} = \left(\frac{r_1 - r_2 e^{-\alpha_0 p}}{1 - r_1 r_2 e^{-\alpha_0 p}}\right)^2 \tag{2.21}$$

Being on resonance causes the reflected intensity to be at a minimum, because the field that is directly reflected from the cavity is 180 degrees out of phase with the cavity field that is transmitted out of the cavity. Assuming no intra-cavity losses and that $r_1 = r_2$,

we have

$$\frac{I_{ref}}{I_{inc}} = \frac{r_1^2(2 - 2cos(\frac{\omega p}{c}))}{(1 + r_1^4 - 2r_1^2 cos(\frac{\omega p}{c}))} \tag{2.22}$$

On resonance, $\omega p/c$ is a multiple of 2π, $cos(\omega p/c)$ is 1, and the numerator is zero. As the laser frequency increases or decreases from resonance by a small amount, $\delta\omega$, the numerator increases to some finite value:

$$\frac{I_{ref}}{I_{inc}} = \frac{r_1^2(2 - 2cos(\frac{(\omega+\delta\omega)p}{c}))}{(1 + r_1^4 - 2r_1^2 cos(\frac{(\omega+\delta\omega)p}{c}))} = \frac{r_1^2(2 - 2cos(\frac{\delta\omega p}{c}))}{(1 + r_1^4 - 2r_1^2 cos(\frac{\delta\omega p}{c}))} \tag{2.23}$$

The cosine of sums simplifies to a term only in $\delta\omega p/c$ because, on resonance, $\omega p/c$ is a whole number multiple of 2π:

$$\begin{aligned} cos\left(\frac{(\omega + \delta\omega)\, p}{c}\right) &= cos\left(\frac{\omega p}{c}\right) cos\left(\frac{\delta\omega p}{c}\right) - sin\left(\frac{\omega p}{c}\right) sin\left(\frac{\delta\omega p}{c}\right) \\ &= cos\,(q2\pi)\, cos\left(\frac{\delta\omega p}{c}\right) - sin\,(q2\pi)\, sin\left(\frac{\delta\omega p}{c}\right) \\ &= cos\left(\frac{\delta\omega p}{c}\right) \end{aligned} \tag{2.24}$$

Since $\frac{\delta\omega p}{c}$ is very small for all frequencies even beyond the full width half maximum, $cos(\frac{\delta\omega p}{c})$ can be approximated by second order MacLaurin series:

$$cos(\frac{\delta\omega p}{c}) = 1 - \frac{1}{2}(\frac{\delta\omega p}{c})^2 + ... \tag{2.25}$$

We can now express $\frac{I_{ref}}{I_{inc}}$ as:

$$\frac{I_{ref}}{I_{inc}} = \frac{r_1^2(\frac{\delta\omega p}{c})^2}{(r_1^2 - 1)^2 + r_1^2(\frac{\delta\omega p}{c})^2} \tag{2.26}$$

Recognizing that c/p is equal the frequency spacing between each TEM_{00} mode, Δf_{FSR}, we have:

$$\frac{I_{ref}}{I_{inc}} = \frac{r_1^2(\frac{\delta\omega}{\Delta f_{FSR}})^2}{(r_1^2 - 1)^2 + r_1^2(\frac{\delta\omega}{\Delta f_{FSR}})^2} \tag{2.27}$$

We can simplify this expression by dividing the numerator and denominator by r_1^2:

$$\frac{I_{ref}}{I_{inc}} = \frac{(\frac{\delta\omega}{\Delta f_{FSR}})^2}{\left(\frac{1-r_1^2}{r_1}\right)^2 + (\frac{\delta\omega}{\Delta f_{FSR}})^2} \tag{2.28}$$

$\frac{1-r_1^2}{r_1}$ is related to the definition of an important cavity parameter called finesse [23].

$$\mathcal{F} \equiv \frac{\pi\sqrt{g_{rt}}}{1-g_{rt}} \approx \frac{\Delta f_{FSR}}{\Delta f_{FWHM}} \tag{2.29}$$

In this case, since we're assuming that the mirror reflectivities are equal and that there are no internal losses, we have:

$$\mathcal{F} = \frac{\pi r_1}{1-r_1^2} \tag{2.30}$$

The Δf_{FWHM} is essentially the width of the resonance peak. More precisely, it is the width of the resonance peak (in frequency space) when $\frac{I_{ref}}{I_{inc}}$ is at half its maximum value. This can be demonstrated by setting $\frac{I_{ref}}{I_{inc}} = \frac{1}{2}$ and solving for $\delta\omega$:

$$\frac{I_{ref}}{I_{inc}} = \frac{(\frac{\delta\omega}{\Delta f_{FSR}})^2}{\left(\frac{\pi}{\mathcal{F}}\right)^2 + (\frac{\delta\omega}{\Delta f_{FSR}})^2} = \frac{1}{2} \tag{2.31}$$

$$\delta\omega = \pm\frac{\pi\Delta f_{FSR}}{\mathcal{F}} \tag{2.32}$$

Since $\omega = 2\pi f$, we have:

$$\delta f = \pm\frac{\Delta f_{FSR}}{2\mathcal{F}} \tag{2.33}$$

By definition, this δf is $\frac{\Delta f_{FWHM}}{2}$. Solving for $\mathcal{F}$, we have:

$$\frac{\Delta f_{FWHM}}{2} = \pm\frac{\Delta f_{FSR}}{2\mathcal{F}} \Rightarrow \mathcal{F} = \frac{\Delta f_{FSR}}{\Delta f_{FWHM}} \tag{2.34}$$

We can simplify our expression for the reflected intensity by multiplying the numerator

and denominator by $\left(\frac{\pi}{\mathcal{F}}\right)^2$:

$$\frac{I_{ref}}{I_{inc}} = \frac{\left(\frac{\delta f}{\frac{\Delta f_{FWHM}}{2}}\right)^2}{1+\left(\frac{\delta f}{\frac{\Delta f_{FWHM}}{2}}\right)^2} = \frac{\left(\frac{\delta f}{\Delta f_{HWHM}}\right)^2}{1+\left(\frac{\delta f}{\Delta f_{HWHM}}\right)^2} \tag{2.35}$$

This expression is convenient for characterizing the dependence of the reflected intensity on relatively small variations in optical frequency from resonance. If we do not assume the mirror reflectivities to be the same and that there are internal losses, our expression for reflected intensity becomes:

$$\frac{I_{ref}}{I_{inc}} = \frac{\left(\frac{\delta f}{\Delta f_{HWHM}}\right)^2 + \left(\frac{r_1 - r_2 e^{-\alpha_0 p}}{1 - r_1 r_2 e^{-\alpha_0 p}}\right)^2}{1+\left(\frac{\delta f}{\Delta f_{HWHM}}\right)^2} \tag{2.36}$$

In both cases, we observe that $\frac{I_{ref}}{I_{inc}}$ increases from its initial value and approaches 1 as δf increases from 0 to well beyond Δf_{HWHM} . These expressions for the reflected intensity are only accurate when $\delta f \ll \Delta f_{FSR}$.

2.3 The Gaussian Model

2.3.1 The Full Scalar Wave Equation

The plane wave approximation is sufficient for a basic understanding of how the transmitted, reflected or intra-cavity electric fields of a Fabry-Perot cavity are affected by certain cavity parameters. Other important parameters require a more sophisticated model for the optical beam. Assuming we have a beam propagating in the z direction, we would like our model to account for the finite transverse (i.e. in 'x' and 'y') amplitude of the beam. Under all conditions in our experiment, we need only consider x and y coordinates that are just off axis from z. We can also safely assume that there are no rapid changes in amplitude in the z direction, since we will not be doing any radical focusing. This assumption allows us to use the paraxial wave equation, in which the

second partial derivative in z can be dropped from the Laplacian. A full derivation is presented in the second appendix. The reader is also referred to a couple of standard textbooks on the subject [24] [23]. In the text, we will merely state the paraxial wave equation and a solution to it. The full scalar wave equation is:

$$[\Delta^2 + k^2]\tilde{E} = [\frac{\partial^2 \tilde{u}}{\partial x^2} + \frac{\partial^2 \tilde{u}}{\partial y^2} + \frac{\partial^2 \tilde{u}}{\partial z^2} - 2ik\frac{\partial \tilde{u}}{\partial z}]e^{-ikz} = 0 \tag{2.37}$$

With the paraxial approximation, we have:

$$\frac{\partial^2 \tilde{u}}{\partial x^2} + \frac{\partial^2 \tilde{u}}{\partial y^2} - 2ik\frac{\partial \tilde{u}}{\partial z} = 0 \tag{2.38}$$

Our solution to the paraxial wave equation is:

$$\tilde{E}(x, y, z) = \frac{1}{R(z)} e^{-ikz} e^{-ik\frac{x^2+y^2}{2R(z)}} \tag{2.39}$$

This makes good physical sense as does the quadratic transverse phase variation. Let's take a look at the expression for the intensity of the beam:

$$I(x, y, z) = |\tilde{E}(x, y, z) * \tilde{E}^*(x, y, z)| = \frac{1}{R(z)^2} = \frac{1}{z^2} \tag{2.40}$$

It makes good physical sense that the intensity of a diverging beam decreases; however, what does not make physical sense is that this solution suggests that the transverse profile of the beam is unbounded.

2.3.2 A Complex Radius of Curvature

We need a real term in the exponent to specify the transverse profile of the beam. If we were to specify the transverse radius of the beam as w(z), we have:

$$\begin{aligned} e^{-ik\frac{x^2+y^2}{2R(z)}} &\Rightarrow e^{-[ik\frac{x^2+y^2}{2R(z)} + \frac{x^2+y^2}{2w^2(z)}]} \\ &= e^{-ik\frac{(x^2+y^2)}{2}(\frac{1}{R(z)} - i\frac{\lambda}{\pi w^2(z)})} \end{aligned} \tag{2.41}$$

The real part of the exponent specifies a Gaussian transverse beam profile. We do not include the propagation constant in this term, since we have assumed that the beam is propagating only in the z direction. From this approach, we can specify a complex radius of curvature, $\tilde{q}(z)$:

$$\frac{1}{\tilde{q}(z)} = \frac{1}{R(z)} - i\frac{\lambda}{\pi w^2(z)} \tag{2.42}$$

We can now rewrite our paraxial solution to the wave equations with the complex radius of curvature:

$$\tilde{E}(x,y,z) = \frac{1}{\tilde{q}(z)} e^{-ikz} e^{-ik\frac{x^2+y^2}{2\tilde{q}(z)}} \tag{2.43}$$

Intuitively, one would conclude that the complex radius of curvature propagates linearly in z; however, it might be helpful to establish this with a bit more mathematical rigor. If we assume a trial solution to the scalar amplitude with the same phase term but with an unspecified amplitude term,

$$\tilde{u}(x,y,z) = A(z) e^{-ik\frac{x^2+y^2}{2\tilde{q}(z)}} \tag{2.44}$$

we can apply the paraxial wave equation to it. After some algebra, we have:

$$-2ik[\frac{1}{\tilde{q}(z)} + \frac{A^{'}(z)}{A(z)}] + \frac{k^2(x^2+y^2)}{\tilde{q}(z)}[q^{'}(z) - 1] = 0 \tag{2.45}$$

Therefore, we conclude that:

$$q^{'}(z) - 1 = 0 \tag{2.46}$$

and

$$\frac{1}{\tilde{q}(z)} + \frac{A^{'}(z)}{A(z)} = 0 \tag{2.47}$$

Thus, we have the following differential equations:

$$\int_{\tilde{q_0}}^{\tilde{q}(z)} d\tilde{q} = \int_{z_0}^{z} dz \Rightarrow \tilde{q}(z) - \tilde{q}_0 = z - z_0 \tag{2.48}$$

This confirms our assumption concerning the linear propagation of the complex radius of curvature in z.

$$\int_{A_0}^{A(z)} \frac{dA(z)}{A(z)} = -\int \frac{dz}{\tilde{q}(z)} = -\int_{z_0}^{z} \frac{dz}{z + (\tilde{q}_0 - z_0)} \tag{2.49}$$

Solving, we get

$$ln(\frac{A(z)}{A_0}) = ln(\frac{\tilde{q}_0}{\tilde{q}(z)}) \Rightarrow \frac{A(z)}{A_0} = \frac{\tilde{q}_0}{\tilde{q}(z)} \tag{2.50}$$

which is consistent with our intuitive conclusion that A(z) is proportional to $\frac{1}{\tilde{q}(z)}$. Rewriting our expression for scalar amplitude, we have:

$$\tilde{u}(x, y, z) = A_0 \frac{\tilde{q}_0}{\tilde{q}} e^{-ik\frac{x^2+y^2}{2\tilde{q}(z)}} \tag{2.51}$$

2.3.3 Hermite-Gaussian Mode Functions

This solution represents the lowest-order Gaussian mode for an optical beam. More general solutions that can specify higher order modes can be derived using roughly the same methodology as before. Once again, this derivation will be relegated to an appendix. In the text, we will merely state a solution which can specify higher order modes. The reader is referred to some general textbooks for an outline of this discussion [23] or an even more in-depth treatment [25] [26]. These equations give rise to what are known as the 'standard' Hermite-Gaussian (i.e. the solution in rectangular coordinates) solutions to the paraxial wave equation. These solutions will be valid for the lowest-order mode and all higher order modes. Our expression for the scalar amplitude in both transverse coordinates is:

$$\tilde{u}_{n,m}(x, y, z) = (\frac{2}{\pi})^{\frac{1}{2}} (\frac{\tilde{q}_0}{2^{n+m} n! m! w_0 \tilde{q}}) (\frac{\tilde{q}^* \tilde{q}_0}{\tilde{q}_0^* \tilde{q}})^{\frac{(n+m)}{2}} H_n(\frac{\sqrt{2}x}{\tilde{p}}) H_m(\frac{\sqrt{2}y}{\tilde{p}}) e^{\frac{-ik(x^2+y^2)}{2\tilde{q}}} \tag{2.52}$$

where 'n' and 'm' are the transverse mode numbers and H_n and H_m are normalized Hermite polynomials, whose form varies with the transverse mode number.

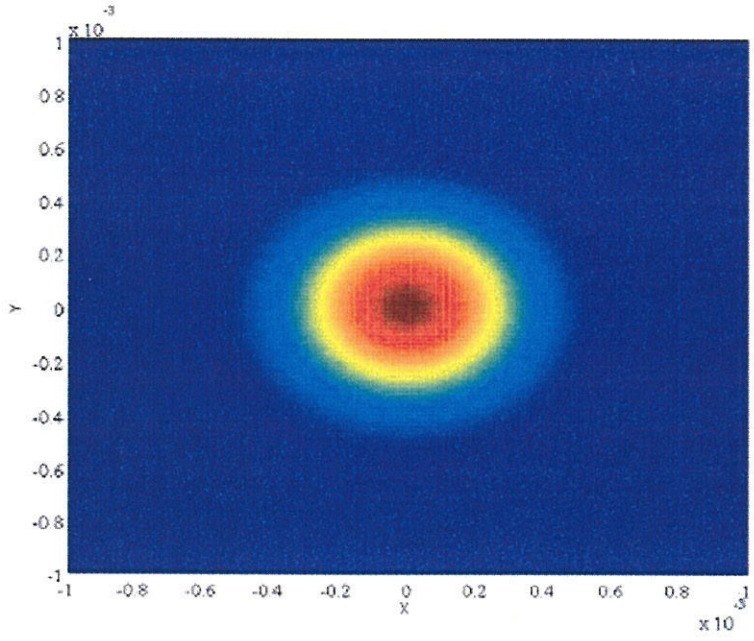

Figure 2.4: Gaussian TEM_{00} Mode

The expression for the TEM_{00} mode is:

$$\tilde{u}_{0,0}(x,y,z) = (\frac{2}{w_0^2\pi})^{\frac{1}{2}} \frac{\tilde{q}_0}{\tilde{q}} e^{\frac{-ik(x^2+y^2)}{2\tilde{q}}} \tag{2.53}$$

This is essentially (2.51) with A_0 as the product of the Gaussian normalization and our scaling factor. The intensity is clearly dependent upon the real radius of curvature, the spot size (w(z)), and is Gaussian in the transverse coordinates, x and y. The shape of this mode along any plane in the z axis is Gaussian in the transverse coordinates (x,y) and is, therefore, roughly circular and is depicted in Figure 2.4. It is this mode that we want to couple to our Fabry-Perot cavity. There is a more commonly used expression for the higher order modes, using a phase angle, defined as:

$$tan\psi(z) = \frac{\Re(1/\tilde{q})}{\Im(1/\tilde{q})} = \frac{\pi w(z)^2}{\lambda R(z)} \tag{2.54}$$

This phase angle characterizes the quantitative relationship between the real and imaginary parts of the complex radius of curvature. What it tells us is how the cur-

vature of the wavefront changes with respect to the beam waist. In the absence of focusing, $\psi(z)$ will asymptotically approach $\pi/2$ as z$\rightarrow \infty$. If a beam is focused, $\psi(z)$ will decrease through zero if the focusing is sharp enough to go below the minimum beam waist, w_0, which, in our case, is defined by certain cavity parameters. This phase shift is called the 'Guoy' phase shift. We can use the following definition to simplify our expressions for the Hermite-Gaussian modes:

$$\frac{i}{\tilde{q}} = \frac{exp(i\psi(z))}{|\tilde{q}|} \Rightarrow exp(i\psi(z)) = \frac{i\sqrt{\tilde{q}\tilde{q}^*}}{\tilde{q}} = i\sqrt{\frac{\tilde{q}^*}{\tilde{q}}} \tag{2.55}$$

For the TEM_{00} mode, we have would like to express $\frac{\tilde{q}_0}{w_0\tilde{q}}$ in terms of $\psi(z)$. From (2.55), we know that:

$$exp[i(\psi(z) - \psi_0(z))] = -\sqrt{\frac{\tilde{q}^*\tilde{q}_0}{\tilde{q}\tilde{q}_0^*}} = \frac{w(z)}{w_0}\frac{\tilde{q}_0}{\tilde{q}} \tag{2.56}$$

We can now express the TEM_{00} mode as:

$$\tilde{u}_{0,0}(x,y,z) = (\frac{2}{\pi})^{\frac{1}{2}}\frac{1}{w(z)}exp[i(\psi(z) - \psi_0) - \frac{ik(x^2+y^2)}{2\tilde{q}}] \tag{2.57}$$

From2.55 and 2.57, we can now express any higher order modes in terms of $\psi(z)$:

$$\tilde{u}_{n,m}(x,y,z) = (\frac{2}{\pi})^{\frac{1}{2}}\frac{1}{n!m!2^{(n+m)}}H_n(\frac{\sqrt{2}x}{\tilde{p}})H_m(\frac{\sqrt{2}y}{\tilde{p}})exp[i(n+m+1)(\psi(z)-\psi_0)-\frac{ik(x^2+y^2)}{2\tilde{q}}] \tag{2.58}$$

The main contributors to the different shapes of each mode of the scalar amplitude function are the Hermite polynomials. The amplitude of the lowest-order mode ($H_0 = 1$) is Gaussian in x and y; its shape, therefore is spherical as in Figure 2.4. For the first order mode in either x or y, $H_{0,1} = 2y; H_{1,0} = 2x$, the amplitude is antisymmetric around the other axis, making the amplitude bi-lobal around that axis. Hermite polynomials follow the recursion relation:

$$H_{n+1} = 2xH_n - 2nH_{n-1} \tag{2.59}$$

This model provides us with an ability explain some of the observed phenomena of a

'real' optical beam that the plane wave approximation cannot account for. Perhaps the most important of these are the Gaussian modes that define certain cavity parameters (they will be discussed in the next chapter). The incoming optical beam must be mode matched to the TEM_{00} mode of the cavity in order to ensure maximum stability of the lock and a simple spatial distribution of the intra-cavity field. In the process of trying to mode match the cavity, it is possible to observe many higher-order modes whose shapes are defined by the Hermite-Gaussian Mode Functions.

Chapter 3

Experimental Setup

Our discussion of the experimental setup used in our experiment will be prefaced by a brief discussion of the experimental methods in which the resonance condition can be met.

3.1 Maintaining Resonance

3.1.1 Scanning

Meeting the resonance condition requires an ability to change the length of the cavity or the frequency of the laser (or both). Depending upon the type of laser being used, it may be convenient to scan the laser far enough in frequency space to observe a resonance peak. Generally, the laser must be able to scan at least one free spectral range to ensure that the resonance condition is met at least once during the scan. Whenever the laser frequency causes a resonance condition to be satisfied during a continuous scan, a resonance peak is observed (assuming the optical beam is properly aligned and coupled). For example, a Ti:Saph laser (Coherent MBR-110) can scan on the order of 40 GHz with the MBR-110E Servo Controller, which corresponds to a cavity length of 3.75 mm. As long as a cavity is longer than 3.75 mm, the MBR-110 can scan far enough to observe a resonance. Scanning the laser has the advantage (over a piezo) of being more or less free of non-linearities during the scan. Being thus free would lead to a more accurate characterization of the free spectral range and resonance peak Δf_{FWHM}.

The simplest way to change the length of the cavity is to place a piezo-electric device between one mirror of the cavity and the outside mounting of the cavity. Applying a voltage to the piezo causes it to change length. Since it is attached to one of the cavity mirrors, when it changes length, the cavity length also changes. Whenever the cavity length is such that the resonance condition is satisfied, a resonance peak will appear (assuming the cavity is properly aligned). Since the precise voltage that is required to meet a resonance condition cannot be precisely predicted or discovered, applying a time-varying, sawtooth voltage to the piezo with sufficient amplitude to ensure that the length of the cavity changed by the distance that corresponds to one free spectral range ($\lambda/2$). Scanning either the laser frequency or the length of the cavity will make it possible to determine the resonance Δf_{FWHM} and the Δf_{FSR}, which, together, define the cavity finesse:

$$\mathcal{F} \equiv \frac{\pi\sqrt{g_{rt}}}{1 - g_{rt}} \approx \frac{\Delta f_{FSR}}{\Delta f_{FWHM}} \tag{3.1}$$

With $\mathcal{F}$, one can solve for $\sqrt{g_{rt}}$, which provides information about the round trip losses within the cavity at the moment at which $\mathcal{F}$ is measured.

3.1.2 Locking the Cavity

Scanning the piezo or the laser can keep the cavity on resonance for a very short time (i.e. the time during the scan when the resonance condition is met). To keep the cavity on resonance, however, requires a more sophisticated technique. Manually adjusting the voltage to the piezo can get the cavity near resonance; however, slow thermal and vibrational noise associated with the cavity and faster frequency noise associated with the laser quickly cause the cavity to drift off of resonance. These types of noise can be suppressed by creating an error signal that indicates the extent to which the cavity has drifted off of resonance. The error signal could then be fed back to the piezo to compensate for the slower thermal and vibrational noise and to an acousto-optic modulator to compensate for the higher-frequency noise.

When the frequency of the laser causes the resonance condition to be satisfied, the

reflected signal from the cavity is zero (assuming no intra-cavity losses) because the promptly- reflected beam destructively interferes with the cavity leak signal.

$$\tilde{E}_{refl} = r_1\tilde{E}_{inc} + it_1\tilde{E}_{circ}\frac{\tilde{g}_{rt}(\omega)}{r_1} \tag{3.2}$$

The promptly-reflected signal is reflected from the outside surface of the first cavity mirror with amplitude reflection coefficient r_1. The cavity leak signal arises when the cavity is close to resonance. Under these circumstances, the intra-cavity field, E_{circ}, is transmitted through the first mirror with amplitude transmission coefficient t_1. The two components of the intra-cavity field are the incident beam that is transmitted through the first mirror and the intra-cavity beam itself whose magnitude and phase are determined by the round trip gain factor, $\tilde{g}_{rt}(\omega)$. The ratio of the reflected field to the incident field is commonly referred to as the reflection coefficent, $(F(\omega))$, and is expressed as:

$$\frac{\tilde{E}_{refl}}{\tilde{E}_{inc}} = F(\omega) = \frac{(r_1 - r_2e^{\frac{i\omega p}{c}-\alpha_0 p})}{(1 - r_1r_2e^{\frac{i\omega p}{c}-\alpha_0 p})} \tag{3.3}$$

The ratio of the reflected to the incident intensity can be expressed as:

$$\frac{I_{refl}}{I_{inc}} = F(\omega)F^*(\omega) = \frac{(r_1^2 + r_2^2e^{-2\alpha_0 p} - 2r_1r_2e^{-\alpha_0 p}cos(\frac{\omega p}{c}))}{(1 + r_1^2r_2^2e^{-2\alpha_0} - 2r_1r_2e^{-\alpha_0 p}cos(\frac{\omega p}{c}))} \tag{3.4}$$

Assuming no intra-cavity losses and that $r_1 = r_2$, we have

$$\frac{I_{ref}}{I_{inc}} = \frac{r_1^2(2 - 2cos(\frac{\omega p}{c}))}{(1 + r_1^4 - 2r_1^2cos(\frac{\omega p}{c}))} \tag{3.5}$$

On resonance, $\omega p/c$ is a multiple of 2π and $cos(\omega p/c)$ is 1 and the numerator is zero. As the laser frequency increases or decreases from resonance by a small amount, $\delta\omega$, the numerator increases to some finite value. From our previous treatment of this (2.35), we know that:

$$\frac{I_{ref}}{I_{inc}} = \frac{r_1^2(2 - 2cos(\frac{(\omega+\delta\omega)p}{c}))}{(1 + r_1^4 - 2r_1^2cos(\frac{(\omega+\delta\omega)p}{c}))} = \frac{(\frac{\delta\omega}{\pi\Delta f_{FWHM}})^2}{1 + (\frac{\delta\omega}{\pi\Delta f_{FWHM}})^2} \tag{3.6}$$

As before (2.36), if we do not assume $r_1 = r_2 e^{\alpha_0 p}$, we have:

$$\frac{I_{ref}}{I_{inc}} = \frac{\left(\frac{\delta f}{\Delta f_{HWHM}}\right)^2 + \left(\frac{r_1 - r_2 e^{-\alpha_0 p}}{1 - r_1 r_2 e^{-\alpha_0 p}}\right)^2}{1 + \left(\frac{\delta f}{\Delta f_{HWHM}}\right)^2} \tag{3.7}$$

Although very small changes in frequency cause a significant change in the reflected intensity, the reflected intensity ends up being the same value for equal increases or decreases in frequency from resonance; therefore, the reflected intensity alone cannot be used to generate an error signal.

3.1.3 Pound-Drever-Hall

An error signal that does change signs depending upon whether the frequency increases or decreases from resonance can be generated in accordance with the method of Pound-Drever-Hall [27]. This method allows us to determine the phase relationship between the promptly reflected field and the intra-cavity field which is transmitted through the first cavity mirror when the cavity is on or near resonance. It requires that the optical beam be phase modulated with an electro-optic modulator (EO). At first order approximation, the field that comes out of the EO contains an unmodulated component, a component at the optical frequency plus the modulation frequency and and a component at the optical frequency minus the modulation frequency. The reflected POWER will contain a term that represents the beat of the unmodulated component with each of the modulated components. When the 'beat' component is mixed down at the modulation frequency and the high frequency components are filtered out, we are left with a term that is proportional to the amount and direction by which the cavity is off of resonance: the error signal. The Pound-Drever-Hall method is central to this experiment; therefore, a detailed treatment of phase modulation and mixing down is warranted. Phase modulating at a modulation frequency, Ω, results in the following:

$$\tilde{E}_{inc} = E_0 e^{i(\omega t + \beta sin(\Omega t))} = E_0 e^{i\omega t} e^{i\beta sin(\Omega t)} \tag{3.8}$$

$$e^{i\beta sin(\Omega t)} = \sum_{p=-\infty}^{p=\infty} J_p(\beta)e^{ip\Omega t} = (..... + J_{-1}(\beta)e^{-i\Omega t} + J_0(\beta) + J_1(\beta)e^{i\Omega t} + ...) \quad (3.9)$$

Using only the zero and first-order terms, we have:

$$\tilde{E}_{inc} = E_0(-J_1(\beta)e^{i(\omega-\Omega)t} + J_0(\beta)e^{i\omega t} + J_1(\beta)e^{i(\omega+\Omega)t}) \quad (3.10)$$

The reflected field can be expressed as the product of the incident field and the frequency-dependent reflection coefficient:

$$\tilde{E}_{refl} = E_0(-J_1(\beta)F(\omega-\Omega)e^{i(\omega-\Omega)t} + J_0(\beta)F(\omega)e^{i\omega t} + J_1(\beta)F(\omega+\Omega)e^{i(\omega+\Omega)t}) \quad (3.11)$$

The reflected intensity is:

$$\begin{aligned} I_{refl} = E_0^2((J_1^2(\beta) \mid F(\omega-\Omega) \mid^2 + & J_0(\beta)^2 \mid F(\omega) \mid^2 + J_1^2(\beta) \mid F(\omega+\Omega) \mid^2 \\ & + 2J_0J_1(\Re(F(\omega)F^*(\omega+\Omega) - F^*(\omega)F(\omega-\Omega))cos(\Omega t)) \\ & + i\Im(F(\omega)F^*(\omega+\Omega) - F^*(\omega)F(\omega-\Omega))sin(\Omega t)) \\ & + J_1^2(F^*(\omega-\Omega)F(\omega+\Omega)e^{-i2\Omega t} + F^*(\omega+\Omega)F(\omega-\Omega)e^{i2\Omega t})) \end{aligned} \quad (3.12)$$

The terms in Ω result from the beat of a sideband with the cavity signal and the terms in 2Ω result from the beat of one sideband with the other. The phase and sign information is contained in the Ω terms. On or very close to resonance, the side bands are promptly reflected from the cavity; therefore, we can safely assume that $F^{(*)}(\omega \pm \Omega) = -1$. This leaves $(F^*(\omega) - F(\omega))$ as the argument for the terms in Ωt. Since $\Re(F(\omega)) = \Re(F^*(\omega))$, the coefficient of the $cos(\Omega t)$ term is zero. Also, since $\Im(F^*(\omega)) = -\Im(F(\omega))$, the coefficient of the term in $sin(\Omega t)$ becomes $-4J_0J_1i\Im(F(\omega))$. A simplified expression for I_{refl}, therefore, becomes:

$$I_{refl} = E_0^2((2J_1^2(\beta) + J_0(\beta)^2 \mid F(\omega) \mid^2 - 4J_0J_1i\Im(F(\omega))sin(\Omega t) + 2J_1^2(cos(2\Omega t))) \quad (3.13)$$

In order to come up with an expression for the error signal, we can rewrite the reflec-

tion coefficient in terms similar to (2.23) with analogous results:

$$F(\omega) = \frac{r_1 - r_2 e^{(\frac{i(\omega+\delta\omega)}{\Delta f_{FSR}} - \alpha_0 p)}}{1 - r_1 r_2 e^{(\frac{i(\omega+\delta\omega)}{\Delta f_{FSR}} - \alpha_0 p)}} = \frac{r_1 - r_2 e^{(i\frac{\delta\omega}{\Delta f_{FSR}} - \alpha_0 p)}}{1 - r_1 r_2 e^{(i\frac{\delta\omega}{\Delta f_{FSR}} - \alpha_0 p)}} \tag{3.14}$$

Since we need only the imaginary part of the reflection coefficient, we need the denominator to be real:

$$\begin{aligned} F(\omega) &= \frac{(r_1 - r_2 e^{-\alpha_0 p} e^{i\frac{\delta\omega}{\Delta f_{FSR}}})}{(1 - r_1 r_2 e^{-\alpha_0 p} e^{i\frac{\delta\omega}{\Delta f_{FSR}}})} \frac{(1 - r_1 r_2 e^{-\alpha_0 p} e^{-i\frac{\delta\omega}{\Delta f_{FSR}}})}{(1 - r_1 r_2 e^{-\alpha_0 p} e^{-i\frac{\delta\omega}{\Delta f_{FSR}}})} \\ &= \frac{r_1 + r_2^2 r_1 e^{-2\alpha_0 p} - r_1^2 r_2 e^{-\alpha_0 p} e^{-i\frac{\delta\omega}{\Delta f_{FSR}}} - r_2 e^{-\alpha_0 p} e^{+i\frac{\delta\omega}{\Delta f_{FSR}}}}{r_1^2 r_2^2 e^{-2\alpha_0 p} - r_1 r_2 e^{-\alpha_0 p}(e^{-i\frac{\delta\omega}{\Delta f_{FSR}}} + e^{+i\frac{\delta\omega}{\Delta f_{FSR}}}) + 1} \end{aligned} \tag{3.15}$$

Using a first-order series approximation for $e^{\pm i\frac{\delta\omega}{\Delta f_{FSR}}}$, we have:

$$F(\omega) = \frac{(r_1 + r_2^2 r_1 e^{-2\alpha_0 p} - r_1^2 r_2 e^{-\alpha_0 p} - r_2 e^{-\alpha_0 p}) - i\frac{\delta\omega}{\Delta f_{FSR}} r_2 e^{-\alpha_0 p}(1 - r_1^2)}{(1 - r_1 r_2 e^{-\alpha_0 p})^2} \tag{3.16}$$

We are interested in the imaginary part of the reflection coefficient. It is:

$$\Im(F(\omega)) = \frac{-i\frac{\delta\omega}{\Delta f_{FSR}} r_2 e^{-\alpha_0 p}(1 - r_1^2)}{(1 - r_1 r_2 e^{-\alpha_0 p})^2} \tag{3.17}$$

Assuming the mirrors have equal reflectivities and that the intra-cavity losses are very low, we can approximate $\Im(F(\omega))$:

$$\Im(F(\omega)) \approx \frac{-i\frac{\delta\omega}{\Delta f_{FSR}} r e^{-\alpha_0 p}}{1 - r^2 e^{-\alpha_0 p}} = -i\frac{\delta\omega}{\Delta f_{FSR}}\frac{\mathcal{F}}{\pi} = -i\frac{\delta\omega}{\pi \Delta f_{FWHM}} \tag{3.18}$$

$$\Im(F(\omega)) = -i\frac{\delta\omega}{\pi \Delta f_{FWHM}} \tag{3.19}$$

When these assumptions are not warranted, as in our experiment, we express $\Im(F(\omega))$ as:

$$\Im(F(\omega)) = -i\frac{\delta\omega}{\pi \Delta f_{FWHM}} \left(\frac{e^{-\alpha_0 p/2}(1 - r_1^2)}{1 - r_1 r_2 e^{-\alpha_0 p}} \right) \tag{3.20}$$

Our expression for I_{refl} is now:

$$I_{refl} = E_0^2(2J_1^2(\beta) + J_0(\beta)^2 \mid F(\omega) \mid^2 -4J_0J_1\frac{\delta\omega}{\pi\Delta f_{FWHM}}\left(\frac{e^{-\alpha_0 p/2}(1-r_1^2)}{1-r_1r_2e^{-\alpha_0 p}}\right)sin(\Omega t) + 2J_1^2(cos(2\Omega t))) \tag{3.21}$$

The phase of the side bands is representative of the phase of the promptly reflected portion of the reflected field. When a side band beats with the reflected cavity signal, the resulting term in Ω provides an indication of the extent to which the cavity is off resonance. In order to generate the error signal, the voltage out of the high frequency photodetector that detects reflected signal must first be demodulated by electronically mixing it with the voltage from the voltage-controlled oscillator that drives the EO (the frequency of the EO VCO voltage is the f_{EO}). This signal is commonly referred to as the local oscillator (LO). Electronic mixing is akin to multiplying the signals. Our mixed-down signal is:

$$LO = V_0 sin(\Omega t + \theta(\Omega, t)) \tag{3.22}$$

Where $\Theta(\Omega, t)$ is a time- and frequency-dependent phase difference between the EO LO and the optical signal. Therefore, the demodulated signal is:

$$\begin{aligned} LO \times I_{refl} = {} & V_0E_0^2(2J_1^2(\beta)sin(\Omega t + \theta(\Omega,t)) + J_0(\beta)^2 \mid F(\omega) \mid^2 sin(\Omega t + \theta(\Omega,t)) \\ & - 4J_0J_1\frac{\delta\omega}{\pi\Delta f_{FWHM}}\left(\frac{e^{-\alpha_0 p/2}(1-r_1^2)}{1-r_1r_2e^{-\alpha_0 p}}\right)sin(\Omega t)sin(\Omega t + \theta(\Omega,t)) \\ & + 2J_1^2 sin(\Omega t + \theta(\Omega,t))(cos(2\Omega t))) \end{aligned} \tag{3.23}$$

All of these terms are in Ωt and can be filtered out except the term in $\delta\omega$, which has a dc component:

$$\begin{aligned} sin\,(\Omega t)\,sin\,(\Omega t + \theta\,(\Omega, t)) = {} & \frac{1}{2}\,(1 - cos\,(\Omega t))\,cos\,(\theta\,(\Omega, t)) \\ & + sin\,(\Omega t)\,cos\,(\Omega t)\,sin\,(\theta\,(\Omega, t)) \end{aligned} \tag{3.24}$$

After low-pass filtering the terms in Ω, we are only left with $\frac{1}{2}cos\left(\theta\left(\Omega,t\right)\right)$. Therefore, our error signal is:

$$E = -2E_0^2 V_0 J_1(\beta) J_0(\beta) \frac{\delta\omega}{\pi \Delta f_{FWHM}} \left(\frac{e^{-\alpha_0 p/2}(1-r_1^2)}{1 - r_1 r_2 e^{-\alpha_0 p}} \right) cos(\theta(\Omega, t)) \tag{3.25}$$

We now have an error signal that is proportional to the amount by and direction in which the laser frequency differs from resonance. The error signal is negative when the laser frequency is above a resonance frequency and positive when below resonance. Therefore, it can be fed back to the piezo and to an acousto-optic modulator through a servo to lock the laser to the cavity linewidth, ensuring that the resonance condition is maintained continuously. Since the phase factor can cause the sign and magnitude of the error signal to change, it must be appropriately managed. There are a number of things that can be done to keep it near 0, including adjusting Ω and the cable length between the LO source and the EO and mixer. This scenario assumes that the EO phase modulates perfectly; however, this is not the case. Despite our best attempts at aligning the EO, there ends up being some residual amplitude modulation at the $f_{EO}\left(\Omega\right)$ due to polarization modulation. A better model for the effect of the EO on the incident field would be:

$$\tilde{E}_{inc} = E_0 e^{i(\omega t + \beta sin(\Omega t))}(1 + \epsilon sin(\Omega t)) \tag{3.26}$$

where ϵ indicates the extent of amplitude modulation. Our final expression for the error signal with amplitude modulation is

$$\begin{aligned} E = &-2E_0^2 V_0 J_1(\beta) J_0(\beta) \frac{\delta\omega}{\pi \Delta f_{FWHM}} \left(\frac{e^{-\alpha_0 p/2}(1-r_1^2)}{1 - r_1 r_2 e^{-\alpha_0 p}} \right) cos(\theta(\Omega, t))(1+\epsilon^2) \\ &+ \epsilon E_0^2 V_0 \left(\left(2J_1^2(\beta) + J_0(\beta)^2 \left(\frac{\left(\frac{\delta f}{\Delta f_{HWHM}}\right)^2 + \left(\frac{r_1 - r_2 e^{-\alpha_0 p}}{1 - r_1 r_2 e^{-\alpha_0 p}}\right)^2}{1 + \left(\frac{\delta f}{\Delta f_{HWHM}}\right)^2} \right) \right) \right) \end{aligned} \tag{3.27}$$

The only important result here is that the error signal has a dc component due to residual amplitude modulation. We can see that the dc offset is affected by laser power,

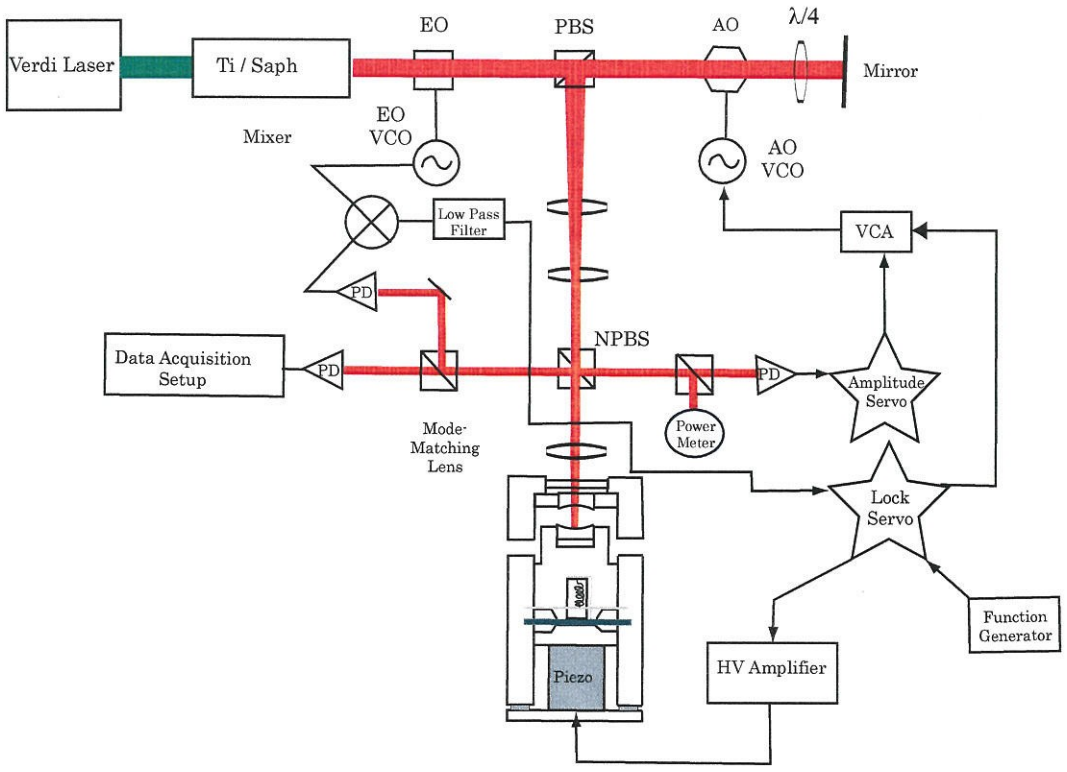

Figure 3.1: Full Experimental Setup

modulation depth, the extent of amplitude modulation, proximity to resonance, and cavity parameters such as mirror reflectivity, intra-cavity losses, etc.... This dc offset must be appropriately managed when trying to lock the cavity, as discussed in the section on servo design.

3.2 Overall Setup

A schematic of the major electronic and optical components in our experiment is shown in Figure 3.1. The most intuitive way to begin this discussion is with a description of the path of the optical beam from the Verdi to the photodetectors. An 8.0 W Coherent Verdi laser (532 nm) pumps the tunable Coherent MBR-110 Titanium Sapphire laser (Ti:saph). With our optics set, the Ti:saph is tunable between 768 nm and approximately 860 nm. The Ti:Saph laser locks to a reference cavity via a servo-lock. The frequency of the Ti:saph can also be scanned and locked using an etalon. Locking with

the etalon is the only way to prevent the laser from staying single mode (which is a requirement for cavity-enhanced spectroscopy). After leaving the Ti:saph, the optical beam goes through a Faraday rotator to prevent back reflections from being fed back into the laser. The beam passes through a sequence of lenses and polarizing beam splitters before going to the EO. After passing through the EO, the phase-modulated beam makes two passes through the AO before going through a sequence of lenses which are used to mode-match the beam to the TEM_{00} mode defined by the cavity (the details of optical alignment will be discussed in a later chapter). A portion of the beam out of the AO is diverted to a photodetector that is the input to an amplitude servo, that helps to suppress intensity noise on the laser (either from the Ti:saph or added by the EO and/or AO). The beam finally passes through the mode-matching lens and into the cavity.

The beam is then reflected from the cavity and directed through a non-polarizing beam splitter either to a power meter or to two different photodetectors (PD): one for observing the DC power and one for detecting the higher-frequency components, which contain the phase-modulated signal that will generate the error signal. The high frequency components are detected with an AC-coupled APD from Menlo Systems (APD-210) which can detect signals from 1.0 MHz to 1.0 GHz. The voltage from this photodector is mixed down (with a Minicircuits mixer) with the the output of the voltage-controlled oscillator that ultimately drives the EO (after going through an RF amplifier). From 3.23, we know that the mixed-down signal will contain a low frequency (nearly DC) component and components at multiples of the modulation frequency. The low frequency/DC component is what contains the phase information that constitutes the error signal. It must be separated from the high frequency signal via a low pass filter (which rejects signals above a specified frequency). The error signal will be the output of the low pass filter. On resonance the phases of the promptly reflected field and the intra-cavity field are exactly 180 degrees out of phase and will perfectly destructively interfere. Slightly above resonance, the frequency of the laser will be a bit

higher than the resonance condition requires which will generate a positive phase difference between the intra-cavity field and the promptly reflected field. Slightly below resonance, the frequency of the laser will be a bit lower than the resonance condition requires, which will generate a negative phase difference between the two fields. Thus, the sign of the phase of the reflected signal will tell us whether the laser frequency is above or below the resonance frequency. This error signal will be used to control the laser frequency via an acousto-optic modulator (AO) and a piezo-electric device (piezo) after being properly conditioned by a servo (which will be discussed in detail in the next chapter).

The piezo is used to compensate for slow variations in frequency by changing the length of the cavity. It must be driven at frequencies below its resonance frequency (which is 138 kHz for the piezo used in this experiment (Thor Labs AE0505D08)) and below lower frequency structural resonances of the piezo due to its placement in the cavity. The piezo is generally only useful for compensating for low frequency noise. An AO can compensate for higher frequency noise by changing the frequency of the optical beam. The AO contains a crystal into which an RF-driven transducer sends acoustic waves. These acoustic waves set up a standing wave in the crystal which causes a Bragg diffraction of the input beam and a corresponding change in the frequency of the laser light. The frequency shift in the first-order beam, for example, is the frequency of the acoustic wave, f_{EO}, which is dictated by the frequency of the RF signal that causes the standing wave in the crystal. The frequency of the RF signal is controlled by a voltage-controlled oscillator (VCO) and is roughly proportional to the input voltage to the VCO. The limiting factor in the ability of an AO to compensate for frequency fluctuations in a laser is the amount of time it takes to change the frequency of the acoustic wave in the AO crystal. The Brimrose TEM-110-25-850 that we are using can compensate for fluctuations up to 100 kHz. The DC lock signal is monitored through a DC-coupled Hammamatsu C5460-01 100 kHz bandwidth APD. The Hammamatsu detector is designed for low-frequency, low-power signals. Its band-

width corresponds to the maximum bandwidth of our optical setup (limited by the AO response). Data is acquired with a Compuscope 14200 data acquisition card with 128 Mbytes of on-board memory. This card has 14 bit resolution and can acquire at up to 100 Msamples/sec on single channel. The data acquisition scheme was controlled by a MATLAB 'm file', written for this purpose.

3.3 Cavity

3.3.1 Design Considerations

The construction of the present cavity was based on lessons learned from the measurements made in the first-generation cavity, which was 1.0 cm in length, had commercially-available mirrors with an advertised finesse of approximately 11,000, and was designed to hold organic solvent in the chamber between the mirrors; however, solvent often slowly leaked out. Furthermore, the cavity required removal, disassembly, and cleaning after each use, which was particularly menacing, given the difficulty associated with the optical alignment of the cavity. The five major design considerations for this cavity are to improve the quality of mirrors, to make the cavity shorter, to ensure that the cavity is solvent tight, to make it possible to introduce solvent into the cavity without disturbing the optical alignment, and to make it possible to control the length of the cavity with a piezo-electric device so that the cavity can be locked on resonance.

3.3.2 Mechanical Features

We wanted to include the highest quality mirrors we could find in order to maximize the cavity-enhancement. We had mirrors custom made by Research Electro-Optics in Boulder, Colorado. Our coating run was intended to produce mirrors with $\mathcal{L} < 20ppm$ at a center wavelength of 770 nm and a radius of curvature of 5 cm (coating run L6-170/L3-532). These mirrors are roughly ten times better than the previous mirrors. We wanted a shorter cavity to provide better temporal resolution (since the average photon spends less time in the cavity) and to cause fewer solvent-mediated losses. The

cavity length was designed to be adjustable from hundreds of microns to approximately 5 mm. The mirrors can be adjusted in their mounts by loosening the two screws in each mount and adjusting the position of the mirror within the mount. This cavity has a solvent-tight glass window ('W') on the front of the cavity and includes a sheet of Kalrez ('K') at the back of the cavity to ensure that no solvent gets into the chamber that holds the piezo. The cavity is constructed of stainless steel rings which were designed to be used in vacuum systems. The vacuum seals on the rings and within the cavity are established by ensuring that the 'knife edge' of the stainless steel rings makes strong contact with the malleable copper rings on adjacent pieces. Careful assembly of the cavity and occasional replacement of copper rings or knife-edge containing pieces are required to keep the cavity solvent tight. The fourth design criterion was to be able to add and remove solvent with the least amount of disturbance to the cavity. This cavity has fittings above and below the solvent chamber in the cavity. Stainless steel tubing is attached at each fitting and, attached to the steel tubing, are isolation valves to which organic solvent safe tubing is attached. The piece that directly contacts the piezo is attached to the brass piece ('A2') that holds one of the cavity mirrors via a spring ('S') so that piezo movement is directly and smoothly coupled to that cavity mirror. Each time the cavity is assembled, the eight screws that hold together all of the rings that make up the cavity must be tightened carefully to ensure adequate that the piezo is properly and evenly compressed between the two surrounding pieces. Turning each nut 2.5 full turns past hand tight turned out to be adequate to ensure that that the piezo made sufficient contact with piece A2 to ensure smooth movement of the second cavity mirror in response to an applied to voltage to the piezo.

3.3.3 Solvent System

The main goals of the cavity solvent system are to ensure that the cavity is filled uniformly, the solvent has minimal exposure to air, and there is minimal vibrational disturbance to the cavity. Filling the cavity from the top proved inadequate for preventing bubbles. Suctioning the solvent through the cavity from the bottom valve

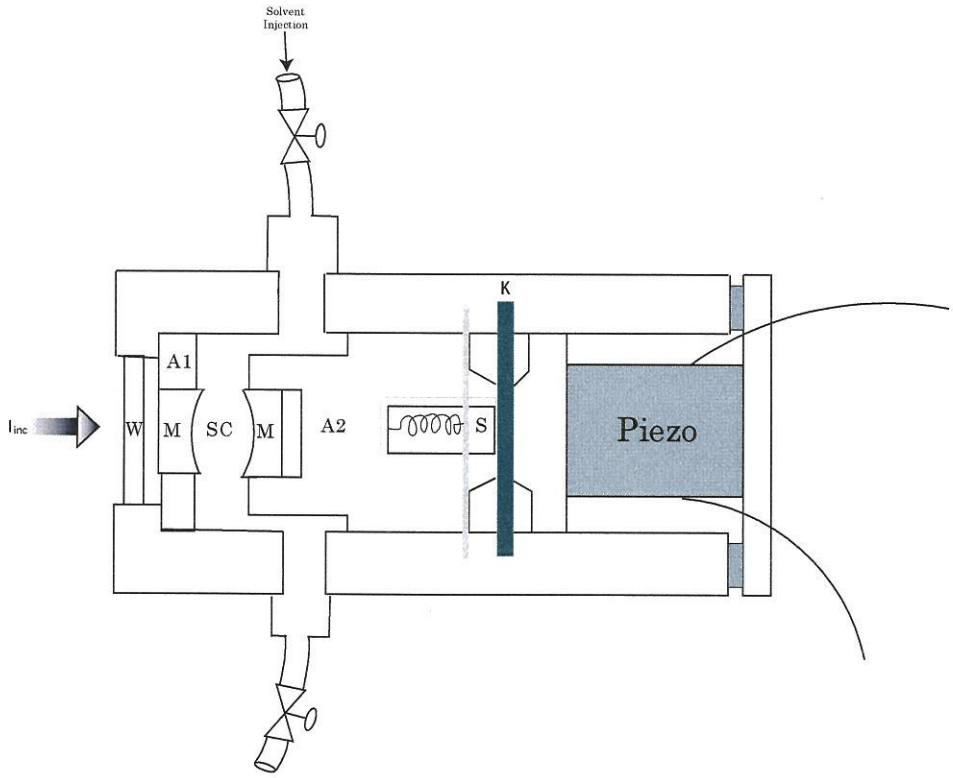

Figure 3.2: Cavity Schematic

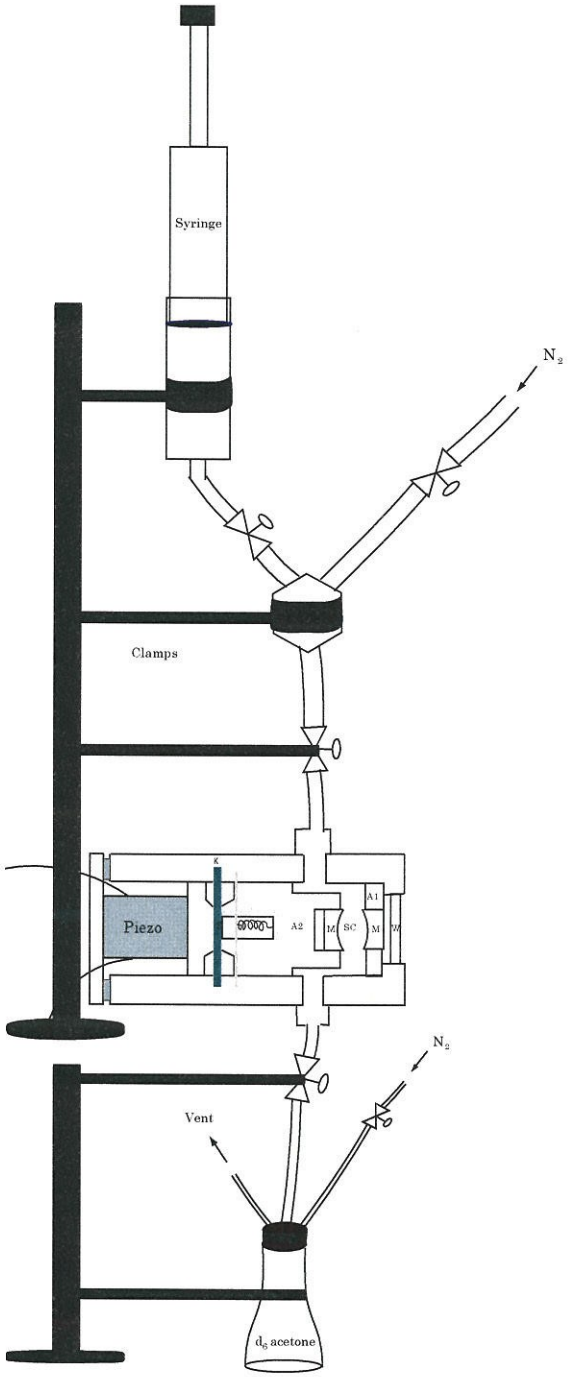

Figure 3.3: Solvent System

using a syringe-like device and then pushing some solvent back into the cavity with the syringe proved to be the most reliable means of filling the cavity with bubble-free solvent. Clamping all elements of the solvent system was the best way to minimize vibrational transients to the cavity. The cavity is very sensitive to vibrational and rotational motion initiated by even touching the tubing. In fact, even gently pulling on the tubing was sufficient to rotate the cavity enough to require optical realignment. Our solvent of choice (d_6-acetone) is optically-transparent at 780 nm; however, the longer it is exposed to air, the less transparent it becomes. Therefore, it is very important to minimize the exposure of our solvent to air. Purging the cavity with dry nitrogen before filling with acetone and keeping the acetone under nitrogen (as shown in Figure 3.3) immediately upon opening, adequately minimizes the exposure of acetone to air.

Chapter 4

Optical Considerations

Optical alignment and Gaussian mode matching are both crucial to cavity-enhanced spectroscopy. The optical beam must be aligned and its waist managed as it passes through each optical element in our experimental setup and as it enters the cavity. In addition, the incoming beam must be mode-matched to the cavity.

4.1 Gaussian Mode Matching

4.1.1 Practical Features of Gaussian Beams

As was mentioned (2.3.2), the complex radius of curvature of Gaussian beams propagates linearly in z:

$$\tilde{q}(z) = \tilde{q}_0 + z \tag{4.1}$$

$\tilde{q}_0$ is also represented as z_R and called the Rayleigh range, which is defined as the distance it takes for the beam waist, w_0, to increase by $\sqrt{2}$. This can be demonstrated by substituting z_R into 4.1 and solving for the the beam waist. The propagation rule for $\tilde{q}(z)$ is commonly written in terms of z_R. Using the propagation law and the definitions of z_R and $\frac{1}{\tilde{q}}$, the spot size $w(z)$, the real radius of curvature (R(z)), and the phase angle $\psi(z)$ can be rewritten in terms of z and z_R:

$$w(z) = w_0^2(1 + \frac{z_R^2}{z^2}) \tag{4.2}$$

$$R(z) = z + \frac{z_R^2}{z} \tag{4.3}$$

$$tan\psi(z) = \frac{z}{z_R} \tag{4.4}$$

These equations are useful for characterizing the mode that is defined by a Fabry-Perot cavity.

4.1.2 Mode Matching a Gaussian Beam to a Fabry-Perot Cavity

Since the radius of curvature and beam waist are characterized by $\tilde{q}(z)$ and since the length and radius of curvature of the mirrors of a Fabry-Perot cavity define a w_0 within the cavity and a w at the reflective surface of each mirror, the beam $\tilde{q}(z)$ must be matched with the w and R at the appropriate cavity mirror for optimal use of the optical power of the beam and for the stability of the intra-cavity mode. Given the length of a cavity, L, and the radius of curvature of its mirrors, R, the minimum beam waist, w_0 and the beam waist at each mirror, w, can be specified in terms of L and R. The complex radius of curvature of each mirror is:

$$\tilde{q}(z) = \tilde{q}_0 + z = i\frac{\pi w_0^2}{\lambda} + \frac{L}{2} \tag{4.5}$$

We also know that $\frac{1}{\tilde{q}}$ is $(\frac{1}{R} - \frac{i\lambda}{\pi w_0^2})$; therefore, we can express solve for w_0:

$$\frac{1}{R} = \frac{2L\lambda^2}{L^2\lambda^2 + 4\pi w_0^4} \tag{4.6}$$

$$w_0^2 = \frac{\lambda L}{2\pi}\sqrt{\frac{2R}{L} - 1} \tag{4.7}$$

With a similar strategy, we can solve for w and z_R:

$$w^2(z) = \frac{\lambda L}{\pi}\sqrt{\frac{\frac{R}{L}}{2 - \frac{L}{R}}} \tag{4.8}$$

$$z_R = \frac{L}{2}\sqrt{\frac{2R}{L} + 1} \tag{4.9}$$

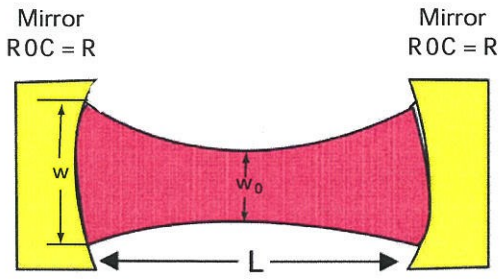

Figure 4.1: Gaussian Mode Defined by Fabry-Perot Cavity

For our cavity whose length, L, is 1.75 mm and whose mirrors have a radius of curvature of 5.00 cm, using these equations, we can determine w_0 to be 40.4 μm and w(z) to be 40.7 μm with an optical beam of wavelength 780 nm. When $R \gg L$ (as in our case), we say that the cavity is near planar. In this situation, our expressions for the beam waist and Rayleigh Range can be further simplified:

$$w_0^2 = \frac{\lambda L}{2\pi}\sqrt{\frac{2R}{L} - 1} \approx \frac{\lambda L}{2\pi}\sqrt{\frac{2R}{L}} \tag{4.10}$$

$$w^2(z) = \frac{\lambda L}{\pi}\sqrt{\frac{\frac{R}{L}}{2 - \frac{L}{R}}} \approx \frac{\lambda L}{2\pi}\sqrt{\frac{2R}{L}} \tag{4.11}$$

$$z_R = \frac{L}{2}\sqrt{\frac{2R}{L} + 1} \approx \frac{L}{2}\sqrt{\frac{2R}{L}} \tag{4.12}$$

The usefulness of these equations is that w_0 and w can be expressed solely in terms of cavity parameters and the optical wavelength. The optical beam must have a radius of curvature, R, of 5 cm at the inner surface of the first mirror and must have a waist, w, of 48.6 μm in order to mode match the beam to this particular cavity. This mode matching can be accomplished reasonably easily by using ABCD matrices and working backwards from these calculated cavity parameters.

4.1.3 ABCD Matrices for Gaussian Beams

The propagation laws for Gaussian beams in free space, through lenses and through dielectric media, can be conveniently applied and calculated using ABCD matrices.

The ABCD matrix has the general form:

$$\begin{bmatrix} A & B \\ C & D \end{bmatrix} \tag{4.13}$$

They can be used to transform rays or Gaussian beams. The general formula for applying ABCD matrices to Gaussian beams is:

$$\tilde{q}_2 = \frac{A\tilde{q}_1 + B}{C\tilde{q}_1 + D} \tag{4.14}$$

where $\tilde{q}_2$ is the complex radius of curvature after the transformation. The matrices for common transformations are:

Free space:

$$\begin{bmatrix} 1 & L \\ 0 & 1 \end{bmatrix} \tag{4.15}$$

Thin lens ($f > 0$ for converging lenses):

$$\begin{bmatrix} 1 & 0 \\ -\frac{1}{f} & 1 \end{bmatrix} \tag{4.16}$$

Interface between regions with different indices of refraction:

$$\begin{bmatrix} 1 & 0 \\ 0 & \frac{n_1}{n_2} \end{bmatrix} \tag{4.17}$$

Curved dielectric at normal incidence ($R > 0$ for concave surfaces):

$$\begin{bmatrix} 1 & L \\ \frac{n_2 - n_1}{Rn_2} & \frac{n_1}{n_2} \end{bmatrix} \tag{4.18}$$

A focusing lens will reduce the radius of curvature of the beam and will cause the beam waist to decrease to a minimum at the focal length of the lens:

$$\tilde{q}_2 = \frac{\tilde{q}_1}{-\frac{\tilde{q}_1}{f}+1} \Rightarrow \frac{1}{\tilde{q}_2} = -\frac{1}{f} + \frac{1}{\tilde{q}_1} = (-\frac{1}{f} + \frac{1}{R_1}) - i\frac{\lambda}{\pi w_1^2} \tag{4.19}$$

A very convenient feature of ABCD matrices is that the transformation of an optical beam by a series of optical elements can be easily computed by multiplying the transformation matrices and applying the effective matrix to complex radius of curvature at the first element. Given a set of transformation matrices from 1 to n, the effective matrix, M_{eff}, is:

$$M_{eff} = \begin{bmatrix} A_{eff} & B_{eff} \\ C_{eff} & D_{eff} \end{bmatrix} = \prod M_n * M_{n-1} * ....M_1 \tag{4.20}$$

It is imperative that the effective matrix be calculated as the product in sequence from the last matrix to the first. This kind of matrix multiplication can be done very easily in a program such as MATLAB.

Given the length of our cavity, and the radius of curvature of the cavity mirrors and the structural elements of the cavity between the first mirror and the outside of the cavity, ABCD matrices can be used to determine the beam waist, w, and the radius of curvature, R, of the beam at the outside edge of the glass window ('W' in Figure 3.2). This beam can then be propagated out any convenient distance from there. A graph of these values from the edge of the outside window ('W') for 30 cm out in the 'z' direction with and without acetone in the cavity are shown in Figure 4.2. Mode-matching the cavity requires that the incoming beam have the beam waist and radius of curvature at whatever distance is chosen. Although the indices of refraction for air and acetone are different, the spot sizes and radii of curvature do not differ much; nevertheless, adding acetone to the cavity requires a moderate amount of realignment.

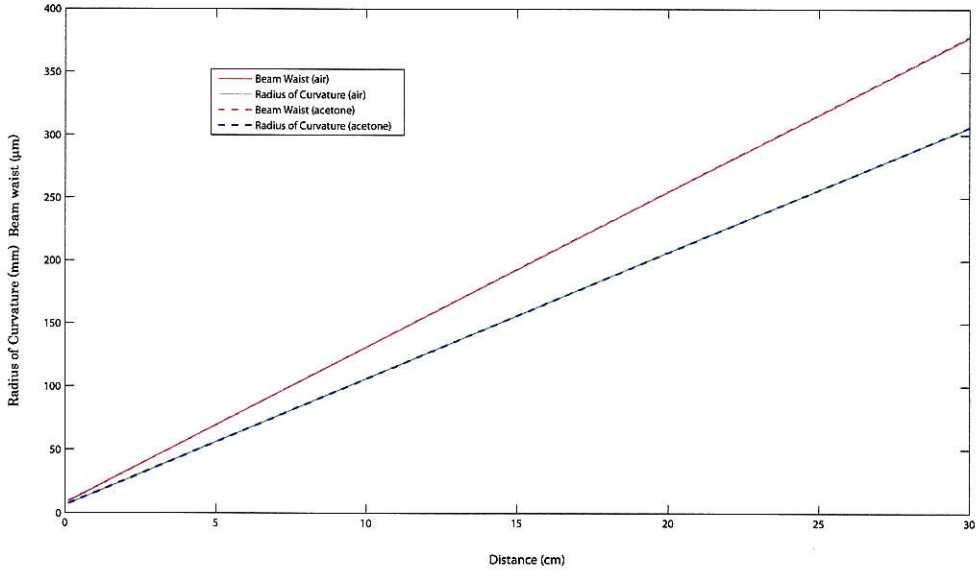

Figure 4.2: Mode Matching

4.1.4 Measuring the Beam Waist

It is necessary to measure the beam waist of the incoming beam in order to mode-match that beam to the cavity. The easiest way to measure the beam waist is to attach a straight razor to a micrometer and position the blade just outside the beam waist in front of a power meter. The micrometer will then be moved until the optical power is reduced by the amount that corresponds to one side of the beam waist and the position of the micrometer will be recorded. It will then be adjusted until the power is reduced by the amount that corresponds to the other side of the beam waist. The power transmission at either side of the beam waist can be determined by integrating the normalized beam intensity in rectangular coordinates, using $\pm$w as the limits of integration in the x direction (assuming that the razor blade is perfectly vertical and moves only in the x direction). The power transmission at the near beam waist would

be:

$$T_{(-w)} = \frac{2}{\pi w^2} \int_{-\infty}^{\infty} \int_{-\infty}^{-w} e^{\frac{-2(x^2+y^2)}{w^2}} dydx \tag{4.21}$$

The power transmission at the far beam waist would be:

$$T_{(+w)} = \frac{2}{\pi w^2} \int_{-\infty}^{\infty} \int_{-\infty}^{+w} e^{\frac{-2(x^2+y^2)}{w^2}} dydx \tag{4.22}$$

These integrals can be solved numerically using Mathematica. $T_{(-w)}$ is 0.977 and $T_{(+w)}$ is 0.023.

4.2 Transverse Mode Frequencies

As was implied in our discussion of the Hermite-Gaussian Mode functions, each transverse mode occurs at a different frequency. Each mode has a different frequency because of the mode-dependent phase shift discussed in the section on Hermite-Gaussian Mode functions. The Guoy phase shift in one length of the cavity is measured from the minimum beam waist to each mirror. On the assumption that each mirror has the same radius of curvature, the minimum beam waist is in the center of the cavity and and the phase shift from the center to each mirror is equal in magnitude but opposite in sign. Although there are many ways to express this phase shift, the most intuitive remains 2.54:

$$tan\psi(z) = \frac{\pi w^2}{\lambda R} \tag{4.23}$$

In one cavity length, the overall phase shift (including the propagation factor (kL)) is:

$$\phi(z_2 - z_1) = kL - (n + m + 1)2tan^{-1}(\frac{\pi w^2}{\lambda R}) \tag{4.24}$$

The resonance condition that applied to plane waves still applies here, namely, that the round-trip phase shift must be an integer multiple of 2π or that the one-way phase shift be an integer multiple of π. Using our definition of the overall phase shift in one

length of the cavity is:

$$kL - (n+m+1)[2tan^{-1}(\frac{\pi w^2}{\lambda R})] = q\pi \tag{4.25}$$

We can express the propagation factor as ω/c and solve for ω:

$$\omega = \left(q + (n+m+1) \left[\frac{2tan^{-1}\left(\frac{\pi w^2}{\lambda R}\right)}{\pi} \right] \right) \frac{c\pi}{L} \tag{4.26}$$

This equation can be simplified by expressing w^2 in terms of R, L, and λ as in 4.8:

$$\omega = \left(q + (n+m+1) \left[\frac{2tan^{-1}\left(\frac{1}{2\frac{R}{L}-1}\right)}{\pi} \right] \right) \frac{c\pi}{L} \tag{4.27}$$

This equation tells us the relative frequency of the higher order Gaussian modes with respect to the TEM_{00} mode. In the near planar case (i.e. $R \gg L$), the Guoy phase shift is very small (for our cavity with $R = 5.0$ cm and $L = 3.5$ mm, the Guoy phase shift is only about 21.5 degrees. This causes each sequential higher transverse mode to be only slightly higher than its associated TEM_{00} mode. This fact is observed when aligning the cavity and knowing that the higher order modes are higher in frequency than the associated TEM_{00} mode is very helpful.

4.3 Optical Alignment

Each element in our optical setup is sensitive to the size of the beam waist (w) and the angle ($\dot{x}$ and $\dot{y}$) and position (x, y) at which the beam passes through the element. The angle and position of the beam can be adjusted with any pair of mirrors. The beam waist can be managed with the appropriate use of lenses, as will be discussed in the following section. Our EO requires that the beam waist be less than 2.0 mm (the size of the aperture) and that it pass as close to the center of the aperture as possible. Misalignments or incorrect polarization can result in frequency or amplitude modulation

on the emergent beam. The good way to maximize the correct polarization through the EO is to include a series of polarizing beam splitters before the EO. Residual frequency modulation can be minimized by setting up a photodiode at the output of the EO and sending the photodiode output to a spectrum analyzer and steering the beam until the peak at the f_{EO} is minimized. The alignment of the AO is particularly challenging. In order to maximize its response time, the beam should be positioned as close as possible to the transducer on the bottom of the AO. The angle at which the beam passes through that AO must be adjusted until the +1 beam (the beam whose frequency has been increased by $1 * f_{AO}$) out of the AO is maximized. This process is more or less trial and error. The +1 beam should be the first one above the non-displaced beam, which can be identified by properly removing the RF signal from the AO. The only beam that is transmitted through an unpowered AO is the 'non-displaced' beam. The next step is to place an iris just before the mirror at the output of the AO such that only the +1 beam hits the mirror. The mirror is then adjusted until the +1 beam hits the AO crystal at exactly the same position that the incoming beam passed through it. It is crucial to have +1 beam overlap the incoming beam to the maximum possible extent. To this end, the appropriate selection of focusing lenses on either side of the AO is very helpful. This second pass beam is directed back through a polarizing beam splitter to a set of mirrors. A quarter wave plate is placed between the mirror and the AO to rotate the polarization of the +1 beam such that it gets reflected by the polarizing beam splitter on the other side of the AO (the transmitted beam heads back towards the EO). An iris should be setup before the first mirror to isolate the emerging +1 beam, which will have a net angular displacement of 0 ($+\theta$ in one direction and $-\theta$ in the opposite direction), and frequency change of $+2f_{EO}$ (one from each pass through the AO) if properly aligned. The easiest way to determine which beam is +2 with zero angular displacement is to add a time-varying voltage of relatively small amplitude to the DC offset that was applied to the AO VCO during alignment and choose the spot that is displaced the least). This technique can also be used to fine tune the second pass alignment.

The alignment of any cavity in reflection will have its own idiosyncracies; however, a few general comments will be made about alignment strategies. It was found that removing the mode-matching lens and both focusing lenses in the path from the last mirror into the cavity is the best starting point. The beam on the last mirror should be at roughly the same x and y positions as the center of the cavity, assuming that the center of the last mirror is placed at the same x and y coordinates as the center of the cavity and that the cavity mirrors are parallel and perfectly vertical (which may not be the case). The beam should be adjusted to hit the center of the first cavity mirror and reflect back onto the last mirror at the same spot. Each of the two of the focusing lenses will be added sequentially, ensuring that the beam passes in the middle of the lens and that the beam is not translated by it. There are several reflection spots from the cavity surfaces. The reflection spot from the reflective surface of the first mirror will likely be large. It must be overlapped with the spot from the reflective surface of the second mirror (this spot should be much smaller). After each lens is added these spots need to be overlapped as well as possible. At this point, a number of transverse modes should be visible on the photodetector, if the piezo is being scanned at least one free spectral range. Each transverse mode is at a different frequency and appears as a separate peak. An illustration of a plenitude of transverse modes is provided in Figure 4.3. From here, one strategy is to choose one transverse mode and steer the beam to maximize its amplitude. After maximizing it, the TEM_{00} should be visible. The relative ratio of the radius of curvatures of the mirrors and the length of the cavity will determine the location (in frequency space) of the TEM_{00} mode in relation to the other transverse modes. In the near-planar case ($R \gg L$), the TEM_{00} mode is at the low frequency side of the group of transverse modes in one free spectral range. Figure 4.4 shows a much better alignment than Figure 4.3 and illustrates the sequence of transverse modes. The lower-order modes are at lower voltages with the TEM_{00} being at the far right or left of the figure. Once one transverse mode is maximized, the piezo offset is adjusted such the highest-order modes progress off the scope until the

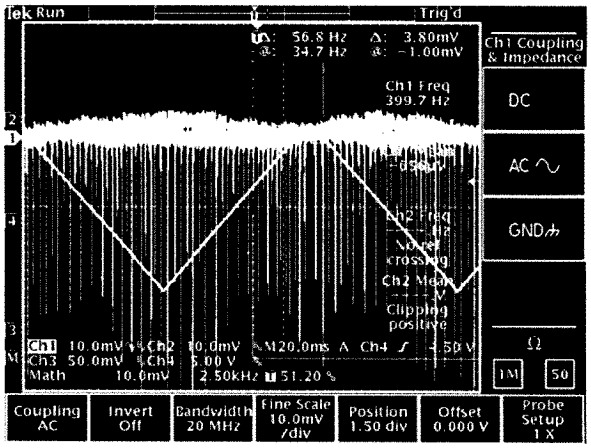

Figure 4.3: Gross Misalignment

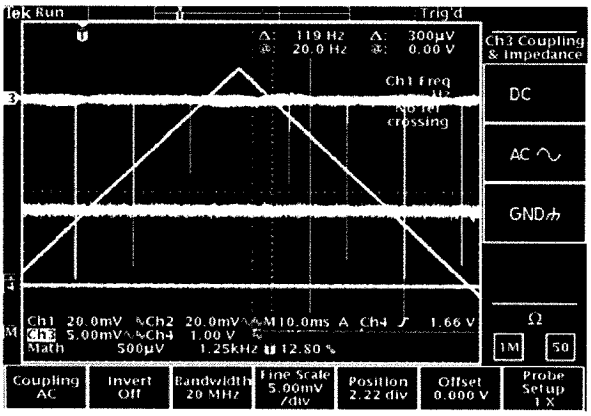

Figure 4.4: Slight Misalignment

end of the sequence of modes is reached (i.e. at the bottom of each piezo scan). This is likely the TEM_{00}. The amplitude of this peak should be maximized. If another peak appears at a lower frequency/piezo voltage, then that is the TEM_{00} mode. This process is repeated until no other peaks appear at lower voltages and all of the power from the other transverse modes has been put into the TEM_{00} mode.

Chapter 5

The Design of the Frequency Servo

5.1 Fundamentals

In order to lock the laser to the cavity, the piezo and the acousto-optic modulator must be controlled with different frequency-dependent voltages, dictated by the individual characteristics of each device. In general, these characteristics are measures of the extent to which the error signal, as depicted in Figure 5.1, can cause each device to change the frequency of the laser or the length of the cavity in order to keep the cavity locked. The slope of the error signal (V/Hz) across the resonance peak (as opposed to the slope across each side band) is what specifically causes each device to respond. The first thing we need to know, therefore, is the slope of the error signal. This slope can be measured directly using an oscilloscope while scanning the piezo. In practice, we can't directly measure the Δf component of the error signal slope. Instead, we measure the Δt_{rp} on the oscilloscope and compare that to our measurement of Δt_{sp} (the temporal spacing between the side bands on the oscilloscope screen). Δt_{sb} corresponds to $2f_{EO}$, which we can measure directly.

$$m_{error} = \left(\frac{\Delta V_{rp}}{\Delta t_{rp}}\right)\left(\frac{\Delta t_{sb}}{2f_{EO}}\right) \tag{5.1}$$

This slope is a function primarily of laser power, photodetector gain/response, cavity mirror reflectivity, and intra-cavity losses; therefore, its value must be re-measured

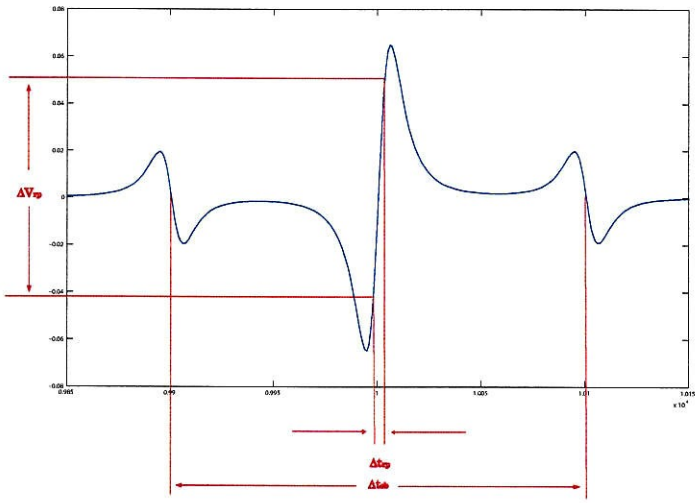

Figure 5.1: Error Signal Slope

whenever any of these parameters changes.

For the piezo, we are concerned with the distance it moves the second mirror (i.e. the change in cavity length) for a given applied voltage. Since the cavity is enclosed and since the distances with which we are concerned are so small, practically speaking, we cannot directly measure the change in distance. We can get an idea of the piezo response directly by scanning the piezo and measuring the difference in voltage between each side band on the resonance signal. The overall hardware gain for the piezo is the product of the slope of the error signal and the piezo response:

$$g_{piezo} = (m_{error})(r_{piezo}) \tag{5.2}$$

This gain (which is unitless) gives us an indication of the extent to which the error signal will cause the piezo to compensate for slow changes in the laser frequency and in the length of the cavity.

For the AO, we are concerned with the degree to which it can change the frequency of the optical beam in response to an applied voltage. An AO consists of a crystal with an attached transducer, which introduces RF radiation into the crystal, setting up a standing wave there. The frequency of the optical beam (f_{beam}) passing through the

AO crystal is changed by the frequency of a standing wave in the AO crystal, (f_{AO}):

$$\Delta f_{beam} = f_{AO} \tag{5.3}$$

The RF signal that establishes this standing wave is generated by a voltage-controlled oscillator (VCO) and its frequency is controlled by the dc voltage that is applied to the VCO. If we measure the dc voltage required to change the frequency of the EO by some relevant amount, we get some insight into the response of the AO:

$$r_{AO} \approx \frac{\Delta f_{A0}}{\Delta V_{VCO}} \tag{5.4}$$

The overall gain of the AO is the product of the error signal slope and the AO response:

$$g_{AO} = (m_{error})(r_{AO}) \tag{5.5}$$

A significant part of understanding the AO response is quantitatively knowing how fast the AO can respond and how its ability to respond changes with frequency. The ultimate limit is dictated largely by the amount of time it takes for changes in the traveling acoustic wavefront to reach the optical beam in the AO crystal. This time varies primarily with the position of the beam with respect to the transducer on the bottom of the crystal and the speed of sound in the crystal. For the Brimrose TEM-110-25-850 (the AO we are using), the response time is approximately $10\mu secs$. This means that it is very difficult to compensate for noise faster than approximately 100 kHz due to phase lag.

Now that we have an idea of the hardware gain of the AO and the piezo, we can consider how we need to condition and amplify the error signal in order to ensure that the piezo and AO are optimally compensating for noise within their bandwidth of operation. The amplification and conditioning are performed by an electronic circuit, commonly referred to as a servo whose main purpose is to keep the laser locked to the cavity. The main parameters we need to know in order to design an appropriate servo are the frequency at which the error signal to each device has unity gain (the 0 dB

point), the frequency at which the AO gain is equal to the piezo gain, and the phase lag associated with each of these frequencies. Phase lag is the difference in phase between the output and the input signals.

5.1.1 AO Branch

In designing the servo, we will first consider the AO branch, then the piezo branch, and, finally, the composite of both branches. The AO branch can be characterized by four important features: the overall DC gain, the 0 dB point, the AC-coupling frequency, and the frequency at which the maximum gain begins to roll off. The 0 dB point of the AO branch must be below 100 kHz, since the AO cannot respond any faster than that, as was previously mentioned. Trying to close at a frequency higher than 100 kHz results in significant oscillations. Since the g_{AO} turns out to be relatively small (compared to the g_{piezo}) over its bandwidth of operation, the gain of the AO branch must be relatively high. Due to the requirement for high gain and because the piezo branch is being relied upon to compensate for lower frequency noise, it will be best to AC-couple the AO branch of the servo. The actual AC-coupling frequency can be chosen within a reasonably wide range. In practice, the upper limit is set by the requirement that there be some region of constant gain over which the piezo branch transfer function can cross. The frequency of the gain roll off will need to be higher than the AC-coupling frequency (assuming the simple servo circuit scheme we are using) but low enough to allow the 0 dB point to be reached by 100kHz using a single pole. From practical experience, we will also want to include a low pass filter to suppress spurious increases in gain at higher frequencies due to the performance of some of the operational amplifiers in the servo. The frequency of the low pass filter needs to be at least a few times higher than the 0 dB point, to avoid reducing our phase margin there. As a note, when we speak of the low pass frequency, what we really mean is the frequency that corresponds to $\frac{1}{2\pi RC}$. It is also the frequency at which there is a 3 dB change in gain. For example, the AC-coupling frequency is the frequency at which the gain is 3 dB lower than (i.e. one half of) its value in the absence of AC-coupling.

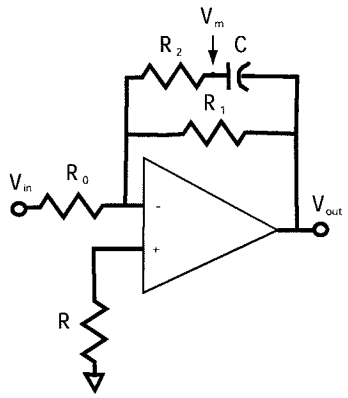

Figure 5.2: Pole Zero

We can set the 0 dB point and the roll off frequency with a single component in the AO servo: the 'pole zero'. In general terms, a 'pole' is a zero in the denominator of the transfer function and a 'zero' is a zero in the numerator. A transfer function is merely the ratio of the output to the input voltage in Laplace space. Poles can either initiate a reduction in gain or terminate an increase in gain, depending upon the dominant element in the transfer function that precedes (in frequency/Laplace space) the pole. In all situations, a stable pole introduces a fixed gain decrease of 20 dB/decade and a 90 degree reduction in phase. A zero does the opposite: it adds 90 degrees of phase and introduces a 20 dB/decade increase in gain. It might be helpful to include a brief discussion of the pole zero component we use in the AO branch of the servo. It is essentially an operational amplifier with parallel feedback paths as illustrated in Figure 5.2. Our goal is to solve for the output voltage of this component (V_{out}) in terms of the input voltage (V_{in}). An adequate way to do this is by making the simplifying assumption that the voltage at the inverting and non-inverting pins of the operational amplifier are equal to zero. We can then easily solve for the sum of the currents at the non-inverting pin in accordance with Kirckhoff's Law, as illustrated in 5.6,

$$\sum_j i_j = 0 \tag{5.6}$$

where j represents each branch adjacent to a node (the node here being the non-

inverting input of the op amp). We have:

$$i_0 + i_1 + i_2 = 0 \tag{5.7}$$

$$i_0 = \frac{-V_{in}}{R_0} \tag{5.8}$$

$$i_1 = \frac{V_{out}}{R_1} \tag{5.9}$$

Solving for i_2 is a little more difficult. We know that the current in each component in branch 2 must be equal. We can specify the voltage between each component as V_m and solve for it in terms of V_{out}:

$$i_2 = i_C = i_{R_2} \tag{5.10}$$

$$i_C = \frac{d}{dt}[V_o - V_m]C \tag{5.11}$$

$$i_{R2} = \frac{V_m}{R_2} \tag{5.12}$$

$$\frac{d}{dt}[V_o - V_m]C = \frac{V_o}{R_2} \tag{5.13}$$

By taking the Laplace transform of each side, we easily solve for V_m:

$$\mathcal{L}[\frac{d}{dt}[V_o - V_m]C] = [V_o(s) - V_m(s)]Cs = \mathcal{L}[\frac{V_m}{R_2}] = \frac{V_m(s)}{R_2} \tag{5.14}$$

Solving for V_m, we have:

$$V_m(s) = \frac{R_2Cs}{1 + R_2Cs}V_o(s) \tag{5.15}$$

Using 5.12, we can solve for i_2:

$$i_2(s) = \frac{Cs}{1 + R_2Cs}V_o(s) \tag{5.16}$$

Taking the Laplace transforms of the other currents is trivial. We can now solve for the ratio of V_{out} to V_{in}, the transfer function:

$$\frac{V_{out}(s)}{V_{in}(s)} = \frac{-R_1(1 + R_2Cs)}{R_0(1 + (R_1 + R_2)Cs)} \tag{5.17}$$

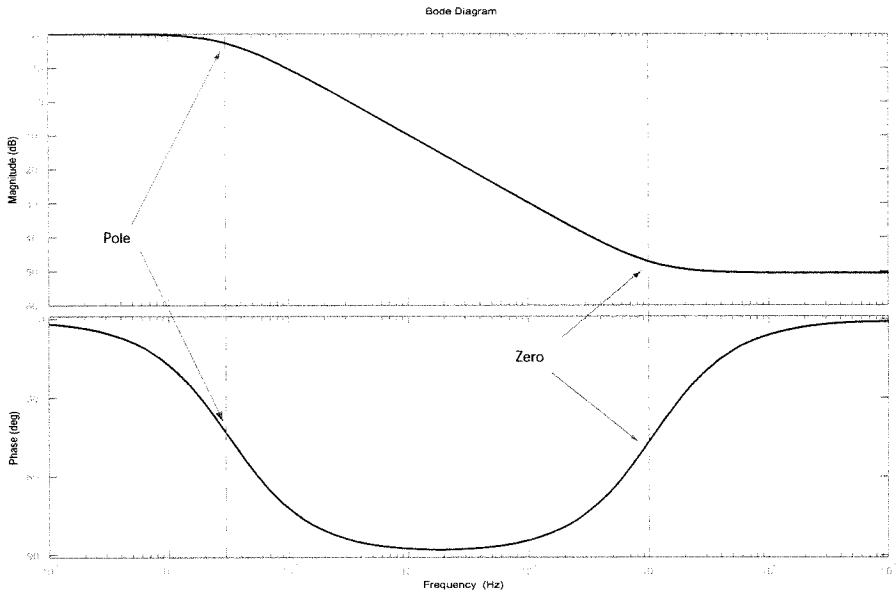

Figure 5.3: Bode Plot of Pole Zero

The frequency of the pole is roughly equal to $1/(R_1 + R_2)C$ and the frequency of the zero is roughly $1/R_2C$. A convenient format in which to illustrate poles and zeros is the bode plot. A bode plot contains a graph of gain (dB) versus the log of frequency and a corresponding graph of phase lag versus the log of frequency. A bode plot of a pole zero is illustrated in Figure 5.3.

From the bode plot, we can observe that a pole causes the gain to begin decreasing at approximately 20 dB/decade and causes a corresponding -90 degree phase lag. At the frequency of the pole (i.e. the frequency at which the numerator is 0), the gain will have decreased by 3 dB and the phase will have decreased by -45 degrees. A zero causes the gain to stop decreasing and the phase to increase by 90 degrees. Although the pole frequency is determined by the sum of R_1 and R_2 times the capacitance $(1/(R_1 + R_2)C)$, from a practical point-of-view, R_1 tends to be much greater than R_2 (since the zero must be at a higher frequency than the pole), so the zero is essentially determined by $1/R_1C$. As the relevant RC product decreases, the frequency of the zero or pole increases. The second significant component in the AO servo is a low pass filter, as illustrated in

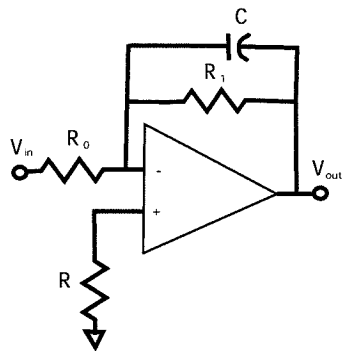

Figure 5.4: Low-Pass Filter

Figure 5.4. The low pass filter we use is similar to the pole zero, except there is no resistor in series with the capacitor. The transfer function of this low pass filter is:

$$\frac{V_{out}}{V_{in}} = \frac{-R_1}{R_0(1 + R_1Cs)} \tag{5.18}$$

A low pass filter has a single pole whose frequency corresponds to $1/R_1C$. The main purpose of a low pass filter is to attenuate higher frequency signals.

It was mentioned that the AO servo is AC-coupled. AC-coupling can be accomplished very simply, by placing a series capacitor just before the input resistor to some stage in the servo. This type of AC-coupling introduces a zero at 0 Hz and a pole at the RC constant for the AC-coupling capacitor and input resistor. If this capacitor (C_0) were placed just before the pole zero stage in Figure 5.2 whose transfer function is 5.17, the overall transfer function would be:

$$\frac{V_{out}(s)}{V_{in}(s)} = \frac{(-R_1C_0s)(1 + R_2Cs)}{(1 + (R_1 + R_2)Cs)(1 + R_0C_0s)} \tag{5.19}$$

and whose bode plot is shown in Figure 5.5. We can see that there is an additional pole at $1/R_0C_0$; however, the pole and zero from Figure 5.3 remain unchanged, except for the extra 90 degrees of phase lag. The overall AO transfer function is shown in Figure 5.6. The only difference between it and Figure 5.5 are the overall DC gain and the low pass filter at 350 kHz (whose purpose is to suppress spurious gain spikes at higher

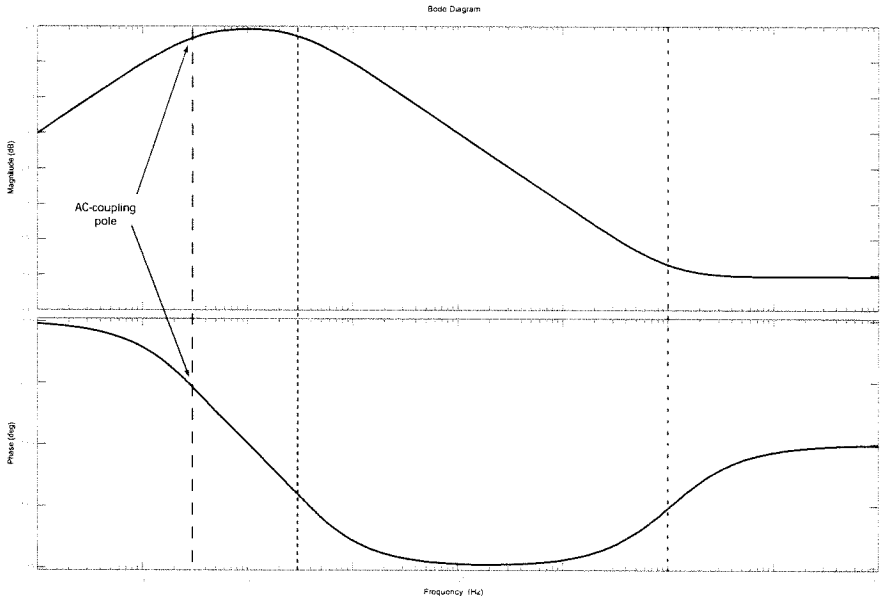

Figure 5.5: Bode Plot of Pole Zero with AC-coupling

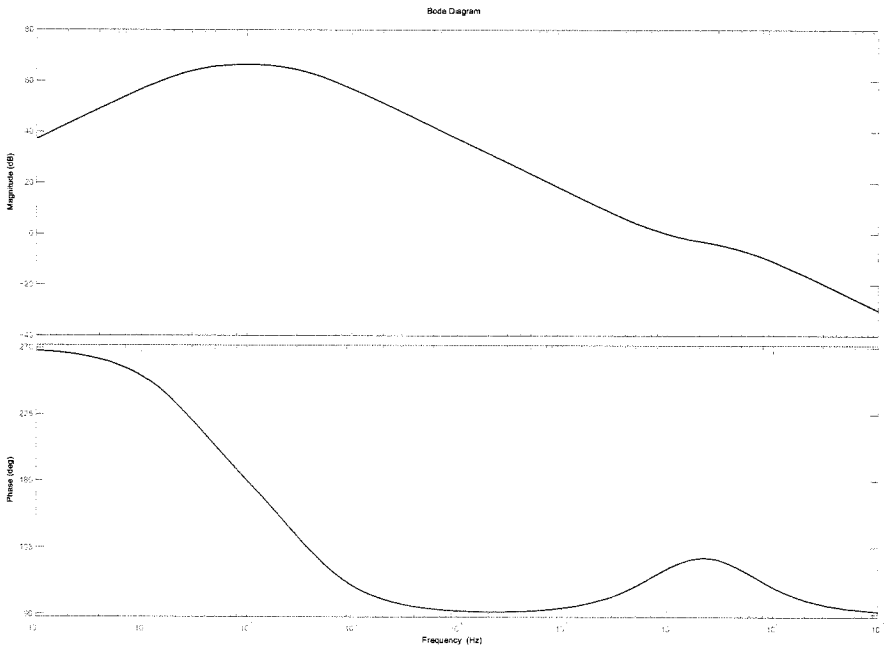

Figure 5.6: AO Transfer Function

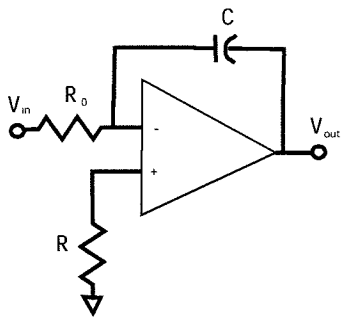

Figure 5.7: Integrator

frequencies, due to op amp anomalies).

5.1.2 Piezo Branch

The 0 dB point of the piezo branch of the servo, as a minimum, must be below the resonance frequency of the piezo (the resonance frequency is the frequency at which the piezo no longer responds predictably), which is 138 kHz for the Thor Labs piezo stack we are using. For a number of practical reasons, we will want the piezo branch to have a 0 dB point at least an order of magnitude lower than its resonance frequency. The key component in the piezo servo is an integrator. An integrator is the component of choice when amplifying low frequency signals, since it theoretically has infinite gain at zero frequency. Practically speaking, the gain at very low frequencies is set by the open loop gain of the particular operational amplifier that is being used as an integrator. We are using an OP627 as an integrator in our servo. The open loop gain of the OP627 is only limiting at frequencies below 1 Hz, as illustrated in Figure 5.8. An integrator looks like the low pass filter in Figure 5.4 without the feedback resistor, as shown in Figure 5.7. The transfer function of an integrator is:

$$\frac{V_{out}}{V_{in}} = \frac{1}{CR_0 s} \tag{5.20}$$

We can see that the integrator has a pole at a frequency of zero and that the phase is constant at -90 degrees. In our servo, we chose to add a low-pass filter at 48 Hz in order to force the overall piezo servo to cross the AO servo where its gain is more or

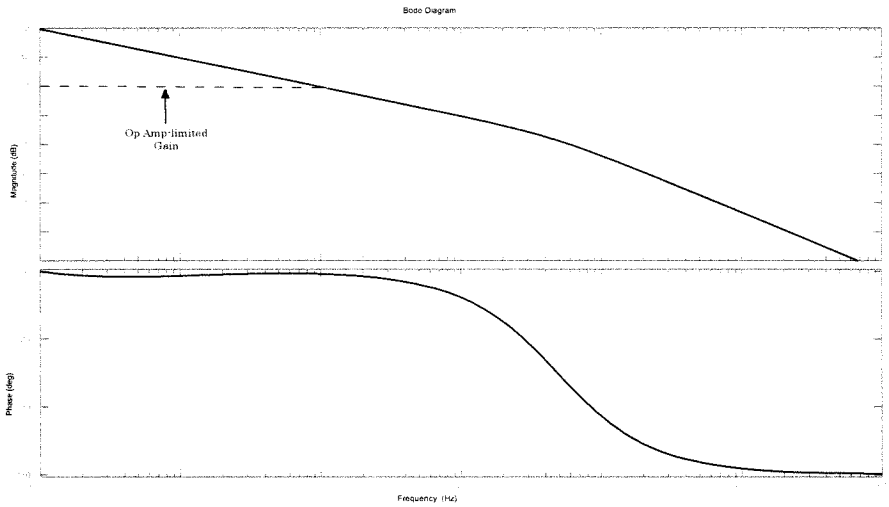

Figure 5.8: Piezo Branch Transfer Function

less constant and to force the piezo branch to close at a lower frequency than would otherwise be possible. The bode plot of the entire piezo branch is shown in Figure 5.8.

5.1.3 Combined Transfer Function

The combined transfer function for the piezo and AO branches is shown in Figure 5.9.

5.2 Practical Considerations

There are a number of practical considerations that inform the proper design of the servo. It was largely these practical considerations that proved to be the largest stumbling block of this experiment and were only fully realized by the fifth and final version of the servo. These considerations will be addressed through the hindsight that came as a result of either neglecting to consider them or improperly considering them. The final version of the main lock servo is shown in Figure 5.10. As a result of the lessons learned in the previous four circuits, the overall circuit has both servos on the same board, a differential amplifier between the error signal and the first stage of the servo with non-inverting amplifiers before each branch, separate gain adjusts for

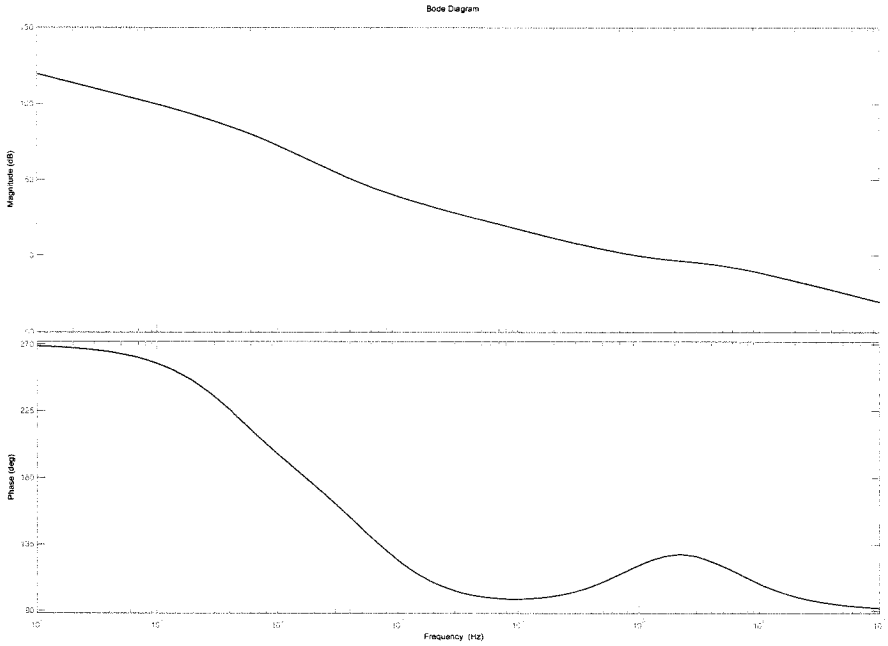

Figure 5.9: Combined Transfer Function

each branch, an isolating op amp between any gain adjust and the next component, a AC-coupled AO servo, an integrated DC offset adder in the AO branch, a low pass filter at 450 kHz on the input stage of the AO servo to suppress high frequency noise on the error signal, a low pass filter in the piezo branch to force the piezo branch to cross the AO branch at a more favorable frequency and to force the piezo branch to close at a lower frequency than would otherwise be possible, an inverter switch in the piezo branch so that it can be changed from inverting to non-inverting as necessary, trimming on the integrator op amp to ensure optimal performance of the integrator, an integrate switch that acts as a low pass filter when the servo is not integrating, an offset adder/subtractor on the error signal input, and a custom/home made high voltage amplifier between the output of the piezo branch and the piezo. Each of these features will be discussed in a bit more detail in the following sections.

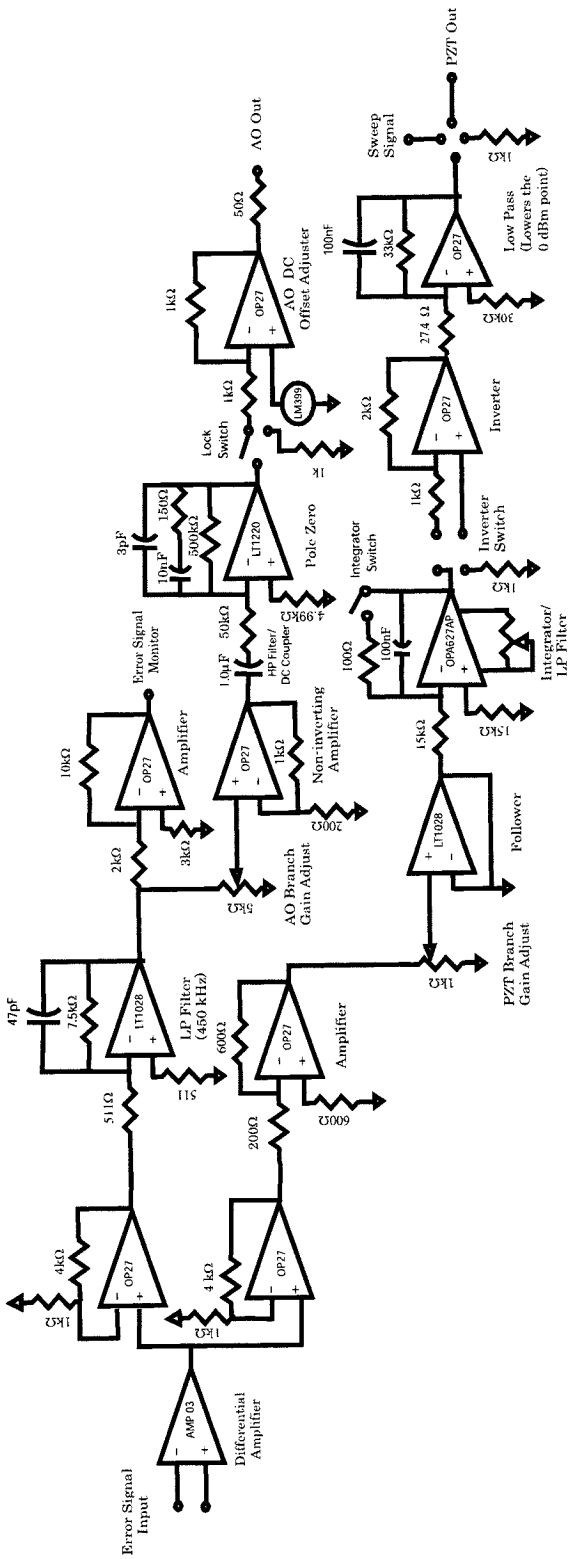

Figure 5.10: Lock Servo

5.2.1 Gain Adjusts

In order for the servo to be functional under various conditions of laser power, photodiode type, and intra-cavity losses and in order to simplify the locking process, it is necessary to be able to adjust the gain of the servo. In the initial two versions of the servo, there was only one gain adjust for both branches. A single gain adjust has the advantage of changing the gain of both branches of the servo by the same amount, thus not changing the frequency at which the gain of the piezo branch equals the gain of the AO branch. It is very important to know what is happening with the transfer function of each branch when the gains are equal in order to prevent instability due to gain spikes or unfavorable phase relationships. Locking with a single gain adjust turned out to be difficult to impossible due to practical considerations in the locking procedure. With a gain adjust in each branch, careful attention had to be paid to potential instabilities with certain combinations of gain settings. Much effort was expended trying to predict which settings would cause such instabilities and making sure that they were not reached during the locking procedure; however, ultimately, acceptable combinations of gain settings was determined empirically. The AO branch was designed such that there would be adequate gain to close slightly above 100 kHz in order to ensure the ability to close as close to 100 kHz as possible. The level of the piezo branch gain was determined by a choice of the frequency range over which the piezo gain would equal the AO branch gain and the the frequency at which the piezo branch should have 0 dB of gain.

5.2.2 Trimming the Integrator

The integrator is the key component in the piezo branch. Since integrators have very high gain at DC (120 dB set by the open loop gain of the OP627), the integrator is very sensitive even to slight imbalances in the input offset voltage due to temperature changes, etc... Therefore, it is necessary to trim the integrator operational amplifier to eliminate any such offset. This amounts to installing a 10 kΩ trim pot between the appropriate pins (1 and 8) of the OP627 and adjusting it until a grounded servo input

causes 0 output from the integrator. Failure to trim an integrator properly causes the integrator to rail at ± 15 Vdc; thus, preventing the piezo from getting an error signal that properly indicates proximity to a resonance condition.

5.2.3 Invertor Stage in Piezo Branch

Because the polarity of the error signal can be changed by changing the frequency at which the EO modulates and because extra stages (which could change the polarity of the branch) might be added to the piezo branch, it is helpful to be able to change the overall polarity of the piezo branch. To this end, we added an invertor stage, which allows the polarity of the piezo to be changed by flipping a switch.

5.2.4 Integrate Switch

The purpose of the integrate switch is to start integrating the error signal in the piezo branch. This can be (and has been) done several ways. We have chosen to place the integrate switch in series with a resistor which is parallel with the integrating capacitor. When the switch is off, the resistor remains in parallel with the capacitor, forming a low pass filter. When the switch is on, the resistor is taken out of the circuit and the op amp begins integrating. The choice in the value of the resistor determines what signal the piezo sees when the integrate switch is off. We can either choose to have the integrator stage low pass when the integrate switch is off, which will result in some feedback to the piezo or we can choose to have it put out little to no voltage, eliminating feedback to the piezo with the switch off. Originally, we chose to have the integrator stage low pass, because the low pass feedback seemed to make it easier to lock. The thought was that sending too much of an impulse to the piezo (by going from no feedback to massive feedback) could cause the AO lock to be lost. We later decided, however, that it would be better if the integrator put out no voltage when the integrator switch is off. This is accomplished by choosing a resistor that is much smaller than the input resistor. Having feedback going to the piezo with the integrate switch off turned out to complicate the locking process instead of helping it, as was previously

thought. If the integrator is trimmed properly, if the DC offset of the error signal is properly eliminated, and if the gain is adjusted correctly, going from 0 piezo feedback to integrated feedback works very well.

5.2.5 Managing the DC Offset of the Error Signal

As is evident from Equation 7.2, the error signal has a DC offset. Appropriately managing the DC offset of the error signal turned out to be the largest stumbling block in this experiment. The DC offset comes from residual amplitude modulation by the EO and is affected by a large number of factors including EO alignment, laser power, modulation depth, RF power applied to the EO, and certain cavity parameters. This offset affects both branches of the servo. Since the piezo branch has very high gain at DC ($\sim 120dB$), it is extremely sensitive to DC offset. From practical experience, locking with the piezo branch requires that the DC offset be zeroed to within tens of millivolts. Inadequate zeroing causes the piezo branch to integrate the DC offset instead of the error signal, which causes the piezo branch to send maximum voltage to the piezo, quickly pushing the cavity far off lock. A simple way to zero the error signal offset is with an adjustable offset adder on the input of the servo. Beyond merely causing the integrator in the piezo branch to rail, a DC offset on the error signal can cause problems common to both branches. It seems counter-intuitive that it should affect the AO branch, since it is AC-coupled and is, on that account, seemingly insensitive to DC offsets. The problem is that a DC offset of sufficient magnitude can cause the error signal to have no zeros. For example, if the DC offset were greater than the amplitude of the main resonance peak, the error signal would never be zero and the servo would not be able to lock. Even in the AC-coupled AO branch, a significant offset could distort the form of the error signal due to significant amplification before the AC-coupling capacitor.

5.2.6 Adding the DC Offset

Both the AO and the piezo require a unique DC offset in order to function properly. Any noise on the DC offset to either the AO or the piezo translates into noise on the lock signal; therefore, it is imperative that each DC offset be as quiet as possible and not prone to drift.

5.2.6.1 AO Branch

The DC offset sent to the AO VCO determines the frequency of the standing wave in the AO crystal. The optical alignment of the beam through the AO crystal is very sensitive even to small changes in the AO frequency; therefore, the beam must be re-aligned after changing the AO frequency. The DC offset to the AO was originally added via an offset adder powered by a battery. This had the advantage of being very quiet and stable; however, was thought to be inconvenient. In the last version of the servo, the offset was added in the last stage of the AO servo via a stable voltage source (LM 399). This was more convenient and very quiet, but had the disadvantage of changing the DC offset by tens of millivolts each time the lock switch was turned on, due to non-ideal performance of some operational amplifiers. Although this phenomenon was far from ideal, it was manageable. If another version of the servo were built, it would definitely be better to add this offset via an external offset adder.

5.2.6.2 Piezo Branch

On a coarse scale, the length of the piezo and the position of the second cavity mirror are controlled by the DC offset going to the piezo. This offset must be manually changed to get the cavity near resonance before attempting to lock. This offset was originally added via a commercial high voltage amplifier (New Focus 3211) whose output impedance was optimized for driving large capacitative loads, such as a piezo. This amplifier had the advantage of being well impedance-matched but was extremely noisy. The next attempt was via a high voltage battery and an adjustable voltage divider circuit. This method was very quiet but the output impedance from the voltage

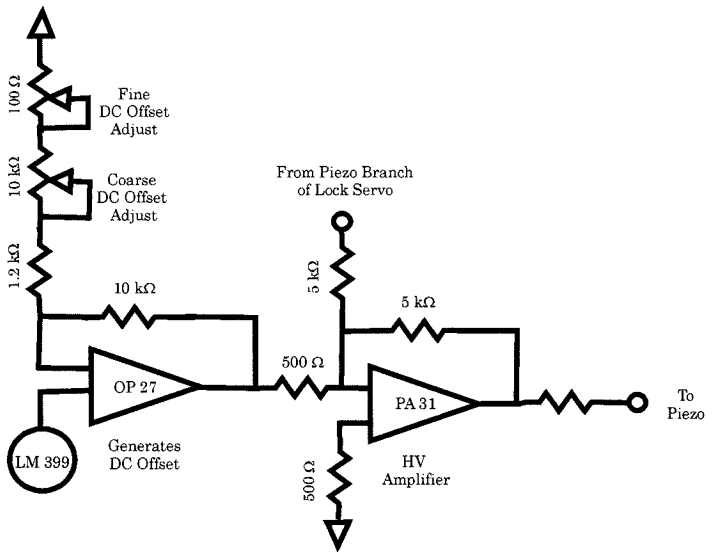

Figure 5.11: High-Voltage Amplifier

divider combined with the capacitance of the piezo to form a low pass filter a prohibitively low frequency, forcing the piezo branch to close at a significantly lower frequency than had been intended. This particular phenomenon was another significant stumbling block, largely because it went undetected for a long time. The final method of adding the DC offset was via a home made high voltage amplifier circuit whose output impedance was optimized for driving large capacitative loads. A schematic of this circuit is shown in Figure 5.11.

5.2.7 60 Hz on Error Signal

The presence of 60 Hz noise on the lock signal proved to be another significant stumbling block. It was first thought that this noise came from a ground loop in the servo. Much time was spent checking solder connections in the servo and in examining all relevant electronic and optical components for 60 Hz noise. After several months, it was determined that the servo was responsible for this noise, and a new version of the servo was built. The 60 Hz noise was still present on the lock signal with this new servo. All electronic components were once again checked for ground loops and 60 Hz noise. The source was still not identified; therefore, the determination was made

to install a differential amplifier at the input of the servo. The error signal from the BNC connector is sent to the non-inverting input of the differential amplifier and the ground/negative of the BNC connector goes to the inverting input. In this arrangement, the servo conditions and amplifies the difference between the error signal and its ground, eliminating any possible differences between the ground plane of the servo and that of the error signal. The differential amplifier did eliminate the 60 Hz noise.

Chapter 6

Cavity-Enhanced Measurements

6.1 Measurement Methodology

The primary advantages of cavity-enhanced spectroscopy over single pass or other multiple-pass, 'pulse' techniques are: (a) significantly increased interaction distance and (b) 'real time' observation.

6.1.1 Beer-Lambert Regime

Standard, single-pass absorption spectroscopy uses the so-called Beer-Lambert Law to determine the power loss due to absorption. Given a sample of absorbers with concentration, C_a (moles/liter), and molar extinction coefficient, ϵ_a $(M^{-1}cm{-}1)$, in a conventional, single-pass spectrophotometer. The sample is in the path of an optical beam of power, P. The reduction in optical power due to absorption, dP, is equal to the incident power multiplied by the absorption caused by the population of absorbers in a cross-sectional slice of the beam of thickness, dz.

$$dP = -P\epsilon_a C_a dz \Rightarrow \frac{dP}{P} = -\epsilon_a C_a dz \tag{6.1}$$

Integrating both sides, we have:

$$\int_{P_{inc}}^{P} \frac{dP}{P} = -\int_{0}^{L} \epsilon_a C_a dz \tag{6.2}$$

$$ln(\frac{P}{P_{inc}}) = -\epsilon_a C_a L \Rightarrow P = P_{inc} e^{-\epsilon_a C_a L} \tag{6.3}$$

$$Absorption_{fractional} = \frac{\Delta P}{P_{inc}} = \frac{P_{inc} - P}{P_{inc}} = 1 - e^{(-\epsilon_a C_a L)} \tag{6.4}$$

6.1.2 Fabry-Perot Regime

Analogously, in cavity-enhanced spectroscopy, the circulating power within the cavity at any time, $P(t_{rt})$, can be expressed in terms of the circulating power during the previous round trip is:

$$P_{circ}(t_{(rt)}) = P_{circ}(t_{(rt-1)}) e^{-\delta_0 - \delta_1 - \delta_2} \tag{6.5}$$

where δ_0 is the round trip loss factor, expressed as $\alpha_0 p$ previously. The reflectivity of the cavity mirrors can also be written in 'delta notation':

$$\delta_i = ln(\frac{1}{r_i^2}) \tag{6.6}$$

The absorption per round trip is:

$$Abs_{rt} = \Delta P_{circ} = P_{circ}(t_{(rt)}) - P_{circ}(t_{(rt-1)}) = P_{circ}(t_{(rt-1)})(1 - e^{-\delta_0}) \tag{6.7}$$

$$Abs_{rt}(fractional) = \frac{\Delta P_{circ}}{P_{circ}(t_{(rt-1)})} = 1 - e^{-\delta_0} \tag{6.8}$$

δ_0 can be directly related to the terms in (6.4):

$$\delta_0 = \alpha_0 p = \epsilon_a C_a L \tag{6.9}$$

We conclude that α_0 is equal to $C_a \epsilon_a$, understanding that the intra-cavity path length per round trip is p.

6.1.2.1 Cavity Enhancement

In order to calculate the enhancement that cavity-enhanced spectroscopy provides over free space measurements, we can examine the sensitivity of each technique to small

changes in the absorption coefficient. From (6.3), the transmitted power in free space measurements is:

$$P = P_{inc}e^{-\alpha_0 L} \tag{6.10}$$

where α is the power absorption coefficient and is equal to $\sigma C_a \epsilon_a$. The reflected output power for a cavity on resonance is:

$$P = P_{inc}\frac{(r_1^2 - g_{rt})^2}{r_1^2(1-g_{rt})^2} \tag{6.11}$$

where g_{rt} is

$$g_{rt} = r_1 r_2 e^{-\frac{\alpha_0}{2}(2L)} \tag{6.12}$$

in a cavity of length, L. We can determine the extent to which the measurement is sensitive to very small changes in α_0, by taking the partial derivative of P_{inc} with respect to α_0. In the free space case, we have:

$$\frac{\partial P_{inc}}{\partial \alpha_0} = LPe^{\alpha_0 L} = LP_{inc} \tag{6.13}$$

With a cavity, we have:

$$\begin{aligned}
\frac{\partial P_{inc}}{\partial \alpha_0} &= \frac{-2r_1^2(1-g)^2(\frac{\partial g_{rt}}{\partial \alpha})}{(r_1^2-g)^2}P + \frac{2r_1^2(1-g)^2(\frac{\partial g_{rt}}{\partial \alpha_0})}{(r_1^2-g)^3}P \\
&= \frac{2r_1^2(1-g)^2 Lg}{(r_1^2-g)^2}P - \frac{2r_1^2(1-g)^2 Lg}{(r_1^2-g)^3}P \\
&= 2LP_{inc}[\frac{g}{1-g} - \frac{g}{r_1^2-g}] \\
&= 2LP_{inc}(\frac{g}{1-g})(\frac{r_1^2-1}{r_1^2-g})
\end{aligned} \tag{6.14}$$

If we assume extremely low losses, $g_{rt} \approx 1$. We now have:

$$\frac{\partial P_{inc}}{\partial \alpha} \approx \frac{2LP}{1-g} = \frac{2LP\mathcal{F}}{\pi} \tag{6.15}$$

The enhancement factor would be the ratio of the two partial derivatives:

$$E = \frac{(\frac{\partial P_{inc}}{\partial \alpha_0})_{cavity}}{(\frac{\partial P_{inc}}{\partial \alpha_0})_{freespace}} = 2(\frac{g}{1-g})(\frac{r_1^2 - 1}{r_1^2 - g}) \approx \frac{2\mathcal{F}}{\pi} \tag{6.16}$$

6.1.3 Measuring Absorption

There are two ways in which absorption can be measured in cavity-enhanced spectroscopy: one while scanning the piezo and the other with the laser locked to the cavity linewidth. It is possible to apply a positive, sawtooth voltage to the piezo which will cause the piezo to move roughly equal distances in either direction from the center DC offset voltage. If the amplitude and offset of the applied voltage are chosen appropriately and the laser is appropriately coupled to the TEM_{00} mode, a resonance condition will be consistently satisfied at one point in each cycle of the applied voltage, assuming no significant piezo hysteresis or thermal transients. On resonance, there will be a peak (a negative peak, in reflection) whose full-width half maximum (Δf_{FWHM}) provides an indication of the overall losses associated with the cavity. The finesse, $\mathcal{F}$, can be related directly to the intracavity losses:

$$\mathcal{F} = \frac{\pi\sqrt{r_1 r_2}e^{-\delta_0/4}}{1 - r_1 r_2 e^{-\delta_0/2}} \approx \frac{\Delta f_{FSR}}{\Delta f_{FWHM}} \tag{6.17}$$

Using delta notation, our expression for finesse becomes:

$$\mathcal{F} = \frac{\pi e^{-(1/4)(\delta_1+\delta_2+\delta_0)}}{1 - e^{-(1/2)(\delta_1+\delta_2+\delta_0)}} \tag{6.18}$$

Assuming $\delta_i \ll 1$, we have:

$$\mathcal{F} = \frac{2\pi}{\delta_1 + \delta_2 + \delta_0} \tag{6.19}$$

Thus, by measuring the finesse, we can determine the sum of the cavity loss factors.

$$\delta_0 + \delta_1 + \delta_2 = \frac{\mathcal{F}}{2\pi} \tag{6.20}$$

Using this equation, we can solve for the difference in the intra-cavity loss factors, assuming that the mirror loss factors do not change between measurements.

$$\Delta\delta_0 = \delta_{0b} - \delta_{0a} = \frac{\mathcal{F}_a}{2\pi} - \frac{\mathcal{F}_b}{2\pi} = \frac{2\pi}{\Delta f_{FSR}}(\Delta f_{FWHMb} - \Delta f_{FWHMa}) \tag{6.21}$$

This could be helpful in determining the round trip losses caused by a particular concentration of an absorber. In such a case, Δf_{FWHMa} would be measured with just solvent in the cavity and would, therefore, be indicative of the losses due to solvent, etc. Δf_{FWHMb} would be measured with some concentration of absorbers in the cavity and would be indicative of the losses due to the solvent, etc. and the absorbers. The advantage of absorption measurements using finesse is that they are not dependent upon the mode-matching factor. The disadvantages are that our ability to measure the Δf_{FWHM} is hampered by piezo non-linearities, resulting in more uncertainty than locked measurements. The other limitation is that the cavity field is not continuously staying at its maximum level.

While the laser is locked to the cavity linewidth, finesse measurements cannot be made. For a cavity in reflection, what can be measured is $\frac{P_{refl}}{P_{inc}}$. From 2.22, on resonance, it is:

$$\frac{P_{refl}}{P_{inc}} = \left(\frac{r_1 - r_2 e^{-\delta_0/2}}{1 - r_1 r_2 e^{-\delta_0/2}}\right)^2 \tag{6.22}$$

Using delta notation for the mirror reflection coefficients, we have:

$$\frac{P_{refl}}{P_{inc}} = \left(\frac{e^{-\delta_1/2} - e^{-\delta_2/2-\delta_0/2}}{1 - e^{-\delta_1/2-\delta_2/2-\delta_0/2}}\right)^2 \tag{6.23}$$

Assuming $\delta_i \ll 1$ as in (6.19), we can use a first-order approximation:

$$\frac{P_{refl}}{P_{inc}} = (\frac{\delta_0 + \delta_2 - \delta_1}{\delta_1 + \delta_2 + \delta_0})^2 \tag{6.24}$$

Solving for δ_0, we have:

$$\delta_0 = (\frac{1 + \sqrt{\frac{P_{refl}}{P_{inc}}}}{1 - \sqrt{\frac{P_{refl}}{P_{inc}}}})\delta_1 - \delta_2 \tag{6.25}$$

If we were to try to solve for a difference in intra-cavity loss factors as in (6.40), we

would need to know δ_1. We can solve for δ_1 by determining an average value for F and $\frac{P_{refl}}{P_{inc}}$ with identical conditions in the cavity. From (6.20), we have:

$$\delta_0 + \delta_1 + \delta_2 = \frac{2\pi}{\mathcal{F}} \tag{6.26}$$

Now we can substitute 6.25 into 6.26 and solve for δ_1:

$$\delta_1 = \frac{\pi}{\langle\mathcal{F}\rangle}\left(1 - \sqrt{\langle\frac{P_{refl}}{P_{inc}}\rangle}\right) \tag{6.27}$$

$\langle\mathcal{F}\rangle$ and $\langle\frac{P_{refl}}{P_{inc}}\rangle$ are the average values of $\mathcal{F}$ and $\frac{P_{refl}}{P_{inc}}$ with only d_6 acetone in the cavity. It was thought that the average of many measurements would provide the most accurate value for δ_1.

Now that we know δ_1, we can solve for $\delta_0 + \delta_2$ from 6.25,

$$\delta_0 + \delta_2 = \frac{\pi}{\langle\mathcal{F}\rangle}\left[\frac{1 + \sqrt{\frac{P_{refl}}{P_{inc}}}}{1 - \sqrt{\frac{P_{refl}}{P_{inc}}}}\right]\left[1 - \sqrt{\langle\frac{P_{refl}}{P_{inc}}\rangle}\right] \tag{6.28}$$

Now we can solve for a difference in loss factors, as in (6.40),

$$\Delta\delta_0 = \delta_{0b} - \delta_{0a} = \frac{\pi}{\langle\mathcal{F}\rangle}\left[\left[\frac{1 + \sqrt{\frac{P_{refl}}{P_{inc}}_b}}{1 - \sqrt{\frac{P_{refl}}{P_{inc}}_b}}\right] - \left[\frac{1 + \sqrt{(\frac{P_{refl}}{P_{inc}})_a}}{1 - \sqrt{(\frac{P_{refl}}{P_{inc}})_a}}\right]\right]\left[1 - \sqrt{\langle\frac{P_{refl}}{P_{inc}}\rangle}\right] \tag{6.29}$$

6.2 Error Propagation

Since measuring the δ_0 due to absorption in cavity-enhanced spectroscopy involves several different measurements (each of which has an error), it would make sense to conduct a brief discussion of how errors are propagated from one measurement to the next. The general formula for propagating the standard deviation in an equation of several variables, whose variance and standard deviation are known and assumed to be uncorrelated is:

$$dF(x,y,z) = \sqrt{(\frac{\partial F}{\partial x})^2(dx)^2 + (\frac{\partial F}{\partial y})^2(dy)^2 + (\frac{\partial F}{\partial z})^2(dz)^2} \tag{6.30}$$

The first measurement is of δ_1, the losses due to the first mirror. From 6.27, we know that:

$$\delta_1 = \frac{\pi}{\langle \mathcal{F} \rangle} \left(1 - \sqrt{\langle \frac{P_{refl}}{P_{inc}} \rangle} \right) \tag{6.31}$$

Before we calculate the error in determining δ_1, we first need to calculate the error in measuring $\mathcal{F}$:

$$\mathcal{F} = \frac{\Delta f_{FSR}}{\Delta f_{FWHM}} \tag{6.32}$$

$$d\mathcal{F} = \sqrt{(\frac{1}{\Delta f_{FWHM}})^2 (d\Delta f_{FSR})^2 + (\frac{\Delta f_{FSR}}{(\Delta f_{FWHM})^2})^2 (d\Delta f_{FWHM})^2} \tag{6.33}$$

$$\begin{aligned} d\delta_1 &= \sqrt{(\frac{\partial \delta_1}{\partial \mathcal{F}})^2 (d\mathcal{F})^2 + (\frac{\partial \delta_1}{\partial \frac{P_{refl}}{P_{inc}}})^2 (d\frac{P_{refl}}{P_{inc}})^2} \\ &= \sqrt{(\frac{\pi}{\mathcal{F}^2})(1 - \sqrt{\frac{P_{refl}}{P_{inc}}}))^2 (d\mathcal{F})^2 + (\frac{\pi}{2\mathcal{F}})(\frac{P_{refl}}{P_{inc}})^{-1/2})^2 (d\frac{P_{refl}}{P_{inc}})^2} \end{aligned} \tag{6.34}$$

From

$$\delta_0 + \delta_2 = \delta_1 \left[\frac{1 + \sqrt{\frac{P_{refl}}{P_{inc}}}}{1 - \sqrt{\frac{P_{refl}}{P_{inc}}}} \right] \tag{6.35}$$

Our error in measuring δ_0 is:

$$\begin{aligned} d(\delta_0 + \delta_2) &= \sqrt{(\left[\frac{1 + \sqrt{\frac{P_{refl}}{P_{inc}}}}{1 - \sqrt{\frac{P_{refl}}{P_{inc}}}} \right])^2 (d\delta_1)^2 + (\frac{\partial(\delta_0 + \delta_2)}{\partial \frac{P_{refl}}{P_{inc}}})^2 (d\frac{P_{refl}}{P_{inc}})^2} \\ &= \sqrt{(\left[\frac{1 + \sqrt{\frac{P_{refl}}{P_{inc}}}}{1 - \sqrt{\frac{P_{refl}}{P_{inc}}}} \right])^2 (d\delta_1)^2 + (\frac{\delta_1 (\frac{P_{refl}}{P_{inc}})^{(-1/2)}}{(1 - \sqrt{\frac{P_{refl}}{P_{inc}}})^2})^2 (d\frac{P_{refl}}{P_{inc}})^2} \end{aligned} \tag{6.36}$$

6.2.1 Estimating the TEM_{00} Mode-Matching Factor

Since we are only monitoring the reflected signal in our experiment, there is no direct way to measure the mode-matching factor. The mode-matching factor is a measure of how well the incoming beam is mode-matched to the cavity. In all of our models, we have implicitly assumed that the mode-matching factor is 1, since we had no way of

measuring it. A way of estimating this factor is presented here.

The cavity finesse, $\mathcal{F}$, can be determined by directly measuring the axial spacing of TEM_{00} modes, Δf_{FSR}, and the cavity linewidth, Δf_{FWHM},

$$\mathcal{F} = \frac{\Delta f_{FSR}}{\Delta f_{FWHM}} \tag{6.37}$$

and can be related directly to the total cavity losses, $\mathcal{L}$:

$$\mathcal{F} = \frac{2\pi}{\mathcal{L}} \tag{6.38}$$

The total losses stem from the transmission of the cavity mirrors, $\delta_1 + \delta_2$, which is a function of the quality and number of dielectric coatings on each mirror, the scattering and absorption losses associated with each mirror, $\delta_{0_1} + \delta_{0_2}$, which stem from imperfections in the surface of each mirror, and other intra-cavity losses, $\delta_{0_{other}}$, which could come from scattering with or absorption by substances within the cavity.
So, our expression for finesse becomes:

$$\mathcal{F} = \frac{2\pi}{\delta_1 + \delta_2 + \delta_{0_1} + \delta_{0_2} + \delta_{0_{other}}} \tag{6.39}$$

Assuming that the transmission, scattering, and absorption losses for each mirror do not change over the course of an experiment, the Δf_{FWHM} of the cavity can be measured in the presence and absence of the absorber, and related directly to the losses due to the absorber.

$$\frac{2\pi}{\mathcal{F}_{(w/abs)}} - \frac{2\pi}{\mathcal{F}_{(w/o)}} = \frac{2\pi}{\Delta f_{FSR}}(\Delta f_{FWHM_{(abs)}} - \Delta f_{FWHM_{(w/o)}}) = \delta_{0_{abs}} \tag{6.40}$$

This absorption value is independent of any assumptions concerning the TEM_{00} mode-matching factor. Measurements of either the reflected or transmitted power do depend on such assumptions. In reflection, only some fraction of the incident power, ϵP_{inc} $(0 < \epsilon < 1)$, is perfectly mode matched to the TEM_{00} Gaussian mode. The remainder,

$(1-\epsilon)P_{inc}$, which is still detected, is essentially stray light and must be excluded for the purposes of determining transmission and loss factors. On resonance:

$$\frac{P_{refl}-(1-\epsilon)P_{inc}}{\epsilon P_{inc}} = (\frac{\delta_{0_T}+\delta_2-\delta_1}{\delta_1+\delta_2+\delta_{0_T}})^2 \approx (\frac{\delta_{0_T}}{\delta_1+\delta_2+\delta_{0_T}})^2 = (\frac{\delta_{0_T}}{\frac{2\pi}{\mathcal{F}}})^2 \tag{6.41}$$

This presents a challenge in determining loss factors, since only P_{refl} and P_{inc} can be directly detected. We can estimate ϵ by measuring $\delta_{0_{abs}}$ as in (6.40) and comparing that value to the value that should be obtained from measuring the cavity reflection signal. Simplifying (6.41) and solving for δ_{0_T},

$$\frac{1}{\epsilon}(\frac{P_{refl}}{P_{inc}}-1)+1 = (\frac{\delta_{0_T}}{\frac{2\pi}{\mathcal{F}}})^2 \tag{6.42}$$

$$\delta_{0_T} = \frac{2\pi}{\mathcal{F}}\sqrt{\epsilon'(R-1)+1} \tag{6.43}$$

where R is $\frac{P_{refl}}{P_{inc}}$ and ϵ' is $\frac{1}{\epsilon}$. $\Delta\delta_{0_{(abs)}}$ is determined by calculating the loss factor in the presence $\delta_{0_{(p)}}$ and in the absence $\delta_{0_{(a)}}$ of an absorber is:

$$\Delta\delta_{0_{abs}} = \delta_{0_{T_{(p)}}} - \delta_{0_{T_{(a)}}} = \frac{2\pi}{\mathcal{F}_p}\sqrt{\epsilon'(R_p-1)+1} - \frac{2\pi}{\mathcal{F}_a}\sqrt{\epsilon'(R_a-1)+1} \tag{6.44}$$

$$\begin{aligned}(\frac{\Delta\delta_{0_{abs}}}{2\pi})^2 &= [\frac{1}{\mathcal{F}_p}\sqrt{\epsilon'(R_p-1)+1} - \frac{1}{\mathcal{F}_a}\sqrt{\epsilon'(R_a-1)+1}]^2 \\ &= (\frac{1}{\mathcal{F}_p})^2(\epsilon'(R_p-1)+1) + (\frac{1}{\mathcal{F}_a})^2(\epsilon'(R_a-1)+1) \\ &\quad - \frac{2}{\mathcal{F}_a\mathcal{F}_p}\sqrt{(\epsilon'(R_p-1)+1)(\epsilon'(R_a-1)+1)}\end{aligned} \tag{6.45}$$

$$\begin{aligned}(\frac{(\Delta\delta_{0_{abs}})^2}{4\pi^2})(\mathcal{F}_a)^2(\mathcal{F}_p)^2 &= (\mathcal{F}_a)^2(\epsilon'(R_p-1)+1) + (\mathcal{F}_p)^2(\epsilon'(R_a-1)+1) \\ &\quad - 2\mathcal{F}_a\mathcal{F}_p\sqrt{(\epsilon'(R_p-1)+1)(\epsilon'(R_a-1)+1)}\end{aligned} \tag{6.46}$$

$$\begin{aligned}&\epsilon'[(\mathcal{F}_a)^2(1-R_p)+(\mathcal{F}_p)^2(1-R_a)] + [(\frac{(\Delta\delta_{0_{abs}})^2}{4\pi^2})(\mathcal{F}_a)^2(\mathcal{F}_p)^2 - (\mathcal{F}_p)^2 - (\mathcal{F}_a)^2] \\ &= -2\mathcal{F}_a\mathcal{F}_p\sqrt{(\epsilon'(R_p-1)+1)(\epsilon'(R_a-1)+1)}\end{aligned} \tag{6.47}$$

To make the algebra more manageable, we can rewrite (6.47) as:

$$(a\epsilon' + b) = c\sqrt{(\epsilon'(R_p - 1) + 1)(\epsilon'(R_a - 1) + 1)} \tag{6.48}$$

Squaring both sides, we have:

$$\begin{aligned} a^2\epsilon'^2 + 2ab\epsilon' &= c^2(\epsilon'(R_p - 1) + 1)(\epsilon'(R_a - 1) + 1) \\ &= c^2[\epsilon'^2(R_p - 1)(R_a - 1) + \epsilon'(R_a + R_p - 2) + 1] \end{aligned} \tag{6.49}$$

$$\epsilon'^2[a^2 - c^2(R_p - 1)(R_a - 1)] + \epsilon'[2ab - c^2(R_a + R_p - 2)] + [b^2 - c^2] = 0 \tag{6.50}$$

Simultaneously monitoring the cavity transmission and reflection would eliminate the uncertainty of both the mode-matching factor and the cavity finesse. This will be discussed further in the final chapter.

6.3 First-Generation Cavity

The first generation cavity was intended merely as a first step in understanding some of the technical issues involved in making measurements in a liquid-filled optical resonator. We also wanted to verify that it would be possible to make solution-based absorption measurements using cavity-enhanced spectroscopy. This cavity was made of aluminum, had medium-quality, commercially available mirrors, was designed to be solvent tight, and contained a single hole through which solvent could be injected. This cavity did not contain a piezo-electric device with which to change the cavity length; therefore, it was necessary to scan the laser in order to see a resonance peak. The Ti:Sapph laser was scanned using a Microlase Optical Systems MBR E-110 Laser Servo Controller. It controls an etalon within the Ti-Sapph that changes the its frequency by up to 40 GHz in each sweep. During some small time during the scan, the laser frequency fulfills a resonance condition and the cavity transmits resonant light from the cavity. This resonant light is what is measured by the oscilloscope and CCD camera. For ease of alignment, we chose to monitor the transmission power of

the cavity. The cavity transmission signal was monitored through both a CCD camera and a photodiode whose output was sent to a Tektronix 3032 digital oscilloscope. The arrangement of transverse modes could be monitored on the oscilloscope and the resonance peak that corresponds to the TEM_{00}, which, in the near-planar regime, is the lowest-frequency mode in each free spectral range could be identified and maximized. The CCD camera was particularly useful because the shape of the transverse mode could be observed as the cavity was aligned to the TEM_{00}. The TEM_{00} is easy to discriminate from the higher-order modes, because it is spherical in shape and the higher-order modes are multi-lobal and generally larger in size.

Once the cavity was properly aligned, the oscilloscope was used to measure the Δf_{FWHM} of the resonance peak. An EO was used in this setup in order to place sidebands on the optical signal. In this case, the sidebands were used as a frequency reference by which to measure the Δf_{FWHM}. The sidebands were modulated at 20 MHz. Therefore, on the oscilloscope, the temporal 'distance' the sidebands is 40MHz. When the Δf_{FWHM} is measured on the oscilloscope, this temporal 'distance' is correlated to the temporal distance between the center of the resonance peak and one sideband and is 'converted' to a true frequency. A complete set of measurements of the Δf_{FWHM} of an air-filled cavity were made in order to determine the actual finesse of the mirrors between 770 nm and 830 nm, the spectral range of the absorption due to the Qy transition in bacteriochlorophyll a (Bchla), the transition in which we are most interested because of the role in plays in electron transfer in Bchla-containing photosynthetic reaction centers. We found that the $\langle \Delta f_{FWHM} \rangle$ between 770 and 800 nm to be 2.87 $\pm$ 0.25 MHz, which corresponds to a $\mathcal{F}$ of 5335 $\pm$ 485, confirming that the reflective coating on the mirrors would give uniform results in the spectral range of interest.

Once the cavity was properly aligned and the cavity parameters were characterized, our first goal was to make a series of finesse measurements with various solvents in the cavity, including acetone, hexanes, heptane, methanol, ethanol, isopropyl alcohol, diethyl fumerate, and water in order to determine the best solvent with which to make absorption measurements of Bacteriochlorophyll a (Bchla). We found that any solvents

with a hydroxyl group (which includes water and the alcohols (methanol, ethanol, and isopropyl alcohol)) absorb or scatter so greatly between 770 nm and 830 nm that the Δf_{FWHM} of the transmitted peak could not be measured, because the resonance peak overlapped with the side bands. The results of measurements with hexanes or heptanes were very promising: the Δf_{FWHM} was 4.00 MHz at 770 nm. While these results would make either of these solvents good candidates for use with Bchla, Bchla's poor solubility in either of these solvents would be problematic enough to preclude using either of them. The results of measurements with acetone or diethyl fumerate were roughly equivalent, though they appeared a bit less promising. Bchla has suitable solubility in both acetone and diethyl fumerate; however, the viscosity of diethyl fumerate and its tendency to stick to the mirrors makes it less suitable than acetone. All things considered, acetone was chosen as the best solvent for making measurements with Bchla. The $\langle \mathcal{F} \rangle$ with acetone was 2828 ± 253. This represent a 47 percent reduction in $\mathcal{F}$, which is less than ideal, but the best we could do at the time.

We wanted to make some preliminary measurements of Bchla absorption in this cavity, to be sure that the cavity would provide roughly the anticipated enhancement factor. Our initial measurements were at concentrations comparable to what the UV/VIS Spectrophotometer requires (25 to 100 μ M). We found that these samples were far too concentrated for our apparatus, since we could not even observe a resonance peak at those concentrations, indicating that the losses due to absorption were higher than the mirror reflectivities. The transmitted intensity can be expressed in terms of the loss factors [23]:

$$\frac{I_{trans}}{I_{inc}} \approx \frac{4\delta_1\delta_2}{(\delta_0 + \delta_1 + \delta_2)^2} \tag{6.51}$$

Assuming equal mirror reflectivities and no internal losses, this ratio would be 1. As the intra-cavity loss factor (δ_0) increases to above the mirror reflectivities, the ratio rapidly approaches 0. After a number of attempts, a 2.0 μM solution of Bchla in acetone was injected into the cavity. The resonance peak with Bchla and acetone in the cavity is shown in Figure 6.1. The Δf_{FWHM} was determined to be 8.73 MHz, which corresponds

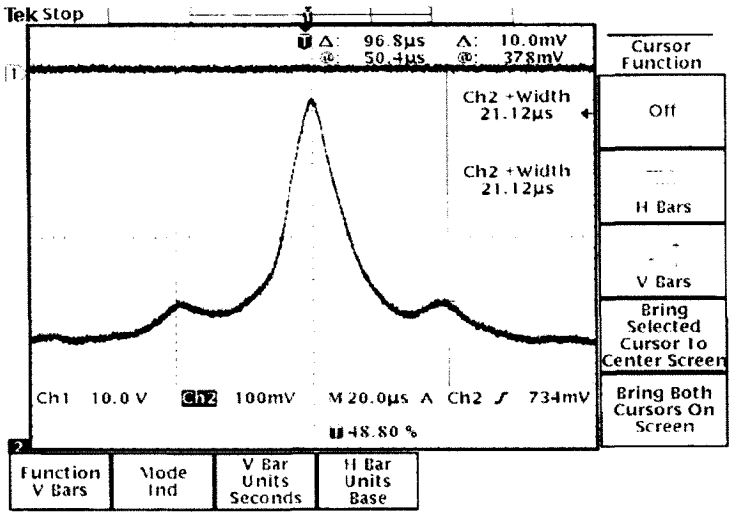

Figure 6.1: Transmission Peak from First-Generation Cavity

to a $\mathcal{F}$ of 1264. The losses due to absorption of Bchla is merely:

$$\delta_{0_{Bchla}} = 2\pi(\frac{1}{F_{Bchla+acetone}} - \frac{1}{F_{acetone}}) = 2\pi(\frac{1}{1264} - \frac{1}{2828}) = 2.80e-4 \tag{6.52}$$

These losses correspond to a molar extinction coefficient of 30.43 $mM^{-1}\ cm^{-1}$. These preliminary investigations demonstrated that cavity-enhanced spectroscopy could be used to make very sensitive absorption measurements. The next step would be to build a cavity with the best possible mirrors and in which the resonance condition can be maintained continuously by locking the cavity. This cavity should also allow for the injection of solvent and absorbers with minimal disturbance to the cavity so that 'real time' absorption measurements can be made.

6.4 Next Generation

The second generation cavity, servo, and optical setup have been described in some detail in the previous chapters. To avoid redundancy, in this chapter we will limit our discussion of these systems to topics that relate directly and practically to making measurements.

6.4.1 Locking the Cavity

The most important aspect of cavity-enhanced spectroscopy is locking the cavity; it also turned out to be the most difficult. The general procedure for locking the cavity with air or solvent is similar. The key point in the lock procedure is managing the DC offset of the error signal. A number of methods of dealing with this offset were attempted; however, the best practical solution was to use a DC voltage offset adder/subtractor. The starting point for attempting to lock the cavity is to be monitoring the reflected DC voltage and the error signal on an oscilloscope and to be scanning the piezo. The DC offset to the piezo should be adjusted so that the resonance peak and error signal are in the middle of a scan (triggering on the piezo scan voltage). We tended to scan at a few hertz and with the lowest practicable amplitude (which is set by the amount of drift in the resonance peak with respect to the scan voltage, caused by some thermal effects and by piezo hysteresis). Another very important factor is the phase of the error signal. This is different for each experimental setup; however, the error signal must be negative on the high frequency side and positive on the low frequency side. The phase of the error signal (i.e. whether the error signal is positive on the high frequency side or the low frequency side) can be changed by adjusting the DC voltage to the EO VCO (which changes the f_{EO}). It should also be noted that changing the f_{EO} can affect the amount of noise the EO adds.

The next step in the locking procedure is to record the DC offset voltage to the piezo and then turn off the scan signal (which reduces the voltage to the piezo by the average amplitude of the scan voltage). The DC offset on the error signal should then be minimized to as close to zero as practicable. The best test of whether it was sufficiently zeroed is to flip the integrate switch and observe how quickly the integrator increases the voltage to the piezo. The more slowly the integrator integrates, the better zeroed the error signal DC offset. The DC offset should be adjusted until the integrator voltage either does not move or moves very slowly. At this point, the DC offset to the piezo should be returned to the recorded voltage (i.e. its value before removing the scan

voltage). As the voltage gets closer to that value, the DC reflected voltage will tend towards the top/bottom of the resonance peak (depending upon whether the photodetector gain is positive or negative): the New Focus detector we used had a positive gain (which means the reflected peak is below baseline) and the Hammamatsu detector has a negative gain (which means the reflected peak is above baseline). A fine adjust to the piezo DC offset is helpful at this point. Only having a single potentiometer to adjust this voltage will make it unnecessarily difficult to get this offset voltage to the appropriate value. It should be possible to adjust the piezo voltage such that the reflected voltage is staying at resonance most of the time. At this point, the output of the AO servo should be sent to the AO so that the AO locks. This can be conveniently done with a "lock switch" that connects the output of the last stage in the AO servo to the AO VCO. The precise gain values in either branch must ultimately be determined empirically, based upon optical power, noise, etc. Once the AO servo has grabbed, the piezo branch of the servo should be connected to the piezo. In our setup, this amounts to flipping an "integrate switch," which initiates integration (with the integrate switch off, there is a resistor parallel to the integrating capacitor, which causes that op amp to low pass at extremely low DC gain). At this point the cavity should be locked.

A locked cavity is susceptible to low-frequency vibrational and thermal noise, particularly when the cavity or components connected to the cavity are touched during an experiment. This requires very high gain at low frequencies. Our piezo branch gain was adjusted several times to enable the servo to keep a lock during strong vibrational transients. In fact, our servo would even remain locked while tapping on the cavity.

Figures 6.2 and 6.3 present a comparison between unlocked and locked reflected power from an air-filled cavity with the Ti:Sapph etalon high voltage supply disconnected. The high voltage supply to the Ti:Sapph etalon was identified as the source of significant frequency noise at 160 kHz, particularly in the face of amplitude noise for several sources. Our initial solution was merely to disconnect the etalon voltage. The disadvantage of doing this is that the Ti:Sapph is susceptible to mode hopping or being in more than one mode at a time. If this happens while the cavity is locked, the lock

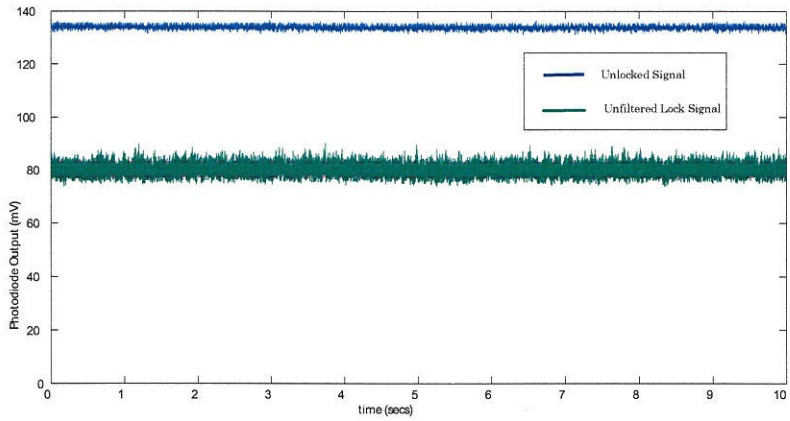

Figure 6.2: Unlocked and Unfiltered Lock On Tektronix Digital Scope

will almost certainly be lost. These data were taken with the Tektronix TDS3034B Scope (9 bit resolution, 10,000 sample maximum) and a 125 MHz New Focus photodetector (1801-FS) with air in the cavity. In Figure 6.3, the comparison is between the lock signal and the unlocked signal, both filtered at 20 MHz by the oscilloscope. The unfiltered lock signal is clearly noisier than the unlocked signal (by a factor of approximately 6). Figure 6.2 compares the locked signal filtered with a 10 kHz low-pass filter with the unlocked signal filtered at 20 MHz on the scope. The filtered lock signal is significantly less noisy (by a factor of 6.6) than the unfiltered signal. Filtering at 10 kHz or lower is justified in our experiment, the only transients we will be observing are less than 1 kHz (i.e. on the diffusion timescale). Motivated by a desire to minimize photobleaching and intensity-related thermal effects within the cavity by minimizing the incident optical power, we decided to rethink our photodetection scheme. The New Focus photodetector has much more bandwidth than we needed (i.e. 125 MHz) and was not designed for low power applications. We decided on a photodetector that was designed for low power application (i.e. in the hundreds of nW and below). With this detector, the resonance peak had an amplitude in the range of 3.5 to 4.5 volts just below maximum input power (as opposed to approximately 100 mV with the New Focus detector with tens of μW of optical power). We also decided that a more sophisticated photodetection scheme was warranted. Instead of taking data on the Tektronix oscil-

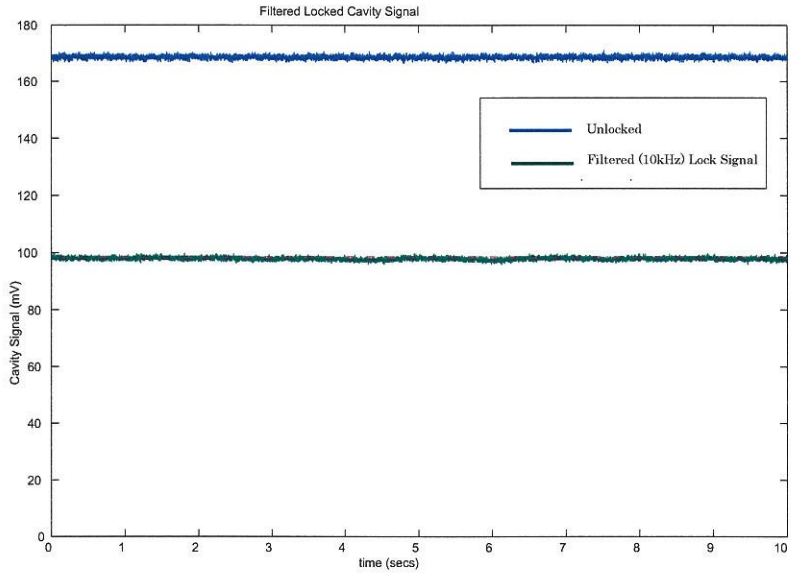

Figure 6.3: 10 kHz Filtered Lock and Unlocked

loscope, we chose to use a Gage Compuscope 14100 data acquisition card. In addition to being of superior quality (i.e. the card has 14 bit resolution, 128 Mbytes of memory, and a sampling rate of up to 100 MS/s), the Gage data acquisition card was procedurally easier to use. We wrote some MATLAB code that specified all of the necessary data acquisition parameters and could initiate data acquisition by pressing a single button. This board could take data for several hours (whereas the oscilloscope could only record 10,000 data points).

Figures 6.4 and 6.5 were taken with the Hammamatsu photodetector and the Gage data acquisition board, controlled by MATLAB (sampled at 60 Hz). In Figure 6.4, there is only air in the cavity. In Figure 6.5, the cavity was filled with d_6 acetone. We found d_6 acetone to be nearly optically transparent between 770 and 800 nm, whereas regular acetone increases losses roughly by a factor of 3.

This might be a convenient time to discuss the special procedures for filling the cavity with solvent and locking under those conditions. The main concern in filling the cavity with solvent is that there be no air bubbles in the beam path. This is particularly difficult to determine the first time a cavity is filled, since some amount of realignment

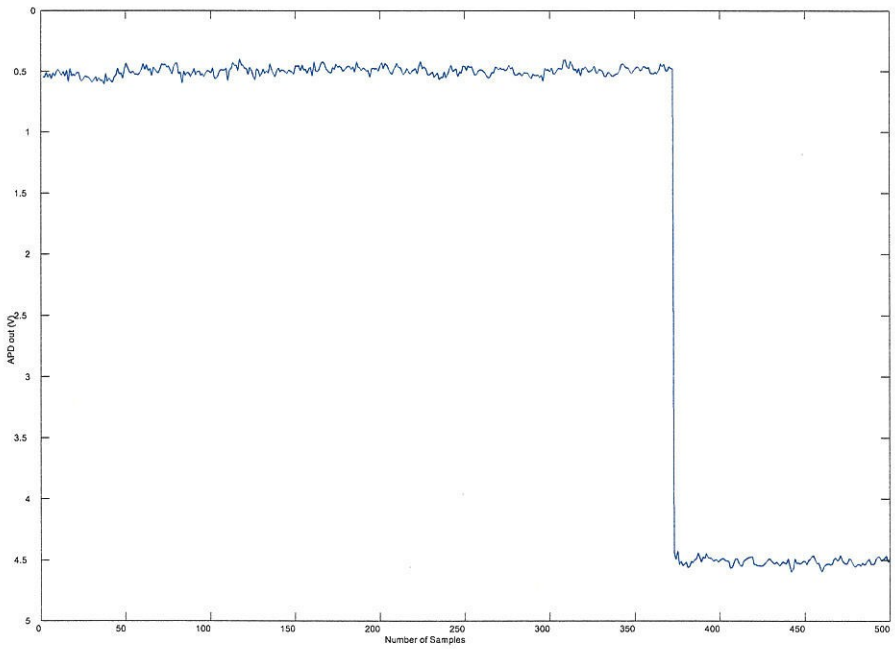

Figure 6.4: Baseline Locked and Unlocked

is necessary after filling (i.e. the absence of modes within a filled cavity may be due either to air bubbles, misalignment, or both). The need for realignment is not so much due to changes in the parameters of the Gaussian mode in the cavity as it is to simple optical alignment. For example, if 'perfect' alignment with air in the cavity required that the beam hit the first mirror at a slight angle (due to the cavity mirrors not being exactly vertical), introducing acetone into the cavity would require a change in such an angle, because the index of refraction inside the cavity would be higher (i.e. there would be less refraction at the inside surface of the first mirror). The geometry of the cavity will dictate how best to fill it to avoid air bubbles. For our cavity, filling from the bottom up by suctioning through the top was the best way to avoid bubbles. If using regular d_6 acetone, another significant issue becomes the hygroscopicity of acetone. This is particularly a problem in the range of 770 to 800 nm, since water seems to absorb significantly. Even the smallest amount of water or deuterated water (i.e. a few volume percent) introduces significant intra-cavity losses. The best solution is to keep the d_6 acetone (and the cavity, if possible) under nitrogen.

Locking with solvent in the cavity is more difficult than locking with air in the cavity. The main reason would seem to be that there are significant solvent-mediated thermal transients. Another possible reason may be solvent-mediated non-linearities in piezo action. At any rate, the procedure for locking a solvent-filled cavity varies primarily in the gain requirements and the sensitivity to low frequency transients. In the initial attempts to lock with acetone in the cavity, the piezo gain seemed to be too low (i.e. the lock was lost during transients which would not have much affected the lock of an air-filled cavity). Increasing the gain in the piezo branch (by a factor of 10) (and associated adjustments to the AO branch to ensure stable crossing of the transfer function of each branch) resulted in the ability to lock stably. Having the piezo branch gain adjustment at maximum when beginning to integrate reliably resulted in a good lock. The most notable feature of Figure 6.5 in comparison to 6.4 is the presence of stronger low frequency transients (almost certainly thermal).

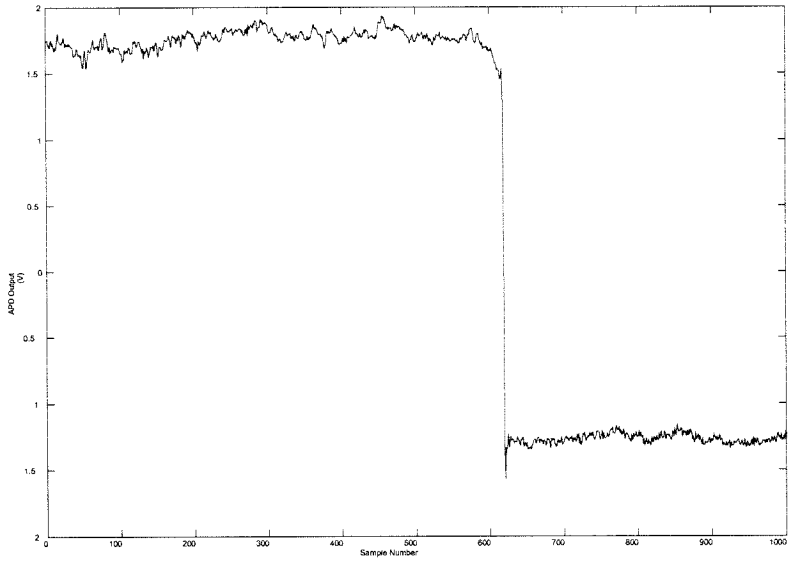

Figure 6.5: d_6 Acetone with Loss of Lock

6.5 Injection

The measurements we made on a concentration series of Bchla in d_6 acetone involved measuring the finesse of the cavity and measuring the reflected power before and after injecting Bchla into a locked cavity. Measuring the finesse amounts to measuring the Δf_{FWHM} and the Δf_{FSR}. As was discussed in 6.20, the finesse measurements are representative of the total losses within the unlocked cavity at the time of the measurement. The limitation of finesse measurements is that they represent a snapshot of the losses. The errors associated with measuring the Δf_{FWHM} are mostly informed by non-linearities in the piezo scan and, to a lessor extent, by instablities/noise on the EO VCO (which sets the frequency of the side bands, which are used as a frequency reference in measuring the Δf_{FWHM}). Another contributor is the jitter in the relative frequency of the laser/cavity on the timescale of the piezo ramp through resonance. Finesse measurements are also prone to errors in measuring the Δf_{FSR}. The most accurate way to measure the free spectral range is to disconnect the piezo from its voltage source and manually tune the Ti:Sapph Servo Controller etalon. This requires the use

of a wavemeter (such as the Burleigh WA 1500) to record the optical frequency at each free spectral range. The basic procedure is to turn adjust the etalon until a resonance is observed on the reflected DC voltage (much like what was observed when adjusting the piezo DC offset when locking) and record the optical frequency and then tune until another resonance is observed and record that optical frequency. The difference in optical frequencies will be the Δf_{FSR}.

Injecting solvent into a locked cavity is a very delicate procedure and took many iterations to find a protocol that worked reliably. The first requirement is to know the volume of the cavity precisely, since this is the volume into which the concentrated sample of Bchla will be diluted. The goals of the injecting procedure are to ensure that all of the injected volume enters the cavity and that the volume reaches the beam volume as quickly as possible with the least amount of vibrational and flow-related disturbance. The best practical method turned out to be using the smallest glass syringe available (1 cc) with a 10 inch spinal needle. The larger syringe was removed and the spinal needle was inserted through the tubing and as deeply through the metal fitting into the cavity as possible. An important factor here was appropriate stabilization of the syringe and tubing. Two separate clamps stabilized the syringe and another stabilized the tubing between the syringe and the cavity. As a first test, the cavity was locked and 100 μL of straight d_6 acetone was injected into the syringe and allowed to enter the cavity by gravity. This caused no perceptible transients. Next, the same amount of d_6 acetone was placed in the glass syringe and forced through with the syringe plunger. This caused significant transients, but the lock was not lost. With this information, we made our first attempt at injected a concentrated sample of Bchla into a locked cavity. We tried 'gravity' injection and forced injection. The advantage of gravity injection is that it causes the least vibrational and flow-related transients. The disadvantage is that it took an unpredictable amount of time for the Bchla to reach the beam. An example of gravity injection is provided in Figure 6.6.

At the beginning of the experiment, a d_6 acetone-filled cavity is locked and the APD voltage from the cavity begins being recorded. A concentrated sample of Bchla is grav-

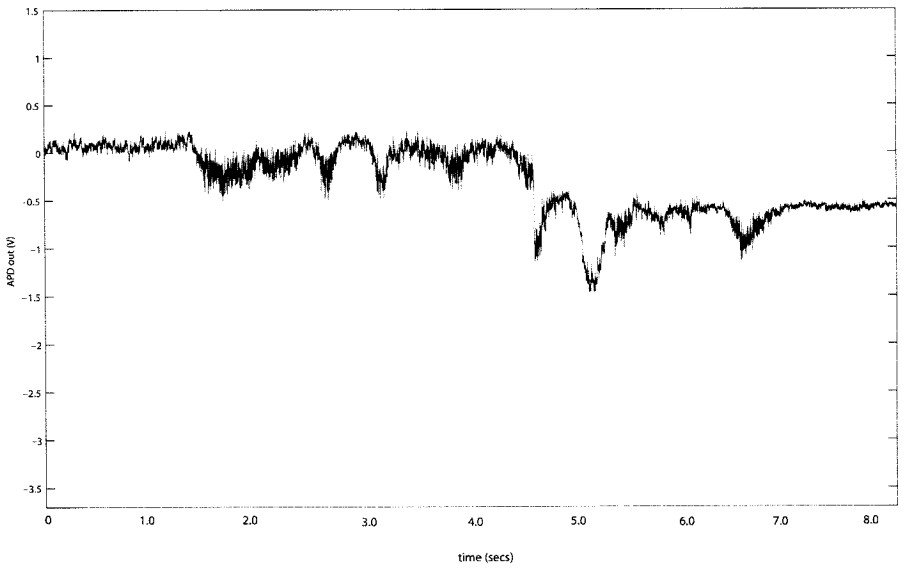

Figure 6.6: Bacteriochlorophyll a Absorption

ity injected into the locked cavity. After some amount of time, the Bchla diffuses through the d_6 acetone within the cavity. As it enters the beam volume, it causes the APD voltage to fluctuate as it decreases to its new equilibrium value. The higher APD voltage(+66.1 mV ($\pm$ 48.2 mV)) at beginning of the figure (to the left) reflects the pre-absorption phase and is, therefore, indicative of the losses due to the two mirrors and to d_6 acetone . This voltage can be converted to $\frac{P_{refl}}{P_{inc}}$, from which the losses can be calculated directly using (6.25). The lower APD voltage at the end of the experiment (to the right) (-561.7 mV $\pm$ 25.6 mV) represents the absorption phase and corresponds to the losses due to the two mirrors, d_6 acetone, and the Bchla. The losses due to Bchla alone can be determined by calculating the intra-cavity losses due to d_6 acetone (given by the higher APD voltage) and subtracting that value from the losses due to d_6 acetone and bacteriochlorophyll (given by the lower APD voltage), the assumption being that the losses associated with each cavity mirror do not change during the experiment.

$$\delta_{0Bchla} = \delta_{0(acetone+Bchla)} - \delta_{0(acetone)} \tag{6.53}$$

This turns out to be a particular application of (6.29). Overall, we have:

$$\delta_{0Bchla} = \delta_{0Bchla+acetone} - \delta_{0acetone}$$
$$= \frac{\pi}{\langle F \rangle}\left[\left[\frac{1+\sqrt{(\frac{P_{refl}}{P_{inc}})_{Bchla+acetone}}}{1-\sqrt{(\frac{P_{refl}}{P_{inc}})_{Bchla+acetone}}}\right] - \left[\frac{1+\sqrt{(\frac{P_{refl}}{P_{inc}})_{acetone}}}{1-\sqrt{(\frac{P_{refl}}{P_{inc}})_{acetone}}}\right]\right]\left[1-\sqrt{\langle\frac{P_{refl}}{P_{inc}}\rangle}\right] \tag{6.54}$$

Figure 6.7 presents an example of series of forced injections of Bchla into a locked cavity. The injection time is indicated by an arrow. The first injection was the most strongly forced of the three depicted in the the figure, as evidenced by the increased noise at the beginning of the trace. This represents a combination of vibrational and flow-related noise due to the force with which the Bchla was injected. Due to the force of the injections, the cavity momentarily lost lock several times during the experiment (as evidenced by the high amplitude excursions of the DC reflected voltage). Despite the noise, it is clear in this figure that the DC reflected voltage deceases and reaches a new steady-state value after each injection, indicating a concomitant increase in the intra-cavity losses.

6.6 Data Summary

The goals of this experiment are (a) to use a cavity-enhanced spectroscopic device to measure the absorption due to a known concentration of Bacteriochlorophyll a (Bchla) in real time and (b) establish the overall sensitivity of the device. The overall sensitivity of the present device at measuring Bchla absorption is summarized in Figure 6.8. Numerous concentrations of Bchla (determined as series dilutions) were introduced into a locked cavity and the overall intra-cavity losses due to Bchla absorption (δ_{0Bchla}) were measured as described above. A plot of these losses as a function of [Bchla] is presented as is a best linear fit of them. The normalized slope of a best fit from free-space, single pass measurements is also presented to demonstrate that the cross section for absorption agrees with the value obtained from conventional measure-

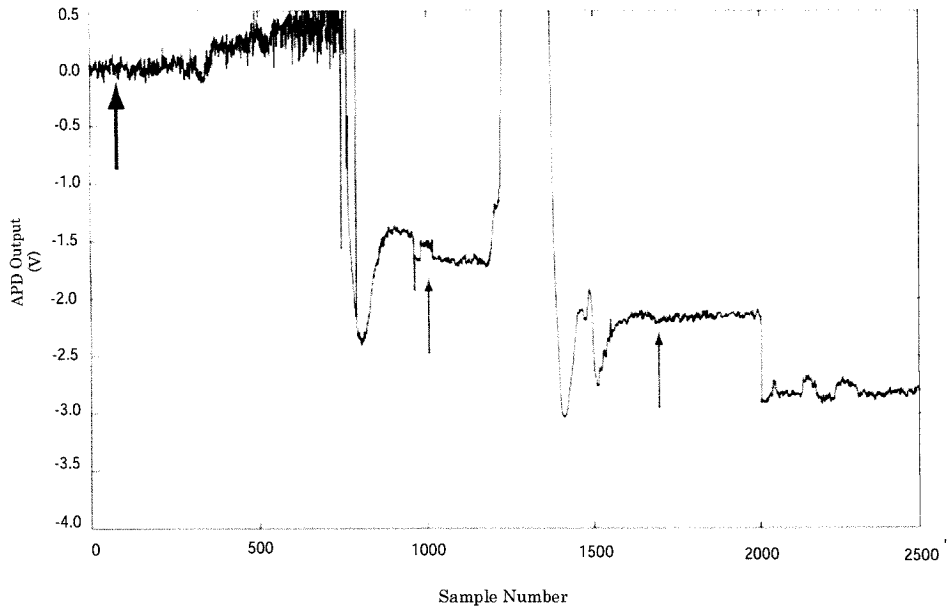

Figure 6.7: Multi-Injection Transients

ments. The sensitivity threshold of this device was determined to be approximately 54.8 pM based upon the normalized residuals in Figure 6.9 and upon an effective sampling bandwidth of 1 kHz. At concentrations below 54.8 pM, the normalized residuals increased significantly (11.0pM (9.3), 1.1pM (12.5)) from the mean (7.76e-2), indicating that those measurements are beyond the sensitivity of this device.

From Figure 6.8, the enhancement factor of cavity-enhanced spectroscopy over free space measurements with the same interaction length is not immediately obvious. In Figure 6.10 the slope of the $log(\frac{P_f}{P_i})$ versus concentration of Bchla is presented for both free space and cavity-enhanced measurements. The main feature of this figure is the ratio of the slopes. It represents the enhancement factor of cavity-enhanced measurements over free space measurements. The actual difference in slopes presented in Figure 6.10 is 19,242, which is within eleven percent of the predicted enhancement factor of $2\mathcal{F}/\pi$ (21,645). The primary purpose of this figure is to demonstrate that the

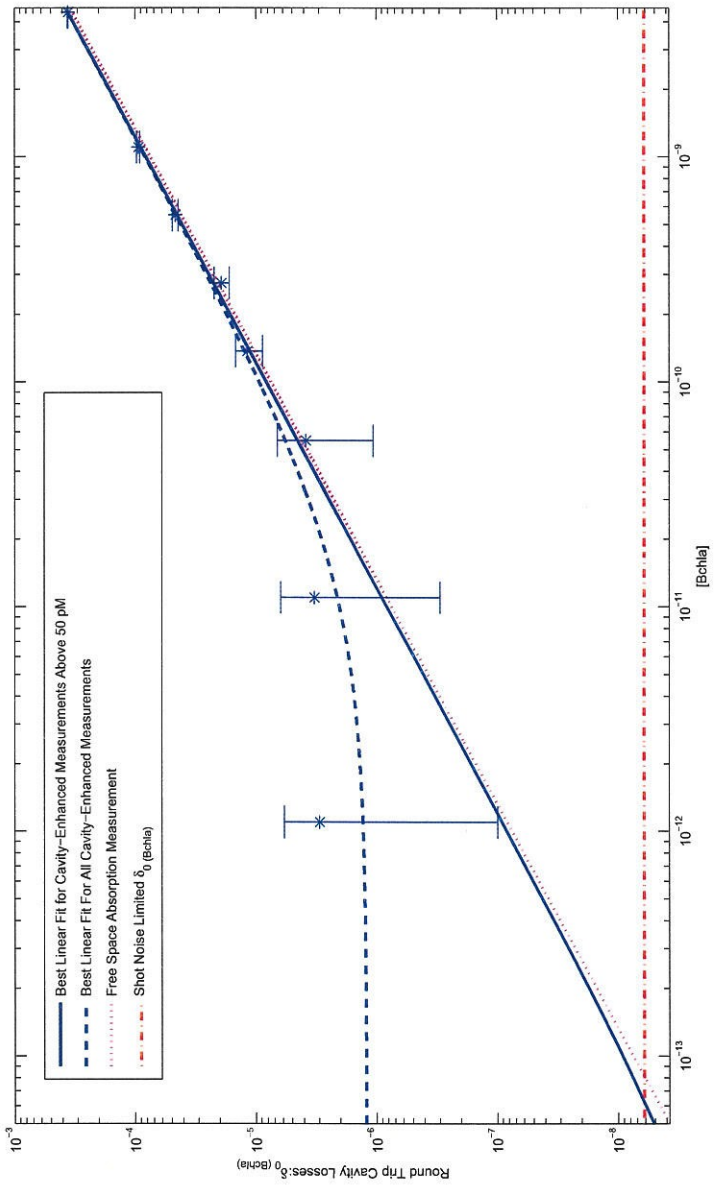

Figure 6.8: Summary of Bacteriochlorophyll Absorption Data

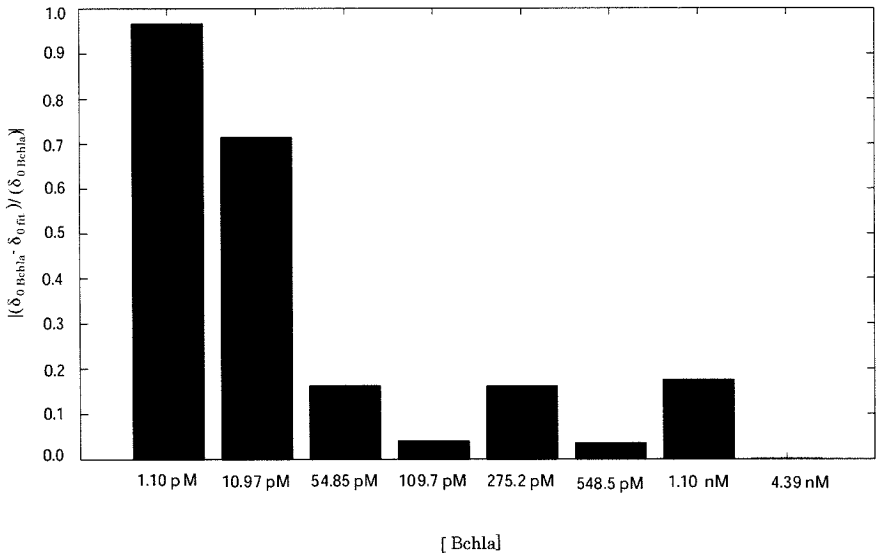

Figure 6.9: Absorption Data Residuals

actual enhancement factor is of the same order of magnitude as the predicted factor. Figure 6.11 shows the round trip losses due to various concentrations of Chlorophyll a at 771 nm. These losses were computed by measuring the Δf_{fwhm} of the cavity resonance in the presence of various concentrations of Chlorophyll a and the Δf_{FWHM} in the presence of acetone alone, as described in equation 6.52. The structure of Chlorophyll a is very similar to the structure of Bacteriochlorophyll a, but its Q_y absorption peak is 100 nm lower (670 nm) and is not purported to absorb appreciably at 780 nm. The purpose of the figure is to demonstrate that the losses we report are due to absorption by Bchla are, in fact, due to absorption and not scattering. At concentrations 50 times higher than the concentrations of Bchla we measured, Chlorophyll a, on average, causes no measurable loss. This result supports our conclusion that the losses we measured due to Bchla are due to Q_y absorption.

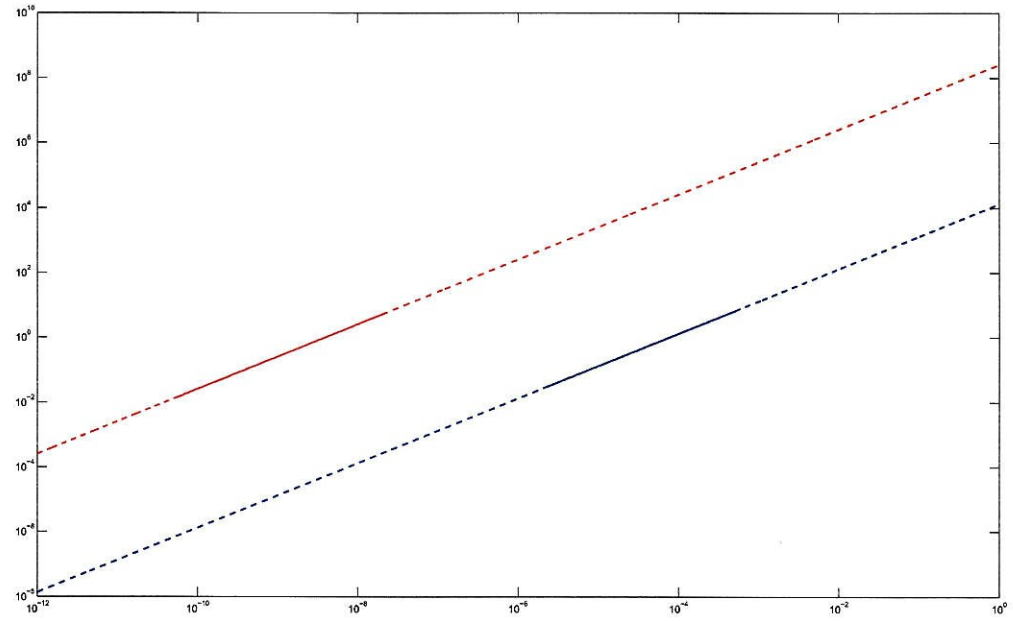

Figure 6.10: Enhancement factor for Cavity-Enhanced Spectroscopy

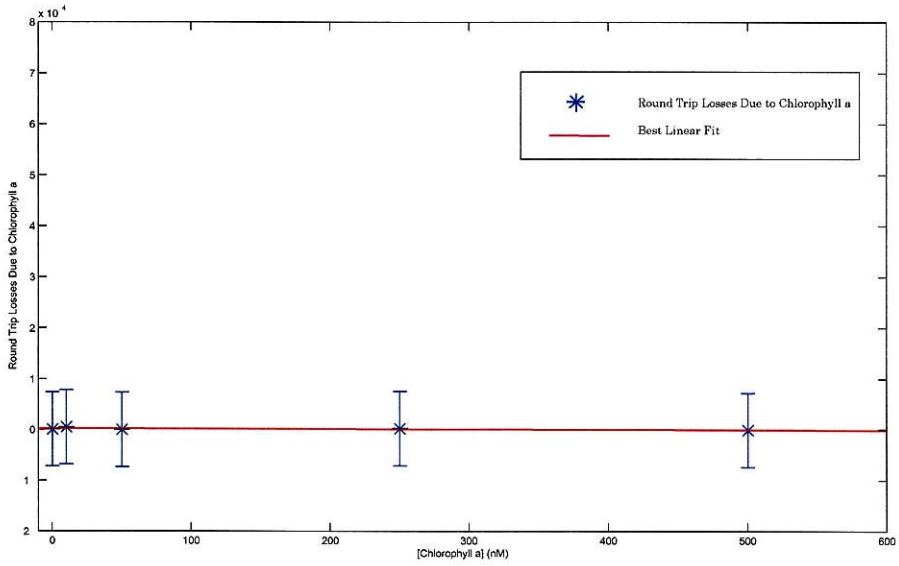

Figure 6.11: Intra-cavity Losses Due to Chlorophyll a

Chapter 7

Noise Considerations

The primary concern in an optical technique such as cavity-enhanced spectroscopy is the control and minimization of all sources of noise: electronic, vibrational, thermal, and laser-associated (which includes amplitude, frequency and shot noise). Electronic noise is associated with power supplies, electronic circuits, and photodetectors. Vibrational noise can be caused by movement on or near the optical table and even by air currents from a nearby fan or air conditioner. The main causes of thermal noise are localized heating in the solvent and on the mirrors and fluid flow-related transients. Our lock servo was designed to control all frequency noise in the bandwidth within which we are interested. Shot noise is unavoidable and will be discussed in a later section. Amplitude noise can be associated with the laser itself or can be added by electro-optical elements such as an EO or an AO. In our previous models of the optical beam, we did not consider amplitude noise; however, it might be useful to do so here, since it can become a significant component of the error signal and DC reflected signal and must be properly addressed.

7.1 Amplitude Noise

7.1.1 Error Signal

Despite our best attempts at aligning the EO, some residual amplitude modulation at the $f_{EO}(\Omega)$ remains. A simple model for the effect of the EO on the incident field would

be:

$$\tilde{E}_{inc} = E_0 e^{i(\omega t + \beta sin(\Omega t))}(1 + \epsilon sin(\Omega t)) \tag{7.1}$$

where ϵ indicates the extent of amplitude modulation. Although this may seem innocuous in so far as it is at a frequency beyond our bandwidth of interest, it adds a component to the error signal we had not anticipated. Following the same procedure as we did in Chapter 2, we come up with our final expression for the error signal with amplitude modulation:

$$\begin{aligned} E = & -2E_0^2 V_0 J_1(\beta) J_0(\beta) \frac{\delta\omega}{\pi \Delta f_{FWHM}} cos(\theta(\Omega, t))(1 + \epsilon^2) \\ & + \epsilon E_0^2 V_0 \left(\left(2J_1^2(\beta) + J_0(\beta)^2 \left(\frac{\left(\frac{\delta f}{\Delta f_{HWHM}}\right)^2 + \left(\frac{r_1 - r_2 e^{-\alpha_0 p}}{1 - r_1 r_2 e^{-\alpha_0 p}}\right)^2}{1 + \left(\frac{\delta f}{\Delta f_{HWHM}}\right)^2} \right) \right) \right) \end{aligned} \tag{7.2}$$

The important result here is that the error signal has a DC component due to residual amplitude modulation. We can see that the DC offset is affected by laser power, modulation depth, the extent of amplitude modulation, proximity to resonance, and cavity parameters such as mirror reflectivity, intra-cavity losses, etc. This DC offset must be appropriately managed when trying to lock the cavity, as discussed in the section on servo design.

7.1.2 DC Amplitude Noise

In considering noise on the DC reflected signal, we make our model one degree more sophisticated. This time we consider both the EO and the AO. As before, we consider the optical field after one pass through the EO (with frequency Ω and amplitude modulation fraction ϵ); however, we also consider the 2 passes through the AO (with frequency $\Omega^{'}$ and amplitude modulation fraction $\epsilon^{'}$). Our model for the reflected field

is:

$$\tilde{E}_{refl} = E_0(J_1(\beta)F(\omega+2\Omega^{'}+\Omega)exp[i(\omega+2\Omega^{'}+\Omega)t] + J_0(\beta)F(\omega+2\Omega^{'})exp[i(\omega+2\Omega^{'})t] - J_1(\beta)F(\omega+2\Omega^{'}-\Omega)exp[\imath(\omega+2\Omega^{'}+\Omega)t])(1+\epsilon sin(\Omega t))(1+\epsilon^{'}sin(\Omega^{'}t))^2 \tag{7.3}$$

The reflected intensity will have the same form as the ideal case, except for the amplitude modulation terms.

$$\begin{aligned} I_{refl} &= E_0^2(2J_1^2(\beta)+J_0(\beta)^2 \mid F(\omega+2\Omega^{'}) \mid^2 \\ &+ 4J_0J_1i\Im(F(\omega+2\Omega^{'})sin(\Omega t) \\ &+ 2J_1^2cos(2\Omega t))(1+\epsilon sin(\Omega t))^2(1+\epsilon^{'}sin(\Omega^{'}t))^4 \end{aligned} \tag{7.4}$$

Since we are interested in examining the noise on the detected signal rather than the mixed-down error signal, it would be helpful to substitute our previously-derived expressions for the reflection coefficient:

$$\begin{aligned} I_{refl} &= E_0^2(2J_1^2(\beta)+J_0(\beta)^2\left(\frac{\left(\frac{\delta f}{\Delta f_{HWHM}}\right)^2+\left(\frac{r_1-r_2e^{-\alpha_0 p}}{1-r_1r_2e^{-\alpha_0 p}}\right)^2}{1+\left(\frac{\delta f}{\Delta f_{HWHM}}\right)^2}\right) \\ &- 4J_0J_1\frac{\delta\omega}{\pi\Delta f_{FWHM}}\left(\frac{e^{-\alpha_0 p/2}(1-r_1^2)}{1-r_1r_2e^{-\alpha_0 p}}\right)sin(\Omega t) \\ &+ 2J_1^2cos(2\Omega t))(1+\epsilon sin(\Omega t))^2(1+\epsilon^{'}sin(\Omega^{'}t))^4 \end{aligned} \tag{7.5}$$

The first two terms are at DC and contain the resonance signal and side bands. The third term, when mixed down with the EO LO is what gives us our error signal. It comes from the beat of a side band with the resonance signal. In its 'raw' detected form, it is modulated at the frequency of the EO LO (36 MHz). The last term comes from the beating of the sidebands with each other and is at two times the frequency of the EO LO. The latter two terms are high enough in frequency that it is quite easy to filter them out; therefore, they will not be given further consideration. The amplitude modulation added by both the AO and EO add DC noise terms in $\frac{\epsilon^2}{2}$, $\frac{13(\epsilon^{'})^2}{4}$, and

$\frac{(\epsilon')^4(\epsilon)^2}{8}$. The first two terms are only in the square of the modulation fraction and contribute to the noise on the DC reflected signal.

7.2 Noise Sources

Our actual sensitivity was $1.20 \times 10^{-7}/\sqrt{Hz}$ ($Absorbance = 5.21 \times 10^{-8}/\sqrt{Hz}$) which is approximately 618 times higher (i.e. worse) than the expected sensitivity in a shot noise-limited regime. In addition to the aforementioned amplitude noise, the sources of noise that kept us from reaching the shot noise limit were frequency noise on the Ti:Sapph laser (largely from a strong 160 kHz noise from the etalon HV), several thermal-mediated noise sources associated with the cavity, vibrational noise on the optical table, and electronic noise introduced by the lock servo. The frequency noise on the Ti:Sapph could be reduced either by optimizing gain settings the Ti:Sapph or by building a separate lock servo. Vibrational noise could be reduced by improved vibrational damping on the cavity mount and on the optical table. One possible solution would be to build a box around all of the components in the experiment and devise a way of injecting solvent through the box. The electronic noise introduced by the servo could be significantly reduced with a better-designed and more sophisticated servo. The thermal mediated noise could be reduced in several ways. The first is to make a cavity that is made of a solvent-safe polymer as opposed to stainless steel. Metal conducts heat well; consequently, having a metal cavity almost certainly contributes to thermal noise. Another possible solution is to conduct the experiment at a lower temperature, perhaps as low as the sublimation temperature of dry ice (-78.5 °C). The flow-mediated noise that is encountered during the injection of absorbers into the cavity could be reduced by improving the injection apparatus. For example, a thin tube could be inserted into the cavity and positioned in the vicinity of the beam path. Absorbers could be delivered through that tube with a micro pump, causing much less turbulence than the present setup. In summary, all of the sources of noise could be significantly reduced, in theory, all the way to the shot noise limit. Gas phase cavity-

enhanced spectroscopic measurements have been made at the shot noise limit. [15]

7.3 Amplitude Servo

In order to eliminate amplitude noise introduced by the AO and EO and present on the Ti:Sapph, an amplitude servo was built, as illustrated in Figure 7.1. This servo essentially compares a stable DC voltage to the output from a photodetector that is downstream of the AO and attempts to eliminate that difference (the assumption being this difference in voltages is due to amplitude noise). The servo accomplishes this through a voltage-controlled attenuator, which attenuates the voltage going to the AO VCO. This attenuation causes a change in the AO frequency and a concomitant change in the optical power transmitted through it. This servo made it possible to lock the cavity with the etalon high voltage source connected, largely because it removed amplitude noise that was adding to the 160 kHz.

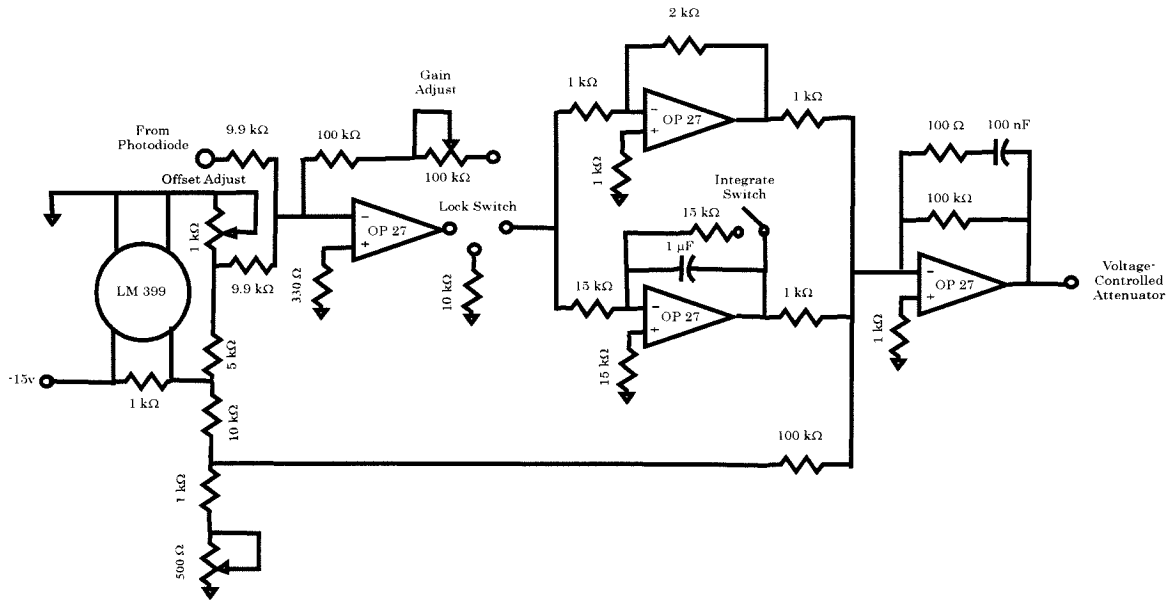

Figure 7.1: Amplitude Servo

7.4 Shot Noise

Shot noise is an intrinsic property of photon detection and is the one type of noise that cannot be circumvented by manipulating detection conditions. Therefore, it is considered the fundamental noise floor in photon detection. In the simplified case in which an optical beam of frequency, ν, and power, P, is incident on a photodetector that is assumed to have no dark current, the rate at which the photons are detected is:

$$r = \frac{\eta P}{h\nu} \tag{7.6}$$

where η is the quantum efficiency of the detector. The average number of photons arriving in a time interval, T, is:

$$\langle N \rangle = rT = \frac{\eta P T}{h\nu} \tag{7.7}$$

The actual number of photons that arrive within this time interval will fluctuate around $\langle N \rangle$. The probability that precisely N photons will arrive within n identical intervals (having divided T into n subintervals) is given by the binomial distribution. $\langle N \rangle / n$ can be viewed as the probability that one photon will arrive within a single segment, n, assuming n is sufficiently large.

$$p_n(N) = \frac{n!}{N!(n-N)!}(\frac{\langle N \rangle}{n})^N(1 - \frac{\langle N \rangle}{n})^{n-N} \tag{7.8}$$

Using Stirling's approximation and taking the continuous limit of this distribution as $n \to \infty$ yields the Poisson distribution:

$$\begin{aligned} p_n(N) &= \frac{\langle N \rangle^N}{N!} \lim_{n\to\infty} \frac{(\frac{n}{e})^n}{n^N(\frac{n-N}{e})^{n-N}}(1 - \frac{\langle N \rangle}{n})^{n-N} = \frac{e^{-N}\langle N \rangle^N}{N!} \lim_{n\to\infty} \frac{n^{n-N}}{(n-N)^{n-N}}(1 - \frac{\langle N \rangle}{n})^{n-N} \\ &= \frac{e^{-N}\langle N \rangle^N}{N!} \lim_{n\to\infty} \frac{(1 - \frac{\langle N \rangle}{n})^{n-N}}{(1 - \frac{N}{n})^{n-N}} = \frac{e^{-\langle N \rangle}\langle N \rangle^N}{N!} \end{aligned} \tag{7.9}$$

$\langle N \rangle$ turns out to be the expectation value of N:

$$\begin{aligned}\int_0^\infty Np(N)dN &= \int_0^\infty N\frac{\langle N\rangle^N e^{-\langle N\rangle}}{N!}dN = \int_0^\infty \frac{\langle N\rangle^N e^{-\langle N\rangle}}{(N-1)!}dN \\ &= \langle N\rangle \int_0^\infty \frac{\langle N\rangle^{(N-1)} e^{-\langle N\rangle}}{(N-1)!}dN = \langle N\rangle\end{aligned} \tag{7.10}$$

The variance of N, $\langle (\Delta N)^2 \rangle$, is:

$$\langle (\Delta N)^2 \rangle = \langle (N - \overline{N})^2 \rangle = \langle N^2 \rangle - \langle N \rangle^2 \tag{7.11}$$

We can easily determine $\langle N \rangle^2$ by expressing N^2 as $N + N(N-1)$:

$$\langle N \rangle^2 = \int_0^\infty Np(N)dN + \int_0^\infty (N(N-1))p(N)dN \tag{7.12}$$

By definition,

$$\int_0^\infty Np(N)dN = \langle N \rangle \tag{7.13}$$

and

$$\begin{aligned}\int_0^\infty (N(N-1))p(N)dN &= \int_0^\infty \frac{(N)(N-1)\langle N^N\rangle e^{-\langle N\rangle}}{N!} = \int_0^\infty \frac{\langle N^N\rangle e^{-\langle N\rangle}}{(N-2)!} \\ &= \langle N^2\rangle \int_0^\infty \frac{\langle N^{(N-2)}\rangle e^{-\langle N\rangle}}{(N-2)!} = \langle N^2\rangle\end{aligned} \tag{7.14}$$

Therefore,

$$\langle (\Delta N)^2 \rangle = \langle N \rangle \tag{7.15}$$

The photocurrent coming from a detector at any moment, therefore, is proportional to the number of photons that hit the detector within some time interval, τ. The average photocurrent would be:

$$\langle i \rangle = \frac{e\langle N \rangle}{\tau} \tag{7.16}$$

The noise in the photocurrent is the variance of i(t):

$$(i_N)^2 \equiv \langle (\Delta i)^2 \rangle \equiv \langle (i - \langle i \rangle)^2 \rangle \tag{7.17}$$

Thus,

$$\langle (\Delta i)^2 \rangle = \frac{e^2 \langle (\Delta N)^2 \rangle}{\tau^2} \tag{7.18}$$

Using the result from (7.15), we have:

$$\langle (\Delta i)^2 \rangle = \frac{e^2 \langle N \rangle}{\tau^2} \tag{7.19}$$

Finally, from (7.16), we have:

$$\langle (\Delta i)^2 \rangle = \frac{e \langle i \rangle}{\tau} \tag{7.20}$$

Therefore,

$$i_N = \sqrt{\frac{e \langle i \rangle}{\tau}} \tag{7.21}$$

where $\langle i \rangle$ is the photocurrent:

$$\langle i \rangle = S P_{refl} \tag{7.22}$$

and S is the detector sensitivity

7.5 Minimum Detectable Change in δ_0

If we wanted to determine the minimum detectable change in the absorption coefficient, α, in a shot-noise limited regime, we would consider an infinitesimal change in the power incident on the photodetector (in this case, due to shot noise) divided by the partial derivative of that power with respect to alpha:

$$(\delta \alpha)_{min} = \frac{\partial P_o}{\frac{\partial P_o}{\partial \alpha}} \tag{7.23}$$

Since we are considering photodetection, we can write:

$$(\delta\alpha)_{min} = \frac{\partial i}{\frac{\partial i}{\partial \alpha}} \tag{7.24}$$

From (7.21), we know that δi is:

$$\delta i = i_N = \sqrt{\frac{e\langle i \rangle}{\tau}} \tag{7.25}$$

From(7.22), we know that the average photocurrent is:

$$\langle i \rangle = SP_o \tag{7.26}$$

Therefore, $\frac{\partial i}{\partial \alpha}$ is:

$$\frac{\partial i}{\partial \alpha} = S\frac{\partial P_o}{\partial \alpha} = -2LP_oS(\frac{g}{1-g})(\frac{r_1^2-1}{r_1^2-g}) \tag{7.27}$$

Our minimum detectable $\delta\alpha$ becomes:

$$(\delta\alpha)_{min} = \frac{\sqrt{e/(\tau SP_o)}}{2L(\frac{g}{1-g})(\frac{r_1^2-1}{r_1^2-g})} \tag{7.28}$$

Since $\delta_0 = \alpha L$, our minimum detectable change in δ_0 is:

$$(\delta\delta_0)_{min} = (\delta\alpha)_{min}L = \frac{\sqrt{e/(\tau SP_o)}}{2(\frac{g}{1-g})(\frac{r_1^2-1}{r_1^2-g})} \approx \sqrt{\frac{e}{\tau SP_o}}(\frac{\pi}{2F}) \tag{7.29}$$

Although (7.29) would give a reasonable estimate of the minimum detectable δ_0, we would like to be more rigorous in our approach, since P_o is a function of δ_0. Therefore, we will express P_o in terms of δ_0 and then solve for δ_0.

$$P_o = P_{inc}\frac{(\delta_{0(abs)} + (\delta_{0(other)} + \delta_2) - \delta_1)^2}{(2\pi/F)^2} \tag{7.30}$$

$\delta_{0(other)}$ is a measure of the intra-cavity losses due to solvent, light scattering, etc. and is assumed to be constant for the purposes of this calculation. $\delta_{0(abs)}$ is a measure of

the losses due to absorption. Now our expression for $\delta\delta_0$ is:

$$(\delta\delta_0)_{min}(\delta_{0(abs)} + \delta_{0(other)} + \delta_2 - \delta_1) = \sqrt{\frac{e}{\tau S P_{inc}}}(\frac{\pi^2}{F^2}) \tag{7.31}$$

If we assume that $\delta\delta_0 = \delta_{0(abs)}$ (i.e. that the SNR is 1), we have:

$$(\delta_{0(abs)})^2 + \delta_{0(abs)}(\delta_{0(other)} + \delta_2 - \delta_1) - \sqrt{\frac{e}{\tau S P_{inc}}}(\frac{\pi^2}{F^2}) = 0 \tag{7.32}$$

With a finesse of 32,000 and an incident power of 60 nW, the minimum detectable δ_0 would be 6.10×10^{-9} ($1.93 \times 10^{-10}/\sqrt{Hz}$. This would correspond to approximately 700 absorbers in the beam volume (given that our cavity has a beam volume of approximately 11.9 nL).

7.6 Optimization Strategies

The fundamental limit for this technique, given the present state of technology, would be determined by the shot-noise limit and the technology for making highly reflective mirrors. The absolute best mirrors would have a $\mathcal{F}$ of $\sim 1.0 \times 10^6$. This would translate to mirrors whose transmittivity and losses ($\mathcal{T} + \mathcal{L}$) are equal to 3.14e-6. In a shot-noise limited regime, with 10 μW of optical power, a cavity enhanced device of roughly the same length (i.e. 1.75 mm) and mirror radius of curvature (5.0 cm), would have a detection threshold of approximately $1 \times 10^{-12}\sqrt{Hz}$,which translates to less than one strong absorber ($\epsilon = 1 \times 10^5 M^{-1} cm^{-1}$)in the beam volume. The largest challenge in being shot-noise limited with so much optical power (i.e. 10 μW), however, would be the minimization of thermal noise. Keeping the solvent system under nitrogen definitely reduced thermal noise. If it were under nitrogen from the initial filling with solvent until the completion of absorption measurements would likely reduce it even further—possibly below the shot-noise limit.

Chapter 8

Future Directions

8.1 Next Phase Instrument

The next phase in the development of cavity-enhanced spectroscopy would involve improvements and modifications to the cavity design, photo detection scheme and servo.

8.1.1 Cavity Design Improvements

It is believed that some of the thermal-mediated noise was exacerbated by having a metal cavity, which conducts heat very quickly. The next cavity should be constructed of a solvent safe polymer. Our present cavity is very difficult to assemble and reassemble, which added unnecessary difficulty to this experiment. Ensuring that the cavity finesse remains at the highest possible value requires frequent and careful cleaning of the cavity mirrors. This cleaning necessitates that the cavity be disassembled; therefore, having a cavity that is simple to disassemble and reassemble would reduce the total amount of time it takes to clean the mirrors and have the cavity realigned. Given the hygroscopicity of acetone (d_6 or otherwise) and the degradation in the optical transparency of d_6 acetone in the presence of even a few percent of water, the cavity and its associated solvent injection system should remain completely under nitrogen.

8.1.2 Photo Detection

In order to lock the cavity with the Pound-Drever-Hall method, it is necessary to detect the reflected intensity from the cavity. Our present cavity design only permits the de-

tection of the reflected power; however, there would be an advantage in detecting both the transmitted and reflected powers [28]. With our present cavity and photo detection scheme, our measurement of absorption is dependent upon the measurement of $\langle \mathcal{F} \rangle$ and the uncertainty of the mode-matching factor ϵ. In measuring both the reflected and transmitted intensities, we no longer need to depend upon the instantaneous $\mathcal{F}$, the $\langle \mathcal{F} \rangle$, or the mode matching factor in order to determine the losses due to absorption. We had expressed the cavity transmission (6.51) as :

$$\frac{P_t}{P_{inc}} = \frac{4\delta_1\delta_2}{(\delta_0 + \delta_1 + \delta_2)} \tag{8.1}$$

δ_1 and δ_2 are the losses due to transmission ($\mathcal{T}$) of each cavity mirror and δ_0 should be understood as the sum of losses due to each mirror and any intra-cavity losses. For the sake of this discussion, let's rewrite δ_0:

$$\delta_0 = \mathcal{L}_1 + \mathcal{L}_2 + \mathcal{L}_0 \tag{8.2}$$

Assuming each mirror has equal transmission and loss and taking into consideration that the power going into the cavity is only the mode-matched power (ϵP_{inc}), we have:

$$\frac{P_t}{\epsilon P_{inc}} = \frac{4\mathcal{T}^2}{(2\mathcal{T} + \mathcal{L}_0 + 2\mathcal{L})^2} \tag{8.3}$$

With respect to the reflected power, we can rewrite 6.41 with our new notation:

$$\frac{P_{refl} - (1-\epsilon)P_{inc}}{\epsilon P_{inc}} = \frac{P_{refl} - P_{inc}}{\epsilon P_{inc}} + 1 = \frac{(2\mathcal{L} + \mathcal{L}_0)^2}{(2\mathcal{T} + \mathcal{L}_0 + 2\mathcal{L})^2} \tag{8.4}$$

Subtracting 1 from 8.4 and dividing it by 8.3 , we have:

$$-\frac{P_{refl} - P_{inc}}{P_t} = \frac{(2\mathcal{T} + \mathcal{L}_0 + 2\mathcal{L})^2 - (2\mathcal{L} + \mathcal{L}_0)^2}{4\mathcal{T}^2} = \frac{(\mathcal{T} + 2\mathcal{L}) + \mathcal{L}_0}{\mathcal{T}} \tag{8.5}$$

We could measure the losses due to absorption by measuring the reflected, transmitted and incident power in the presence and absence of the absorber:

$$(\frac{P_{inc} - P_{refl}}{P_t})_2 - (\frac{P_{inc} - P_{refl}}{P_t})_1 = \frac{\Delta \mathcal{L}_0}{\mathcal{T}} \tag{8.6}$$

Now we have a measurement of losses due to absorption that is not dependent upon unknown or error-laden parameters such as $\langle \mathcal{F} \rangle$ or ϵ. The precision of this measurement is only dependent upon the noise on the optical signals and the accuracy with which $\mathcal{T}$ can be measured (which has been reported to be a few percent [28]).

8.1.3 Improved Bandwidth

If we were interested in increasing the bandwidth of our experiment, a more sophisticated servo would have to be designed (as discussed in Chapter 4) and a higher bandwidth AO would have to be used.

8.2 Reaction Center Absorption Measurements

Beyond the aforementioned technical challenges, the main obstacles to being able to make absorption measurements on photosynthetic reaction centers are where to place the reaction centers and how to address the absorption of water at the monitoring wavelengths. One possibility is to deposit a reaction-center-containing phospholipid bilayer onto the surface of one of the cavity mirrors. It would be necessary to verify that the presence of the phospholipid bilayer does not significantly degrade the finesse of the cavity. Once that is accomplished, the phospholipid bilayer on the cavity mirror could be supplemented with purified photosynthetic reaction centers and their accessory co-factors and preliminary absorption measurements could be made with them. Once preliminary absorption measurements are completed, an attempt would be made to reduce the concentration of the reaction centers in sequential steps until the limits of the cavity are reached. A simple cavity with high finesse ($\mathcal{F} = 10^5$) mirrors has been constructed and aligned into a new optical setup designed to permit the cavity to be

placed in a vertical position so that the interior faces of the cavity mirrors are horizontal. This setup allows the phospholipid bilayer to be placed onto a horizontal surface (i.e. the bottom cavity mirror). A phosopholipid bilayer was placed on the surface of one of the mirrors in this cavity. The finesse of this cavity was measured with and without a phospholipid bilayer on the bottom mirror. Preliminary measurements suggest that the presence of the bilayer only reduces the cavity finesse by approximately 10 percent.

As was mentioned in the introduction, there are a number of events in the well-characterized electron transfer process in the photosynthetic reaction center that are of a sufficient duration to be candidates for such measurements, such as the thermally induced transfer of an electron between QA to QB or perhaps the role of the 'B' pathway in the reaction center, and perhaps the role of the bacteriopheophytin molecules in electron transfer. Additionally, the cavity could be used to determine the extent to which the reaction center is rotating within the membrane, by observing the frequency of the oscillations in absorption due to the rotation of the reaction center (and hence the rotation of the excitation dipole of the chromaphore), assuming the rotation is slower than the temporal resolution of the cavity. This technique of making single molecule absorption measurements is, of course, not limited to studying the photosynthetic reaction center. Any molecule that participates in a chemical reaction whose progress or state can be monitored by absorption measurements would be a candidate for this technique.

Appendix A: Derivation of the Scalar Wave Equation from Maxwell's Equations

If we assume a neutral, homogeneous, isotropic medium such as air or glass or an uncharged liquid, Maxwell's Equations are [29]:

$$\nabla \cdot \mathbf{E} = 0 \tag{8.7}$$

$$\nabla \cdot \mathbf{B} = 0 \tag{8.8}$$

$$\nabla \times \mathbf{B} = \frac{\mu\epsilon}{c}\frac{\partial \mathbf{E}}{\partial t} \tag{8.9}$$

$$\nabla \times \mathbf{E} = -\frac{1}{c}\frac{\partial \mathbf{B}}{\partial t} \tag{8.10}$$

The first equation (known as Gauss's Law) merely states that the electric field through any closed surface is proportional to the charge enclosed by that surface or that the divergence of the electric field is proportional to the charge density. If there is no enclosed charge, there is no charge density and the divergence of the electric field is zero. The second equation merely states that the net magnetic field through an enclosed surface is zero or that the divergence of the magnetic field is zero, since there are no magnetic monopoles or charges. The next two equations state that a time varying magnetic or electric field induces an electric or magnetic (respectively) field that is perpendicular to the plane of the time varying field (which is what the curl ensures). Our goal is to use Maxwell's equations to come up with an expression that describes the propagation of the electric field of optical beams; therefore, we want to end up with an expression in

terms of the electric field alone. Equation (8.10) describes how a time varying magnetic field induces an electric field perpendicular to the magnetic field. If we take the curl of this equation, the right side will contain the curl of the magnetic field, which can be related to a time-varying electric field via Equation(8.9). Therefore, our strategy will be to take the curl of (8.10) and then to use (8.9) for an expression in terms of the electric field alone.

$$\nabla \times (\nabla \times \mathbf{E}) = -\frac{1}{c}(\nabla \times \frac{\partial \mathbf{B}}{\partial t}) = -\frac{1}{c}\frac{\partial}{\partial t}(\nabla \times \mathbf{B}) \tag{8.11}$$

Now replacing the curl of the magnetic field with the right side of (8.9), we have :

$$\nabla \times (\nabla \times \mathbf{E}) = -\frac{\mu\epsilon}{c^2}\frac{\partial^2 \mathbf{E}}{\partial t^2} \tag{8.12}$$

We can simplify by using a vector identity:

$$\mathbf{A} \times (\mathbf{B} \times \mathbf{C}) = \mathbf{A}(B \cdot C) - (A \cdot B)\mathbf{C} \tag{8.13}$$

and substituting ∇ for $\mathbf{A}$ and $\mathbf{B}$, and $\mathbf{E}$ for $\mathbf{C}$, we have:

$$\nabla \times (\nabla \times \mathbf{E}) = \nabla(\nabla \cdot \mathbf{E}) - \nabla^2 \mathbf{E} \tag{8.14}$$

Since we know that $\nabla \cdot \mathbf{E} = 0$ from Equation 8.7, we have:

$$\nabla \times (\nabla \times \mathbf{E}) = -\nabla^2 \mathbf{E} \tag{8.15}$$

Therefore, (8.12) becomes:

$$\nabla^2 \mathbf{E} - \frac{\mu\epsilon}{c^2}\frac{\partial^2 \mathbf{E}}{\partial t^2} = 0 \tag{8.16}$$

In order to proceed further, we need a time-dependent expression for the electric field. We can do this without making any assumptions about the spatial distribution of the field:

$$\mathbf{E}(q,t) = \mathbf{E}(q)e^{-i\omega t} \tag{8.17}$$

where q is an arbitrary spatial coordinate and ω is the angular frequency of the wave. Taking the second partial derivative of the field with respect to time, we have:

$$\frac{\partial^2 \mathbf{E}}{\partial t^2} = -\omega^2 \mathbf{E}(q) e^{-i\omega t} \tag{8.18}$$

Substituting this result into (8.16), we have:

$$\nabla^2 \mathbf{E}(q) e^{-i\omega t} + \frac{\mu\epsilon\omega^2}{c^2} \mathbf{E}(q) e^{-i\omega t} = 0 = \nabla^2 \mathbf{E}(q) + \frac{\mu\epsilon\omega^2}{c^2} \mathbf{E}(q) \tag{8.19}$$

We will define the square of the propagation constant, k^2, as:

$$k^2 = \frac{\mu\epsilon\omega^2}{c^2} \tag{8.20}$$

Substituting into(8.19), we have the scalar wave equation:

$$[\Delta^2 + k^2]\mathbf{e}E(q) = 0 \tag{8.21}$$

Appendix B: Full Scalar Wave Equation

Let's consider a spherical wave propagating from a point source at the origin; we can represent the electric field as:

$$\tilde{E} = \tilde{E}(r,t) \tag{8.22}$$

where $r = \sqrt{x^2+y^2+z^2}$. We can take partial derivatives of this expression in rectangular coordinates as follows:

$$\frac{\partial E}{\partial x} = \frac{\partial r}{\partial x}\frac{\partial E}{\partial r} \tag{8.23}$$

$$\frac{\partial^2 E}{\partial x^2} = (\frac{\partial r}{\partial x})^2\frac{\partial^2 E}{\partial r^2} + \frac{\partial^2 r}{\partial x^2}\frac{\partial E}{\partial r} \tag{8.24}$$

Now, we can evaluate the Laplacian of $\tilde{E}(r,t)$:

$$\Delta^2[\tilde{E}(r,t)] = (\frac{x^2+y^2+z^2}{r^2})\frac{\partial^2 E}{\partial r^2} + \frac{1}{r}(3 - \frac{x^2+y^2+z^2}{r^2})\frac{\partial E}{\partial r} = \frac{1}{r}(r\frac{\partial^2 E}{\partial r^2} + 2\frac{\partial E}{\partial r}) \tag{8.25}$$

We can see that our final expression for the Laplacian of E(r,t) is merely the second partial derivative of the product (E(r,t)r) with respect to r:

$$\Delta^2 E(r,t) = \frac{\partial^2}{\partial r^2}(rE(r,t)) \tag{8.26}$$

Our scalar wave equation is now:

$$\frac{\partial^2}{\partial r^2}(rE(r)) + k^2(rE(r)) = 0 \tag{8.27}$$

A general solution to this equation would be:

$$\tilde{E}(r) = \frac{e^{-ikr}}{r} \tag{8.28}$$

We can see that the electric field and intensity of the wave decrease as the wave propagates from the source. We also note that the radius of curvature of the spherical wave is r. As the wave propagates from a point source, the radius of curvature increases linearly. This intuition will be helpful when look for a simplified solution in rectangular coordinates. This solution in rectangular coordinates is:

$$\tilde{E}(x, y, z) = \frac{e^{-ik\sqrt{x^2+y^2+z^2}}}{\sqrt{x^2 + y^2 + z^2}} \tag{8.29}$$

Appendix C: The Paraxial Approximation

For the optical beams with which we are concerned, there is no need to consider the full three-dimensional propagation of a spherical wave. Our goal is to model a beam propagating in the z direction with a finite transverse profile. To this end, we will represent the field as the product of a propagation term and a scalar amplitude, $\tilde{u}$:

$$\tilde{E}(x,y,z) = \tilde{u}(x,y,z)e^{-ikz} \tag{8.30}$$

We will now apply the scalar wave equation (8.21) to this expression. First we'll take the Laplacian of our expression for the electric field.

$$\Delta^2[\tilde{u}e^{-ikz}] = [\frac{\partial^2\tilde{u}}{\partial x^2} + \frac{\partial^2\tilde{u}}{\partial y^2} + \frac{\partial^2\tilde{u}}{\partial z^2} - 2ik\frac{\partial\tilde{u}}{\partial z} - k^2\tilde{u}]e^{-ikz} \tag{8.31}$$

To this, we will add $k^2\tilde{u}e^{-ikz}$ and set this sum equal to zero, thus satisfying the wave equation:

$$[\Delta^2 + k^2]\tilde{E} = [\frac{\partial^2\tilde{u}}{\partial x^2} + \frac{\partial^2\tilde{u}}{\partial y^2} + \frac{\partial^2\tilde{u}}{\partial z^2} - 2ik\frac{\partial\tilde{u}}{\partial z}]e^{-ikz} = 0 \tag{8.32}$$

We will only consider the x and y coordinates that are just off-axis from z. We will assume that the beam propagates gently in the z direction with no rapid changes in the amplitude along the z axis (i.e. no radical focusing of the beam). In this case, the second derivative in z can be dropped. For most applications, this is a good assumption. This

is called the paraxial approximation and it gives rise to the paraxial wave equation:

$$\frac{\partial^2 \tilde{u}}{\partial x^2} + \frac{\partial^2 \tilde{u}}{\partial y^2} - 2ik\frac{\partial \tilde{u}}{\partial z} = 0 \tag{8.33}$$

Although there are a number of mathematically rigorous ways to find a solution to the paraxial wave equation, a common sense approach will suffice. Let's consider our solution to the exact wave equation (8.29) in rectangular coordinates. We can rewrite it as:

$$\tilde{E}(x,y,z) = \frac{e^{-ik\sqrt{x^2+y^2+z^2}}}{\sqrt{x^2+y^2+z^2}} = \frac{e^{-ikz\sqrt{1+(\frac{x^2+y^2}{z^2})}}}{z\sqrt{1+(\frac{x^2+y^2}{z^2})}} \tag{8.34}$$

We can expand $\sqrt{1+\frac{x^2+y^2}{z^2}}$ as a MacLaurin series,

$$\sqrt{1+\frac{x^2+y^2}{z^2}} \approx 1 + \frac{x^2+y^2}{2z^2} - \frac{(x^2+y^2)^2}{4z^4} + ... \tag{8.35}$$

Our expression for the field is now:

$$\tilde{E}(x,y,z) = \frac{e^{-ik(z+(\frac{x^2+y^2}{2z})-\frac{(x^2+y^2)^2}{4z^3}+...)}}{z+\frac{x^2+y^2}{2z}-\frac{(x^2+y^2)^2}{4z^3}+....} \tag{8.36}$$

If we are considering axial distances that are much larger than the transverse distances, i.e. $z^2 \gg x^2+y^2$, then $\frac{x^2+y^2}{z^2} \ll 1$ and we can ignore higher-order terms. If we choose the first two terms in the exponent and in the denominator, we have:

$$\tilde{E}(x,y,z) = \frac{e^{-ikz}e^{-ik\frac{x^2+y^2}{2z}}}{z+\frac{x^2+y^2}{2z}} \tag{8.37}$$

This turns out not to be a solution to the paraxial wave equation, due to the second-order term in the denominator. In physical terms, eliminating the quadratic term in the denominator would seem to makes sense, since we are assuming that $\frac{x^2+y^2}{z^2} \ll 1$. Eliminating this term, we have an exact solution to the paraxial wave equation:

$$\tilde{E}(x,y,z) = \frac{e^{-ikz}e^{-ik\frac{x^2+y^2}{2z}}}{z} \tag{8.38}$$

Analogous to the exact solution, z represents the radius of curvature of the wavefront.

$$\tilde{E}(x,y,z) = \frac{1}{R(z)}e^{-ikz}e^{-ik\frac{x^2+y^2}{2R(z)}} \tag{8.39}$$

This makes good physical sense as does the quadratic transverse phase variation. Let's take a look at the expression for the intensity of the beam:

$$I(x,y,z) = |\tilde{E}(x,y,z) * \tilde{E}^*(x,y,z)| = \frac{1}{R(z)^2} = \frac{1}{z^2} \tag{8.40}$$

It makes good physical sense that the intensity of a diverging beam decreases; however, what does not make physical sense is that this solution suggests that the transverse profile of the beam is unbounded.

Appendix D: Derivation of the Hermite Gaussian Mode Functions

A general expression for the scalar amplitude of the n, m transverse mode is:

$$\tilde{u}_{n,m}(x, y, z) = \tilde{u}_n(x, z)\tilde{u}_m(y, z) \tag{8.41}$$

We are assuming that the overall scalar amplitude can be expressed as the product of the amplitude in each transverse coordinate. We will begin by suggesting a trial solution in one transverse coordinate [23]:

$$\tilde{u}_n(x, z) = A(\tilde{q}(z))f(x)e^{-ik\frac{x^2+y^2}{2\tilde{q}(z)}} \tag{8.42}$$

We are assuming that the scalar amplitude of the higher-order transverse modes will contain a term in the transverse coordinate, which we are calling f(x). What we also know is that this term will change form as the mode number changes. Let's apply the paraxial wave equation in x and z to this trial solution. We come up with a differential equation:

$$\frac{\partial^2 f}{\partial x^2} + \frac{2ik}{\tilde{q}}x\frac{\partial f}{\partial x} - \frac{ik}{\tilde{q}}[1 + \frac{2\tilde{q}}{A}\frac{dA}{d\tilde{q}}]f = 0 \tag{8.43}$$

This differential equation is similar in form to an expression for a damped harmonic oscillator. It is a special case of the Sturm-Liouville system, known as the Hermite Differential equation::

$$H_n^{''} - 2xH_n^{'} + 2nH_n = 0 \tag{8.44}$$

The problem with this solution is that the amplitude of each transverse mode would change as the wave propagates in z. It would be preferable to have a solution that does not change with z propagation. To this end, we can suggest that our Hermite polynomial solution contain a scaling factor, $\tilde{p}(z)$:

$$f = H_n(\frac{x}{\tilde{p}(z)}) \tag{8.45}$$

Applying the paraxial wave equation to our revised expression for the scalar amplitude, we have:

$$f'' - \frac{2ik}{\tilde{q}}[\tilde{p} - \tilde{q}\frac{d\tilde{p}}{dz}]xf' - \frac{ik\tilde{p}^2}{\tilde{q}}[1 + \frac{2\tilde{q}}{A}\frac{dA}{d\tilde{q}}]f = 0 \tag{8.46}$$

Setting coefficients equal, we have:

$$\frac{2ik}{\tilde{q}}[\tilde{p} - \tilde{q}\frac{d\tilde{p}}{dz}] = \frac{2}{\tilde{p}} \Rightarrow \frac{dp}{p} = \frac{dz}{\tilde{q}} + \frac{idz}{k\tilde{p}^2} \tag{8.47}$$

$$-\frac{ik\tilde{p}^2}{\tilde{q}}[1 + \frac{2\tilde{q}}{A}\frac{dA}{d\tilde{q}}] = 2n \Rightarrow \frac{dA}{A} = \frac{id\tilde{q}}{k}\frac{n}{\tilde{p}^2} - \frac{1}{2}\frac{d\tilde{q}}{\tilde{q}} \tag{8.48}$$

These equations can be solved by relating $\tilde{p}(z)$ to the complex radius of curvature. A standard, physically convenient, arbitrary definition of the scaling factor, $\tilde{p}$ is:

$$\frac{1}{\tilde{p}(z)} = \frac{\sqrt{2}}{w(z)} \tag{8.49}$$

This is physically convenient in so far as the scalar amplitudes of the transverse modes will not change as the wave propagates in z. We can relate $\tilde{p}$ to the complex conjugates of $\tilde{q}$, from the definition of q:

$$\frac{1}{\tilde{q}} = \frac{1}{R(z)} - \frac{i\lambda}{\pi w^2(z)} \tag{8.50}$$

Subtracting the complex conjugates of q and doing a bit of algebra, we have an expression for p in terms of q:

$$\frac{1}{\tilde{p}^2} = \frac{ik}{2}(\frac{1}{\tilde{q}} - \frac{1}{\tilde{q}^*}) \tag{8.51}$$

Substituting this solution in 8.48, we have:

$$\frac{dA}{A} = \frac{id\tilde{q}}{k}\frac{ikn}{2}(\frac{1}{\tilde{q}} - \frac{1}{\tilde{q}^*}) - \frac{1}{2}\frac{d\tilde{q}}{\tilde{q}} = \frac{n}{2}(\frac{d\tilde{q}^*}{\tilde{q}^*} - \frac{dq}{\tilde{q}}) - \frac{1}{2}\frac{d\tilde{q}}{\tilde{q}} \tag{8.52}$$

Integrating, we have:

$$ln(\frac{A}{A_0}) = ln(\frac{\tilde{q}^*\tilde{q}_0}{\tilde{q}_0^*\tilde{q}})^{\frac{n}{2}} + ln(\frac{\tilde{q}_0}{\tilde{q}})^{\frac{1}{2}} \Rightarrow A = A_0(\frac{\tilde{q}^*\tilde{q}_0}{\tilde{q}_0^*\tilde{q}})^{\frac{n}{2}}(\frac{\tilde{q}_0}{\tilde{q}})^{\frac{1}{2}} \tag{8.53}$$

We complete our expression for transverse mode amplitudes in x by normalizing the Hermite polynomial functions:

$$\tilde{u}_n(x,z) = (\frac{2}{\pi})^{\frac{1}{4}}(\frac{1}{2^n n! w_0})^{\frac{1}{2}}(\frac{\tilde{q}^*\tilde{q}_0}{\tilde{q}_0^*\tilde{q}})^{\frac{n}{2}}(\frac{\tilde{q}_0}{\tilde{q}})^{\frac{1}{2}} H_n(\frac{\sqrt{2}x}{\tilde{p}})e^{\frac{-ikx^2}{2\tilde{q}}} \tag{8.54}$$

Our expression for the scalar amplitude in both transverse coordinates is merely the product of the amplitude in each transverse coordinate:

$$\tilde{u}_{n,m}(x,y,z) = (\frac{2}{\pi})^{\frac{1}{2}}(\frac{\tilde{q}_0}{2^{n+m}n!m!w_0\tilde{q}})(\frac{\tilde{q}^*\tilde{q}_0}{\tilde{q}_0^*\tilde{q}})^{\frac{(n+m)}{2}} H_n(\frac{\sqrt{2}x}{\tilde{p}})H_m(\frac{\sqrt{2}y}{\tilde{p}})e^{\frac{-ik(x^2+y^2)}{2\tilde{q}}} \tag{8.55}$$

Appendix E: Locking Protocol

1. Adjust optical power into cavity to less than 60 μW (which corresponds to about 3 W of circulating power in the cavity. This is the 'thermal' limit for this setup). The lower limit to optical power is set by the necessity of having a sufficient error signal to lock. The Menlo Systems detector needs around 500 nW for the error signal amplitude to be sufficient to lock.
2. Make sure that the Thor labs noise eater is operating 'within range' (green light on) and that it reduces the optical power by at least 10 percent . There are certain situations in which the noise eater adds 10 kHz noise. Watch for that and make appropriate adjustments to the power adjustment knob.

3. Engage the amplitude servo lock and integrator and ensure that the servo reduces optical power by at least another 10 percent.

4. Adjust the piezo offset voltage until the TEM_{00} peak is at the center of the scan voltage and note the value of the piezo offset on the voltmeter.

5. Turn the scan off (which should increase the piezo offset by a couple hundred millivolts) and re-adjust the piezo offset voltage to the value while scanning. This value will bring the cavity VERY close to resonance. At this point, the error signal and cavity signal should begin to oscillate with the amplitude of the error signal and resonance peak of the TEM_{00} mode. BE SURE THAT THIS IS THE AMPLITUDE of the oscillation you observe. Despite best attempts at alignment and mode matching, 2 or three other transverse modes do exist in the cavityand the cavity can be locked to them.

6. Increase the resolution of the error signal and make sure its DC offset is close to zero. If it's not, then use the offset adjuster to make sure it is.

7. Flip on the Integrator switch. If the integrator signal races off..then adjust the integrator offset until the integrator signal barely moves up (with the inverter switch down (non-inverting).

8. With the integrator switch off, readjust the piezo offset with the fine adjust knob until the oscillations are observed.

9. With the AO gain knob about three ' turns' from 0 and the error and cavity signals oscillating, turn on the AO lock switch. The AO should catchif it doesn't, re-adjust the piezo offset with the 'fine adjust' knob until it catches (the cavity signal should lock at the bottom of the resonance peak).

10. With the AO locked, quickly flip the integrate switch (the gain can be all the way to maxbut start at lower gainmaybe about halfway between 0 and max) and, if the gain isn't all the way to maximum, then increase it to max.

11. Increase the AO gain until the unity gain noise (151 kHz) increases, then reduce it until it reaches a minimum. The best position for the AO gain seems to be about 4 to 5 half turns from 0.

Appendix F: Data Acquisition MATLAB Code

```
% This is an m file which captures and
% retrieves data from one or more CompuScopes.
% Only the data from the first channel is
% retrieved and displayed.
%Adds the directory where the Gage DLL files are located
addpath 'C:\Gage OLD\CompuScope SDK\SDK for MATLAB'
% Set at least 1 of the system variables
% so it's defined in the first call.
system.board(1).opmode = 2;
% The 1 means look for GAGESCOP.INC in the Windows directory
boards_found = gagecall(0, 1, 0, system);
%If not all boards are found, exit.
if (boards_found < 1)
   disp('CompuScope boards not found');
   return;
end filename=input('How shall I name this datafile?','s'); mr=0;
dp=input('How many samples do you want to collect (per record, if
applicable)?'); sr=input('At what sample rate would you like to
collect data? (100,50,25,10,5,2,or 1 MS/s or kS/s)');

% Set up the rest of the system structure.
for i = 1:boards_found
```

```
        system.board(i).opmode = 2;
        system.board(i).sample_rate = sr;
        system.board(i).range_a = 1;
        system.board(i).couple_a = 1;
        system.board(i).range_b = 1;
        system.board(i).couple_b = 1;
        system.board(i).source = 4;
        system.board(i).source_2 = 5;
        system.board(i).slope = 1;
        system.board(i).imped_a = 0;
        system.board(i).imped_b = 0;
        system.board(i).range_e = 3;
        system.board(i).couple_e = 2;
        system.board(i).level = 143;
        system.board(i).slope_2 = 2;
        system.board(i).level_2 = 128;
        system.board(i).depth = dp;
        system.board(i).use_multiple_record = mr;
        system.board(i).use_external_clock = 0;
        system.board(i).external_clock_rate = 1000000;
        system.board(i).use_cal_table = 1;
        system.board(i).diff_in_a = 0;
        system.board(i).diff_in_b = 0;
end

system.capture.capture_type = 1; system.capture.trigger_timeout =
16.8; system.capture.busy_timeout = 65535;
system.capture.ensure_pre_trigger = 0;
%provides the option of multiple record, which essentially fills
```

```
the DAQ board memory in 'continuous'
%data streaming.  this is the suggested mode in triggering on 60Hz
line voltage and trying to take
%data at a fast sampling speed between each trigger.  if matlab
needs to interface with the DLL files
%between each 60 Hz triggering pulse, then the data will not be
taken in real time, even though MATLAB
%will not indicate that triggers are being missed
 due to processing time, etc!

 if (system.board(1).opmode == 1)
        channels_found = boards_found;
else
        channels_found = boards_found * 2;
end if mr==1 multirec=input('How many multiple record data sets do
you want to take? (1 to 65530)'); else multirec=-1; end for i =
1:channels_found
        system.channel(i).enable = 1;
        system.channel(i).start_point = 0;
        system.channel(i).transfer_length = dp;
        system.board(i).mulrec_acquisitions = -1;
        system.channel(i).mr_group_start = 1;
        system.channel(i).mr_groups = multirec;
end
% Set up the board parameters.
ret = gagecall(1, 0, 0, system);

if (ret <= 0)
  error ('Errors in one or more capture parameters, program stopped');
```

```
end

% Let the DLL handle the trigger timeout and
% the busy timeout.
trigger_timeout = 1; busy_timeout = 1;

% Capture the data.
change=input('Are you ready to take data? (yes = 1)');
   if change ==1
   disp('Here we go!')
   end
daq_run=input('How many data acquisition runs do you want to
make?');
%turns on power to board: in the absence of this gagecall function, the
%power is automatically turned on just before data capture and off just
%after capture is complete.  controlling it with this gagecall improves
%system performance.
gagecall(8,1,0,system); a=zeros(dp,daq_run); for n=1:daq_run
%the following commented code was to diagnose triggering issues by using a
%clock to figure out whether triggers were being missed.
   %timetr1=clock;
   %initiates trigger detection and data capture.  the return value
   %indicates whether a trigger is detected and whether data capture is
   %complete:  5=trigger detected and capture complete
   tc=gagecall(2, trigger_timeout, busy_timeout, system);
   trigcap(n)=tc;
%timetr2=clock;
%eetimeS(n)=timetr2(1,6)-timetr1(1,6);
%eetimeM(n)=timetr2(1,5)-timetr1(1,5);
```

```
%if eetimeM(n)>0
 %    eetimeS(n)=60.*eetimeM(n)+eetimeS(n);
%end

if (system.board(1).opmode == 1)
   channels = boards_found;
else
   channels = boards_found * 2;
end

% Disable all channels but channel 1.
for i = 2:channels
   system.channel(i).enable = 0;
end
% Get the data from channel  1 and convert to voltages.
a(:,n) = gagecall(3, 1, 0, system); end
%turns off power to board
gagecall(8,0,0,system);
%the following code was also used for triggering diagnosis
%if mr==1
%a=a(:,1:multirec);
%disp('Time to find a trigger and capture the last daq run is');
%disp(eetimeS(n));
disp('Now processing data');

for k=1:daq_run;
    m=((dp/2)-2):((dp/2)+2);
    b(1,k)=sum(a(m,k))/(5);
end
```

```
%a = reshape(a,prod(size(a)),1);
plot(b);

save(strcat('z:\Cavity-Enhanced Spectroscopy\Data
Files\','daq_runs',num2str(daq_run),num2str(filename)),'a','b'); for
y=1:n;
    disp(trigcap(y));
end
%end
```

Appendix G: Transients

With an acetone-filled cavity, we observed occasional diffusion timescale transients of unknown origin. It is possible that these transients are caused by clusters of water or localized populations of acetone in which one or more of the deuterium atoms is replaced with a hydrogen atom. The lock level at the depth of the transient roughly corresponds to the observed losses with regular acetone. Proton NMR experiments could aid in determining the nature of these transients. An example of one of these transients is provided in Figure 8.1.

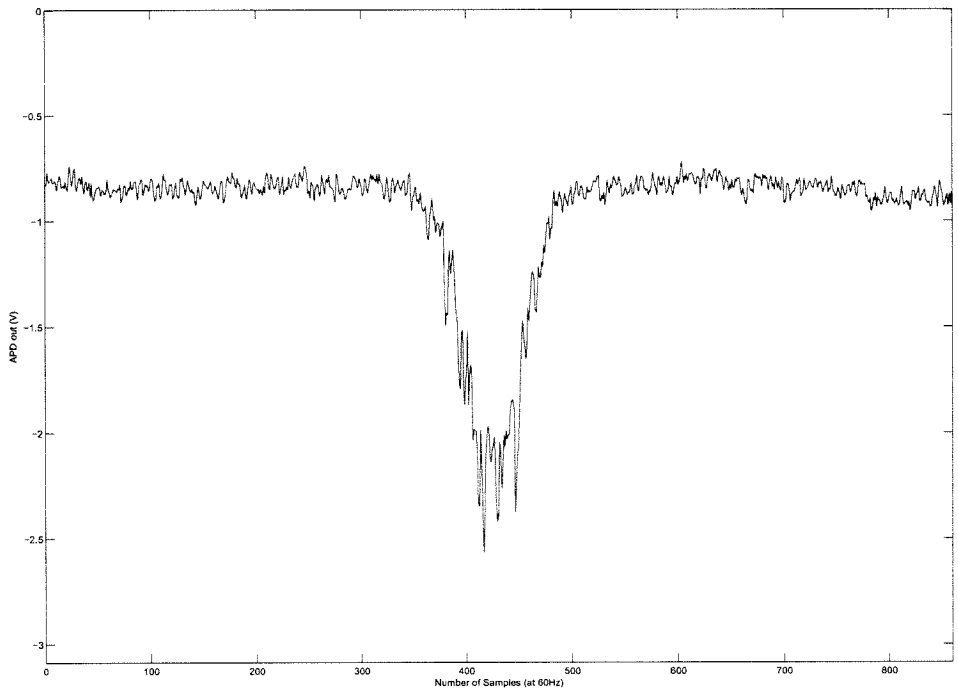

Figure 8.1: Diffusion Timescale Transient

Appendix H: Effective Beam Volume

Inside a locked Fabry-Perot cavity on resonance, the TEM_{00} mode has the following spatial distribution.

$$W = e^{\frac{-2(x^2+y^2)}{w(z)^2}} sin^2(kz) \tag{8.56}$$

The mode is Gaussian in x, y; however, the beam waist, w(z), change in z. Since there is a standing wave in the cavity, the intensity profile changes in z as $sin^2(kz)$. Analogous to fluorescence correlation spectroscopy (FCS), the effective volume can be expressed as:

$$V_{eff} = \frac{(\int W dV)^2}{\int W^2 dV} \tag{8.57}$$

It turns out to be much easier to evaluate the exponential in x and y first and then to evaluate with respect to z.

$$\int W dV = \int_{-\infty}^{\infty}\int_{-\infty}^{\infty}\int_{0}^{\infty} e^{\frac{-2(x^2+y^2)}{w(z)^2}} sin^2(kz) dx dy dz = \int_{-\infty}^{\infty}\int_{-\infty}^{\infty} e^{\frac{-2(x^2+y^2)}{w(z)^2}} dx dy \int_{-l/2}^{l/2} sin^2(kz) dz \tag{8.58}$$

Shifting to 'cylindrical' coordinates and changing integration limits to make it easier to solve the Gaussian integral:

$$2\int_{0}^{2\pi}\int_{0}^{\infty} e^{\frac{-2(r^2)}{w(z)^2}} r dr d\theta \int_{-l/2}^{l/2} sin^2(kz) dz \tag{8.59}$$

Solving the Gaussian integral by substitution:

$$u = 2r^2/w_0^2 \tag{8.60}$$

$$du = 4rdr/w_0^2 \tag{8.61}$$

$$\int WdV = 2\int_0^{2\pi}\int_0^{\infty} e^{\frac{-2(r^2)}{w(z)^2}} rdrd\theta = w(z)^2/2\int_0^{2\pi}\int_0^{\infty} e^{-u}dud\theta = \pi w(z)^2 \tag{8.62}$$

The beam waist propagates in the z direction as follows:

$$w(z)^2 = w_0^2(1 + \frac{z^2}{\lambda^2/(\pi^2 w_0^4)}) \tag{8.63}$$

The remaining integral is now:

$$\int WdV = \pi w_0^2 \int_{-l/2}^{l/2}(1 + \frac{z^2}{\lambda^2/(\pi^2 w_0^4)})sin^2(kz)dz \tag{8.64}$$

We can solve this integral using a trig identity and the intra-cavity boundary conditions on resonance (i.e. sin(kz) = 0 at each end of the cavity and that $l = q\lambda$), we have:

$$\int WdV = \pi w_0^2 \int_{-l/2}^{l/2}(1 + \frac{z^2}{\lambda^2/(\pi^2 w_0^4)})\frac{1}{2}(1 - cos(2kz))dz \tag{8.65}$$

Due to the boundary conditions, all definite integrals involving either cosine or sine will be zero. Taking this into consideration, we have:

$$\int WdV = \frac{\pi w_0^2}{2}\int_{-l/2}^{l/2}(1 + \frac{z^2}{\lambda^2/(\pi^2 w_0^4)})dz = (\frac{\pi w_0^2 l}{2} + \frac{\lambda^2 l^3}{24\pi w_0^2}) \tag{8.66}$$

The integration of the Gaussian portion is almost exactly the same as before. The

value of this integration differs from the previous case by a factor of two:

$$\begin{aligned}\int W^2 dV &= 2\int_0^{2\pi}\int_0^{\infty} e^{\frac{-4(r^2)}{w(z)^2}} r dr d\theta \int_0^{l} sin^4(kz)dz = \frac{\pi}{2}\int_{-l/2}^{l/2} w(z)^2 sin^4(kz)dz \\ &= \frac{w_0^2\pi}{2}\int_{-l/2}^{l/2}(1+\frac{z^2}{\lambda^2/(\pi^2 w_0^4)})sin^4(kz)dz\end{aligned} \tag{8.67}$$

The integration of $sin^4(kz)$ requires one extra step:

$$\begin{aligned}\int_{-l/2}^{l/2} sin^4(kz)dz &= \int_{-l/2}^{l/2}(1/2(1-cos(2kz)))^2 dz = \frac{1}{4}\int_{-l/2}^{l/2}(1+cos^2(2kz)+2cos(2kz))dz \\ &= \frac{1}{4}\int_{-l/2}^{l/2}(1+\frac{1}{2}(1+cos(4kz))+2cos(2kz))dz\end{aligned} \tag{8.68}$$

The overall integral is now:

$$\int W^2 dV = \frac{w_0^2\pi}{8}\int_{-l/2}^{l/2}(1+\frac{z^2}{\lambda^2/(\pi^2 w_0^4)})(1+\frac{1}{2}(1+cos(4kz))+2cos(2kz))dz \tag{8.69}$$

As with the previous integral, whenever there is a sine or cosine in this integral, its value becomes zero due to the boundary conditions. Taking this into consideration, our integral is:

$$\int W^2 dV = \frac{3w_0^2\pi}{16}\int_{-l/2}^{l/2}(1+\frac{z^2}{\lambda^2/(\pi^2 w_0^4)})dz = (\frac{3\pi w_0^2 l}{16}+\frac{\lambda^2 l^3}{64\pi w_0^2}) \tag{8.70}$$

Our value for V_{eff} is:

$$V_{eff} = \frac{(\frac{\pi w_0^2 l}{2}+\frac{\lambda^2 l^3}{24\pi w_0^2})^2}{(\frac{3\pi w_0^2 l}{16}+\frac{\lambda^2 l^3}{64\pi w_0^2})} \approx \frac{4}{3}\pi w_0^2 l \tag{8.71}$$

Bibliography

[1] J. Allen, G. Feher, T. Yeates, H. Komiya, and D. Rees, PNAS **84**, 5730 (1987).

[2] J. Allen, G. Feher, T. Yeates, H. Komiya, and D. Rees, PNAS **84**, 6162 (1987).

[3] J. Allen, G. Feher, T. Yeates, H. Komiya, and D. Rees, PNAS **85**, 8487 (1988).

[4] J. Deisenhofer, O. Epp, K. Miki, R. Huber, and H. Michel, J. Molec. Biol. **180**, 385 (1984).

[5] J. Deisenhofer, J. Epp, R. Huber, and H. Michel, Nature **318**, 618 (1985).

[6] L. B. et al, Biochemistry **34**, 14712 (1995).

[7] D. Tiede, J. Vazquez, J. Cordova, and P. Marone, Biochemistry **35**, 10763 (1996).

[8] A. Vermeglio and R. Clayton, PNAS **85**, 8487 (1988).

[9] R. H. et al, Biochemistry **31**, 5799 (1992).

[10] N. Woodbury, M. Becker, D. Middendorf, and W. Parson, Biochemistry **24**, 7516 (1985).

[11] M. S. et al, Science **276**, 812 (1997).

[12] D. Kleinfeld, M. Okamura, and G. Feher, Biochemistry **23**, 5780 (1984).

[13] C. Vallance, New J. Chem. **29**, 867 (2005).

[14] B. Paldus and A. Kachanov, Can. J. Phys. **83**, 975 (2001).

[15] J. Ye, L. Ma, and J. Hall, J. Opt. Soc. Am. B **15**, 6 (1998).

[16] A. Hallock, E. Berman, and R. Zare, Analytical Chemistry **74**, 1741 (2002).

[17] A. Hallock, E. Berman, and R. Zare, JACS **125**, 1158 (2003).

[18] A. Hallock, E. Berman, and R. Zare, Applied Spectroscopy **57**, 571 (2003).

[19] A. Pipino, Physical Review Letters **83**, 3093 (1999).

[20] A. Pipino, Applied Optics **39**, 1449 (2000).

[21] J. Nadeau, V. Ilchenko, and D. Kossakovski, Proceedings SPIE **4629**, 172 (2002).

[22] S. Fiedler and A. Hese, Review of Scientific Instruments **76**, 023107 (2005).

[23] A. Siegman, *Lasers*, University Science Books, 1986.

[24] M. Born and E. Wolf, *Principles of Optics*, Cambridge University Press, seventh edition edition, 1999.

[25] L. Mandel and E. Wolf, *Optical Coherence and Quantum Optics*, Cambridge University Press, 1995.

[26] R. Shankar, *Principles of Quantum Mechanics*, Plenum Press, second edition, 1994.

[27] R. D. et al, Appl. Phys. B: Photophys. Laser Chem. **31**, 97 (1983).

[28] C. Hood and H. Kimble, Physical Review A **64**, 033804 (2001).

[29] J. Jackson, *Classical Electrodynamics*, Wiley, 1974.